NAVAL SHIP RESEARCH AND DEVELOPMENT CENTER

Bethesda, Md. 20034

STRESS ANALYSIS OF COMPLEX SHIP COMPONENTS BY A NUMERICAL PROCEDURE USING CURVED FINITE ELEMENTS

by

James Hsienne Ma

STRUCTURES DEPARTMENT
RESEARCH AND DEVELOPMENT REPORT

July 1973

Report 4057

The Naval Ship Research and Development Center is a U. S. Navy center for laboratory effort directed at achieving improved sea and air vehicles. It was formed in March 1967 by merging the David Taylor Model Basin at Carderock, Maryland with the Marine Engineering Laboratory at Annapolis, Maryland.

Naval Ship Research and Development Center
Bethesda, Md. 20034

MAJOR NSRDC ORGANIZATIONAL COMPONENTS

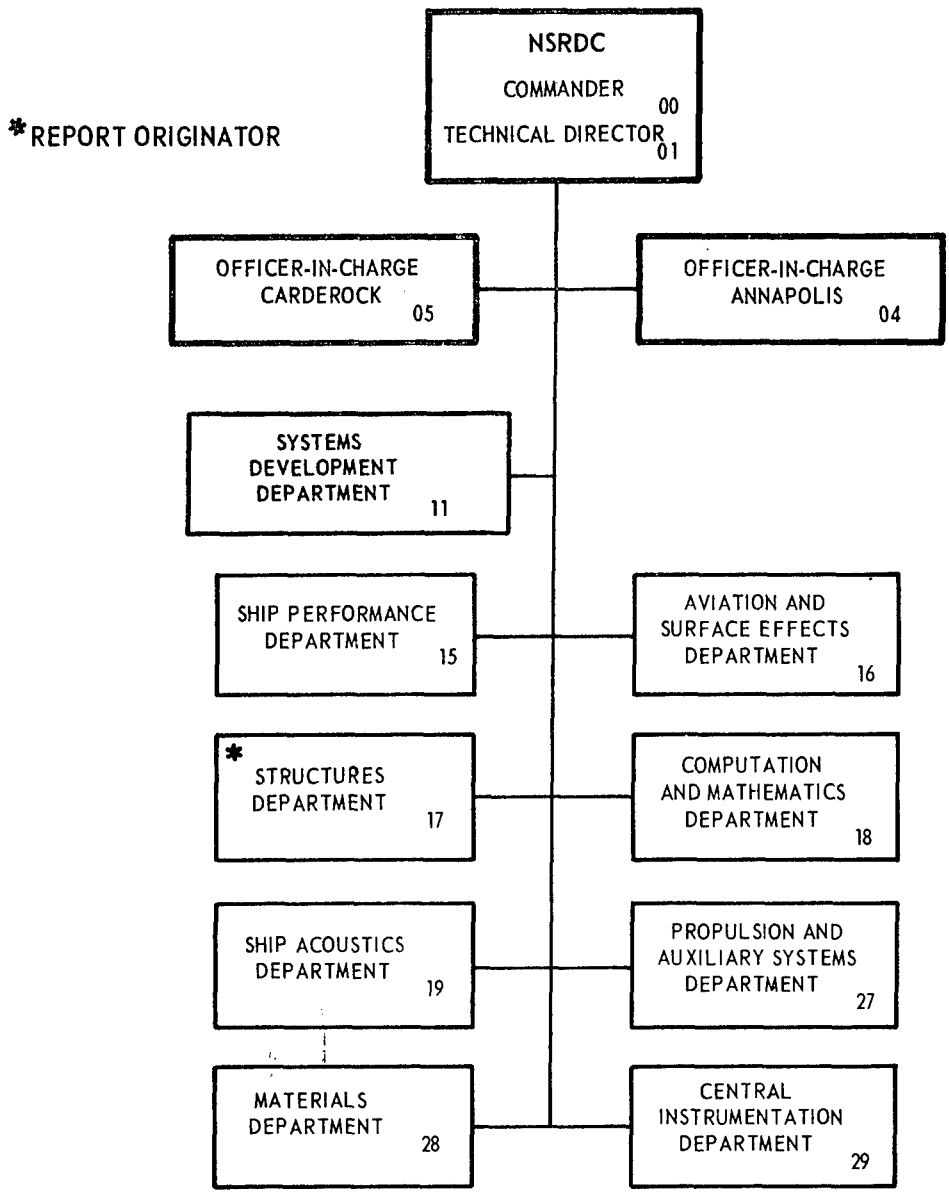

NDW-NSRDC 3960/43b (Rev. 3-72)
GPO 928-108

DEPARTMENT OF THE NAVY
NAVAL SHIP RESEARCH AND DEVELOPMENT CENTER
BETHESDA, MD. 20034

STRESS ANALYSIS OF COMPLEX SHIP COMPONENTS BY A NUMERICAL PROCEDURE USING CURVED FINITE ELEMENTS

by

James Hsienne Ma

July 1973 Report 4057

TABLE OF CONTENTS

LIST OF FIGURES

LIST OF TABLES

ABSTRACT

A numerical procedure for the structural analysis of a general three-dimensional nature has been developed to provide a reliable solution to the problem of determining the strength of propellers, particularly those with unconventional configurations. A finite element displacement model is utilized and compatible solid elements in their general form are adopted. The use of interpolation functions to define pertinent curvilinear coordinates in element space gives the finite element technique, new capabilities for dealing with structures of highly complex geometry. This formulation bypasses the constraints of simplifying assumptions (such as those imposed by classicial plate theory) and allows a closer approximation to the true structural configuration than is possible by other approaches, including most analytical and numerical methods. The performance of the refined elements described in this report is distinctly superior to those obtainable with commonly available elements, for example, those in NASTRAN. A highly skewed propeller blade under prescribed pressure distributions was chosen for demonstration of the generality of the procedure. Good agreement was obtained with measured displacement and experimental stress data.

ADMINISTRATION INFORMATION

The studies described in this report were carried out from the fall of 1971 to the fall of 1972 at the Naval Ship Research and Development Center (NSRDC) and were sponsored by the Naval Ship Systems Command (NAVSHIPS). Funding was provided under Subproject SF 43 422 312, Task 15084 (Structural Analysis for High Performance Surface Ships), Work Unit 1–1730–089.

The material contained in this report was submitted to the Graduate College of the University of Illinois at Urbana-Champaign in partial fulfillment of requirements for the degree of Doctor of Philosophy in Civil Engineering. The headings and other details of format follow University of Illinois rather than NSRDC style.

CHAPTER 1

INTRODUCTION

1.1 General

Recent years have witnessed an increased interest in the development of performance-oriented surface ships for which it is vital to keep weight to a minimum, e.g., high-speed hydrofoils, catamarans, and surface effect ships. A more accurate method of analysis than currently employed in shipyards is imperative if weight saving is to be achieved for such vehicles. The effective use of materials and an increased reliability of design will have far-reaching results over their life spans.

Governed by functional requirements and hydrodynamical considerations, the geometry of ship scantlings is generally complex and their construction contains a high degree of redundancy. It is therefore necessary to make simplifying assumptions in order to reduce the complexity of the mathematical model representing the structure to a form that is amenable to traditional design methods. In consequence, certain characteristic behavior of the elastic body is ignored and the accuracy of the analysis is often open to question. Thus verification requires testing scaled models and, at times, costly prototypes as well.

The rapid advances in digital electronic computers since the mid-1950's coupled with recent development in discrete element methods provide a powerful new tool for structural analysis (Paulling, 1964; Moe and Tonnesen, 1966; and the International Ship Structures Committee, 1969).* Many complicated design problems that were considered insurmountable to a realistic analysis only a few years ago can now be executed almost routinely by using an ordinary computer (Roren, 1969; Ma, 1969; and Abrahamsen, 1970). Specifically a structure system having, say, 1000 degrees of freedom can be solved in a matter of a few minutes on a late model computer (such as CDC 6600, or IBM 360/75, etc.) through appropriate idealization with due consideration for the bandwidth of the resulting system of equations.

During the past decade, the development of finite element methods has exhibited an exponential growth, and the demand for appropriate programs has increased rapidly. The total number of finite element computer programs in which substantial efforts have been expended may have exceeded several hundred (Gallagher, 1970 and Schrem, 1971). Nevertheless, only a rather small number of them (and these only recently) are accessible to engineers in practice. Among these well known programs are NASTRAN, the NASA structural analysis (MacNeal and McCormick, 1967); STRUDL, structural design language (Logcher and Sturman, 1966); FINEL (Adamchak, 1970) and SAMIS (Melosh et al., 1966). Programs of a proprietary nature includes ASKA (Schrem and Roy, 1971); DAISY (Kamel et al., 1969); SESAM-69 (Araldsen and Egeland, 1971); SAP (Wilson, 1970); STARDYNE (Dainora, 1971); and others (Hartung, 1970; and Mallett and Jordan, 1969).

*References are listed alphabetically starting on page 95.

Most of the finite element programs, including larger scale and general purpose programs that are currently available, have little or no data-generation features and their element libraries contain basically one- and two-dimensional elements of linear or constant-strain types. The big cost item of a finite element analysis is frequently the data preparation stage. In areas of steep stress gradient, for example, the good approximation of an important structural response may require the assemblage of a large number of elements, especially when the elements to be used are of lower calibre, such as the constant-stress elements. In the case of an irregular boundary, curved elements will have a distinct advantage. Thus refinement of element characteristics can have a profound impact on the economy and range of solution that the finite element method can provide.

By nature of their geometric proportions, many structural components can be idealized as one- or two-dimensional problems of elasticity and standard methods can be used to obtain reasonably good solutions. For other design tasks, however, no conventional approach can achieve realistic results. Examples are bodies of complex, unsymmetrical shapes and interface problems of two or more geometrical entitles (e.g., the junction of pipes, plates, and/or shells). The rational solution of such problems requires a general analysis in three-dimensional elasticity. It is in this difficult, but important, field of three-dimensional problems that recent developments in the isoparametric element family offer the most promising approach. These refined elements will be utilized in the study reported here.

1.2 Objective and Scope

The objective of the present study was to develop a numerical procedure for the static analysis of a three-dimensional elastic body of arbitrary configuration. More specifically, the purpose was to determine the structural behavior of a marine propeller subjected to a prescribed pressure loading. A highly skewed propeller* was chosen to demonstrate the generality of the approach. The study employed the finite element method in conjunction with curved solid elements. A computer program was developed to implement the procedure for predicting displacements and stresses of a complex structure with reference to an arbitrary curvilinear coordinate system. Linear elasticity and small deformation theory were assumed.

Chapter 2 outlines the finite element method for structural analysis. Certain element characteristics derived from a displacement model are discussed to aid in the selection of appropriate elements for improved computational results.

Although finite element techniques are widely used in the two-dimensional domain of plates and shells, they have had only limited application for the treatment of complex structures in the context of three-dimensional elasticity. The principal reason for this slow

*The marine propeller takes on complex, skewed geometry as a result of design considerations, such as those of vibration and cavitation aspects in blade design (Cox and Morgan, 1972).

progress is the large amount of input data and processing time required to implement a three-dimensional solution when only simple, tetrahedron-type solid elements are utilized. Isoparametric formulation and its associated refined curved elements coupled with a more efficient solution technique (as described in Chapter 3) now make it possible to tackle some of the most difficult problems in solid mechanics.

Some selected problems, including beams, plates, shells, and stiffened plates are solved to evaluate the adequacy and performance of the procedure developed here. Further, a ship component of complex geometry—a skewed propeller blade—is analyzed in Chapter 4 to provide insight into the potential of the procedure as a design tool. Since no analytic solution for the propeller blade problem is known, computed results for displacements and stresses are compared with experimental data.

1.3 Notations

The symbols used in this study are defined where they first appear. For convenience, frequently used symbols are summarized below.

The bar and tilde underscores (or overscores) generally denote a vector and a matrix, respectively. Parentheses and brackets are used alternatively to denote a vector and a matrix. For example, a column vector U^a can be written

$$\underline{U}^a = \{U^a\} = \begin{Bmatrix} \underline{U}_1 \\ \underline{U}_2 \\ \cdot \\ \cdot \\ \cdot \\ \underline{U}_i \end{Bmatrix}$$

with its subvector

$$\underline{U}_i = \{U_i\} = \begin{Bmatrix} u_i \\ v_i \\ w_i \end{Bmatrix}$$

A matrix

$$\underset{\sim}{\theta} = [\theta] = [\hat{V}_1, \hat{V}_2, \hat{V}_3]$$

When vector quantities appear in an equation, standard vector notations will apply. For example, "×" and "." represent cross and scalar product of vectors, respectively.

$[A]$	matrix of functions in nodal coordinates, Eq. (2.2)
$[B]$	matrix relating strain vector to nodal displacements, Eq. (2.4) or (3.8)
$[B']$	matrix relating local strain vector of a shell to nodal displacements, Eq. (3.52)
D	a specified domain, such as a given volume or area
$[D]$	elasticity matrix
$[D']$	elasticity matrix in the local coordinate system for a isotropic shell element
DK	$= \dfrac{E}{(1+\nu)(1-2\nu)}$
E	Young's modulus of elasticity
$\{F\}$	equivalent load vector, also known as generalized load vector
F_x, F_y, F_z	equivalent element nodal force in the x, y, or z direction, respectively; forces are positive in the positive direction of x, y, and z axes
$F_x(I), F_y(I), F_z(I)$	equivalent force in direction of x, y or z axis at node "i," Eq. (3.28)
$[g(\xi, \eta, \zeta)]$	matrix containing functions of curvilinear coordinates
G	$= \dfrac{E}{2(1+\nu)}$ shear modulus of elasticity
H_{ix}, H_{iy}, H_{iz}	weighting coefficient corresponding to position along Gaussian quadrature points ξ_{ix}, η_{iy}, or ζ_{iz}
i	subscript indicating nodal number, or active index
I	moment of inertia of a transverse section of a beam
$\hat{i}, \hat{j}, \hat{k}$	vector having unit value in direction of x, y, or z axis, respectively
$[J]$	Jacobian matrix of coordinate transformation
$\lvert J \rvert$	Jacobian determinant

k	constant factor included in $[D']$ matrix to improve shear deformation
k_{ij}	stiffness coefficient at i th row and j th column
$[K]$	stiffness matrix of entire structure
$[K_e]$	stiffness matrix of an element e
$\underset{\sim}{K}(r \cdot s)$	submatrices of $[K_e]$
ℓ, m, n	direction cosines of a unit vector $\bar{e}$ and $(\hat{i}, \hat{j}, \hat{k})$ representing global rectangular axes (x, y, z)
$[L^a]$	localizing matrix relating element nodal parameter to global structure parameter, Eq. (2.13)
M_x, M_y	bending moment components in the x and y directions
$\bar{n}$	vector normal to a curved surface
$N_i(\xi, \eta), N_i(\xi, \eta, \zeta)$	function of curvilinear coordinates in two or three dimensions, respectively, taking a value of unity at node i and zero at all other nodes
NNPE	number of nodes per element
$\bar{p}$	applied pressure on an element face, Eq. (3.27)
$\{P\}$	global load vector (entire structure)
$\{P^a\}$	external load vector for an element
$\bar{P}_\xi, \bar{P}_\eta, \bar{P}_\zeta$	vectors tangent to curvilinear coordinate lines (ξ, η, ζ)
$q(x, y, z)$	intensity of distributed loads
$\{q\}$	column matrix of generalized coordinates
$\bar{r}$	displacement vector $(= u\hat{i} + v\hat{j} + w\hat{k})$
$\bar{r}_i$	displacement vector of node "i"
$[R]$	rotation matrix for coordinate transformation, Eq. (3.40)
S	area of curved surface

t_i	shell thickness at node i
u, v, w	components of displacement in the direction of x, y and z axes, respectively; displacements are positive in the positive direction of coordinate axes
u_i, v_i, w_i	components of displacement at node i
$\{U\}$	vector of nodal parameters for entire structure, Eq. (2.13)
$\{U^a\}$	nodal displacement vector for an element
$\underline{U}_i$	vector of parameters at node i
$\underline{U}_{is}$	vector of parameters at node i for shell element, Eq. (3.51)
$\hat{V}_1, \hat{V}_2, \hat{V}_3$	unit vectors in directions of local axes x', y' and z', respectively
$\hat{V}_{1i}, \hat{V}_{2i}, \hat{V}_{3i}$	local unit vectors at node i
$\bar{V}_{3i}$	shell thickness vector at node i
Vol	volume of a given solid domain
w_e	work done by external load
w_i	internal work of strain energy
x, y, z	global system of rectangular coordinates
x', y', z'	local system of rectangular coordinates for shell element
x_i, y_i, z_i	coordinates at node i
α, β	rotations of nodal normal about two orthogonal axes
α_i, β_i	rotations of normal at node i
$\{a_j\}$	column matrix of constant coefficients, Eq. (3.21)
$\gamma_{xy}, \gamma_{yz}, \gamma_{xz}$	shearing strain components
$\gamma_{x'y'}, \gamma_{y'z'}, \gamma_{x'z'}$	shearing strain components in the local rectangular coordinates

δ	prefex denoting first variation of a function
δU_i	virtual displacement at node i for an element
$[\epsilon']$	local strain tensor, Eq. (3.42)
$\{\epsilon'\}$	local strain vector for a shell element Eq. (3.52)
ζ	a curvilinear coordinate in the thickness direction in case of a shell element
ζ, η, ξ	curvilinear coordinates at any point within an element
ζ_i, η_i, ξ_i	curvilinear coordinates at node i
$\zeta_{iz}, \eta_{iy}, \xi_{ix}$	position constants for the Gaussian quadrature point i
$[\theta]$	direction casine matrix of a local orthogonal system of axes
ν	Poisson's ratio
$[\sigma]$	stress tensor, Eq. (3.43)
$\tau_{x'y'}, \tau_{y'z'}, \tau_{z'x'}$	shearing stress components in the local rectangular coordinates
$[\phi(x, y, z)]$	row matrix of monomial functions of cartesian coordinate, Eq. (3.1)
$\sum_i$	summation on the running index i
$\int_D$	integration over a domain D

CHAPTER 2

THE FINITE ELEMENT METHOD OF STRUCTURAL ANALYSIS

2.1 Background

The finite element methods of structural mechanics rely heavily on numerical computation and their advent followed the availability of high-speed digital computers. The matrix formulation of structural problems was formally introduced by J. H. Argyris in a series of papers published in 1954–55. About the same period, notable progress in applying finite element methods to the analysis of aircraft and civil engineering structures had been made independently by a number of investigators including M. J. Turner (1956) and his group at the Boeing Company and B. Langefors (1958) in Sweden.

The basic concept of the finite element method is that a real continuum can be treated analytically by subdividing it into a finite number of regions. In each of these regions, the behavior, such as displacement or stress, is described by a separate field. These fields are often chosen in a form that ensures continuity of the described behavior throughout the complete continuum. In other cases, the chosen fields do not ensure continuity but nevertheless they achieve satisfactory solutions. These later cases do not have the assurance of convergence* possessed by the fully continuous analytical models (Melosh, 1963 and Irons and Draper, 1965). The concept of the finite element representation owes much to the early work of A. P. Hrenikoff (1941) and R. Courant (1943); the later was concerned with problems governed by broader field equations than just structural mechanics.

Much progress had been made in the various aspects of finite element analysis. Improved results were realized by introducing new types of elements, such as more powerful refined elements (Argyris, 1965; Felippa, 1966; Mehrain, 1967; Kohnke and Schnobrich, 1969; and Chu and Schnobrick, 1970) or efficient superelements (Araldsen and Egeland, 1971). Successful developments were also cited for various forms of structural behavior representation as in dynamics, plasticity, and large deflection (Argyris, 1965; Przemieniecki et al., 1971; and Zienkiewicz, 1971).

The formulation of the finite element method can be traced to energy procedures, principally the minimum potential energy (MPE) method and the minimum complementary energy (MCE) method. The MPE method is associated with assumed displacement parameters as unknowns and is usually termed the "displacement" or "stiffness" method. On the other hand, the MCE method deals with stress parameters and is termed the "flexibility" approach. Several authors, e.g., Fraeijs deVeubeke (1964), have been concerned with a parallel use of displacement and equilibrium models to obtain lower and upper bounds to the exact solution. Still others (Fraeijs deVeubeke, 1964 and Herman, 1967) used a mixed model and considered both displacements and stresses as primary variables. The ease with which a continuous

*For convergence requirements, see Section 2.3.1.

displacement pattern can be prescribed (compared to the alternative approach of forming an equilibrating internal force field) has aided the widespread use and development of the finite element displacement approach. The displacement model and the stiffness analysis are employed in the present study.

2.2 Finite Element Displacement Approach

The displacement formulation involves derivation of the stiffness matrix of each individual element. The stiffness matrix of the entire assembled structure is then obtained by the direct stiffness method. This matrix, along with the prescribed displacement boundary conditions and loads, is used for the solution of displacements and stresses.

2.2.1 Element Analysis

The basic steps for derivation of the element stiffness matrix are:

a. Express the internal displacements $\{U\}$ of the element in terms of displacement functions $\phi(x, y, z)$, and generalized coordinates $\{q\}$

$$\{U\} = [\phi]\{q\} \tag{2.1}$$

where

$$\{U\} = \begin{Bmatrix} u(x, y, z) \\ v(x, y, z) \\ w(x, y, z) \end{Bmatrix}$$

is a displacement vector consisting of displacement components u, v, w, referenced to the rectangular cartesian coordinate system (x, y, z).

b. Express the nodal displacements $\{U^a\}$ in terms of generalized coordinates $\{q\}$:

$$\{U^a\} = [A]\{q\} \tag{2.2}$$

Here $\{U^a\} = \{U_i(x, y, z)\}$ and

$$U_i(x, y, z) = U(x_i, y_i, z_i) \qquad i = 1, 2, \ldots, n$$

are the displacements at node "i" and n is the number of nodes. Coefficients of matrix $[A]$ are functions of nodal coordinates (x_i, y_i, z_i). Conversely,

$$\{q\} = [A]^{-1}\{U^a\} \tag{2.3}$$

c. Evaluate strains $\{\epsilon\}$ from the assumed displacement. Use the strain-displacement relationship

$$\{\epsilon\} = \mathfrak{L}\{U\} = [G(x, y, z)]\{q\}$$

$$= [G][A^{-1}]\{U^a\}$$

or

$$\{\epsilon\} = [B]\{U^a\} \tag{2.4}$$

where $\mathfrak{L}$ is a differential operator and $[G] = \mathfrak{L}[\phi]$.

d. Compute stresses $\{\sigma\}$ using the elasticity matrix $[D]$ established from the properties of the material

$$\{\sigma\} = [D]\{\epsilon\} \tag{2.5}$$

or

$$\{\sigma\} = [D][B(x, y, z)]\{U^a\} \tag{2.6}$$

e. The condition for equilibrium is obtained by applying the principle of minimum potential energy

$$\delta(w_i + w_e) = 0 \tag{2.7}$$

During a virtual displacement $U^a \rightarrow \delta U^a$, the internal work done is

$$\delta w_i = \delta \int \{\epsilon\}^T \{\sigma\}\, d\,(\text{Vol})$$

$$= \{\delta U^a\}^T \int [B]^T [D][B]\, d\,(\text{Vol})\, \{U^a\}$$

or

$$\delta w_i = \{\delta U^a\}^T [K_e]\{U^a\} \tag{2.8}$$

The external work done by a set of nodal forces $\{P^a\}$ corresponding to the nodal displacements $\{U^a\}$ is

$$\delta w_e = -\{\delta U^a\}^T \{P^a\} \tag{2.9}$$

Substitute into Eq. (2.7). Since the virtual displacements δU^a are arbitrary, we have

$$[K_e]\{U^a\} = \{P^a\} \tag{2.10}$$

where

$$[K_e] = \int [B]^T [D][B]\, d(\text{Vol})$$

$$= [A^{-1}]^T \int [G]^T [D][G]\, d(\text{Vol})\, [A^{-1}] \tag{2.11}$$

expresses the nodal force-displacement relation and is the desired element stiffness matrix.

f. Establish the load generalization. Generally loads are distributed. Concentrated loads at nodes represent special cases. In the finite element context where all the forces can be transmitted only through the prescribed network of nodes, we need to compute the equivalent concentrated nodal loads $\{P^a\}$ for the actual distributed loading $p(x, y, z)$. Equivalence is based on the work done during a virtual displacement consistent with the assumed displacement field $U(x, y, z)$. Since

$$\delta w_e = -\delta \int \{U\}^T \{p\}\, d\,(\text{Vol})$$

Eq. (2.9) gives the equivalent loading vector

$$\{P_d^a\} = [A^{-1}]^T \int [\phi]^T \{p\}\, d(\text{Vol})$$

or

$$\{P_d^a\} = \int [N]^T \{p\}\, d(\text{Vol}) \tag{2.12}$$

The vector $\{P_d^a\}$ is often called the generalized load of element "a" and N is known as shape function. Thus a normal load can produce not only parallel nodal forces but also couples, or their equivalent, and these will depend on the displacement assumption $U(x, y, z)$ used.

2.2.2 Structural Analysis (by Direct Stiffness Method)

The real elastic structure is now represented by a finite number of small, discrete elements. Once their approximation behaviors, identified by their individual stiffness matrices $[K^a]$, have been established, the stiffness matrix $[K]$ for the complete structure is obtained by the proper summation of each element stiffness matrix in the structure. This is done conceptually by joining successive elements at their adjoining nodes and requiring that the conditions of compatibility of displacements and equilibrium of forces have been satisfied at every node throughout the structure. A set of simultaneous equations is generated in terms of displacement parameters $\{U\}$. For compatibility, express in matrix form:

$$\{U^a\} = [L^a]\, \{U\} \tag{2.13}$$

where $\{U^a\}$ is the column vector of element nodal displacements,

$\{U\}$ is the column vector of nodal displacements for the entire structure,

$[L^a]$ is the localizing matrix for element "a" relating the displacements of the element to those of the structure and is with respect to a set of nodal numbering system, and for equilibrium,

$$[K]\{U\} = \{P\} \tag{2.14}$$

Note that

$$[K] = \sum_{a=1}^{M} [L^a]^T [K^a] [L^a]$$

where $[K]$ is the structure stiffness matrix,

$[K^a]$ is the element stiffness matrix,

M is the total number of element in the structure, and

$\{P\}$ is the structure loading vector and is equal to

$$\{P\} = \sum_{a=1}^{M} [L^a]^T \{P^a\}$$

The assembly process is also known as the direct stiffness method. Matrix notation is convenient, general, and applicable to a wide range of structural problems. In practice, further processing takes into consideration the fact that the structure stiffness matrix is banded, symmetric, and sparsely populated. This allows a significant advance (Tezcan, 1966; Irons, 1970; and Jennings and Tuff, 1971) in computational efficiency (the number of arithmetic operations and data storage can often be drastically reduced).

2.3 Characteristics of Finite Element Analysis

2.3.1 Convergence Criteria

The trace of element characteristics follows a prescribed path once the shape function N has been defined. It describes the displacement field within the element in terms of the nodal parameters. The shape function matrix $[N]$ can be determined from Eq. (2.1), (2.3), and (2.12):

$$\{U\} = [N]\{U_i\} \tag{2.15}$$

and

$$[N] = [\phi][A]^{-1} \tag{2.16}$$

The shape functions are usually taken as polynomial expressions in terms of either the global coordinates (x, y, z) or the local coordinate system (ξ, η, ζ).

The reliability of a solution by the finite element method is indicated by the fact that the approximate numerical results come increasingly closer to the correct value as the finite element mesh is repeatedly subdivided into finer and finer meshes (Tong and Pian, 1967 and deAranetes, 1968).

The requirements of convergence fall into two categories: (a) completeness of the displacement field U and (b) interelement continuity. First, the completeness requirement ensures that the energy represented by the functional (such as the integral of potential energy) includes a constant energy state for each element. If this is satisfied, the true energy state of the entire structure can be represented, in the limit, as the mesh layout is refined. Mathematically, this requires that all uniform states of the displacement variables U must be included in each element. This results in the equivalent requirement that "constant strain" and "rigid body" states must be included.

The second requirement is that of continuity between adjacent elements. In order for the functional at the element interface to remain finite, it has been considered necessary to provide continuity of displacement variable U and its derivatives to one order lower than the order of the highest derivative of that variable in the energy integral. The success of certain nonconforming elements, however, has led to a reevaluation of this requirement. Bazeley et al. (1965) suggested a less stringent condition, namely, that reduced continuity must be maintained for the state of constant energy in the region concerned.

2.3.2 Elements of Arbitrary Shapes

Linear elasticity problems can be readily solved by a finite element technique that employs simple triangular or tetrahedral elements. The displacement fields for those elements have often taken the form of polynomials of variables in cartesian coordinates. That is

$$\{U\} = [\phi(x, y, z)]\,\{q\}$$

or

$$\left.\begin{aligned} u\ (x,y,z) &= q_{11} + q_{12}x + q_{13}y + q_{14}z + \cdots \\ v\ (x,y,z) &= q_{21} + q_{22}x + q_{23}y + q_{24}z + \cdots \\ w(x,y,z) &= q_{31} + q_{32}x + q_{33}y + q_{34}z + \cdots \end{aligned}\right\} \tag{2.17}$$

In the case of the constant strain element, the criteria of convergence can be satisfied when the assumed displacement functions ϕ include the complete first order polynomial $[1, x, y, z]$

in addition to the basic requirement of compatibility* of nodal parameters. Additional nodal variables can be introduced to give better element performance with improved representation of the actual deformation. Selective higher order terms are to be added to ensure the continuity of displacement U across the interelement boundary.

The popularity of polynomial displacement expansions $\phi(x, y, z)$ lies in the fact that matrix operation is straightforward and stiffness coefficients can be readily obtained in explicit form by a standard procedure (see Section 2.2). It becomes obvious in application, however, that the property of a displacement variable $U(x, y, z)$ should have no preferred directions. This requires that the complete polynomial expansion be used in the displacement assumption. To implement this, a simple procedure can be found to determine shape functions $[N]$ and displacement patterns $\{U\}$; the tacit assumption is that matrix $[A]$ (Eq. (2.14)) is invertible and that the shape function is correct simply because there is a "match" between the monomials present in the displacement expansion and the corresponding nodal variables (Dunne, 1968). However, this approach is not generally valid.

Complete polynomials for a compatible displacement field are well suited for the triangular and tetrahedral family of elements, but the use of complete polynomial displacement expansion may lead to algebraic difficulties in the case of arbitrary quadrilaterals, hexahedra, and plate bending elements. On the other hand, it is possible to formulate a compatible element that possesses rotational invariance via direct formulation by employing a coordinate transformation (mapping) or a natural coordinate system (Irons, 1966 and Ergatoudis et al., 1968). Additional kinematic capabilities can be incorporated by introducing intermediate nodal parameters (Zienkiewicz et al., 1971). This is another desirable feature of isoparametric elements. A more detailed description will be given in the following chapters.

*This ensures the minimum continuity requirements of displacement at element interface.

CHAPTER 3

ELASTIC ANALYSIS IN THREE-DIMENSIONAL SPACE

3.1 Introduction to Solid Elements

For many years, considerable effort has been devoted to solving problems in the realm of three-dimensional elasticity. The classical, analytical approach for solving a set of governing differential equations derived from a three-dimensional theory is available only for bodies with simple geometric forms and for restricted boundary conditions and limited loading cases. Different numerical procedures (finite difference methods etc.) have been applied to solve these differential equations; their success is generally still limited to special geometric shapes and, at most, is of occasional academic interest. Now that the finite element method has been eminently successful in dealing with certain complex problems such as plane stress and plate bending, it has perhaps even greater potential for the solution of three-dimensional problems.

The approach envisioned here is based on a full three-dimensional analysis and is completely general in nature. It will be shown that the solid elements used in the present study are capable of correctly representing the behavior of a beam, plate, shell, or any of the varied aspects of structural components.

Because the tetrahedron-shaped element (Fig. 3.1) has simplicity and flexibility, it was a natural choice for the earlier development of solid elements (Gallagher et al., 1962). The element shape is defined by four arbitrary, noncoplanar points in space. Any topography may therefore be represented with sufficient accuracy by some assembly of these tetrahedron elements. The drawback to this element shape is the large number of element inputs required to describe a complex surface. The mesh is difficult to visualize, and the amount of data to be processed as well as the number and the bandwidth of the system of equations generated tend to exceed the storage capacity of the average size computer and call for excessive computer times. To reduce these constraints, isoparametric elements, including those with a curved face, have been introduced. These elements represent a great improvement over the tetrahedron because they enable bodies with curved boundaries to be treated with a limited number of elements.

3.2 The Basic Solid Element

A comparison (Clough, 1969) of the performance of solid finite elements has shown that isoparametric hexahedron elements are distinctly superior to any tetrahedron assemblages, both in terms of the properties of the individual elements and their application to analyze real structural systems. Isoparametric elements have the additional advantage of isotropy. It is evident, then, that a general-purpose, three-dimensional finite element analysis program should be constructed around the isoparametric hexahedron element family.

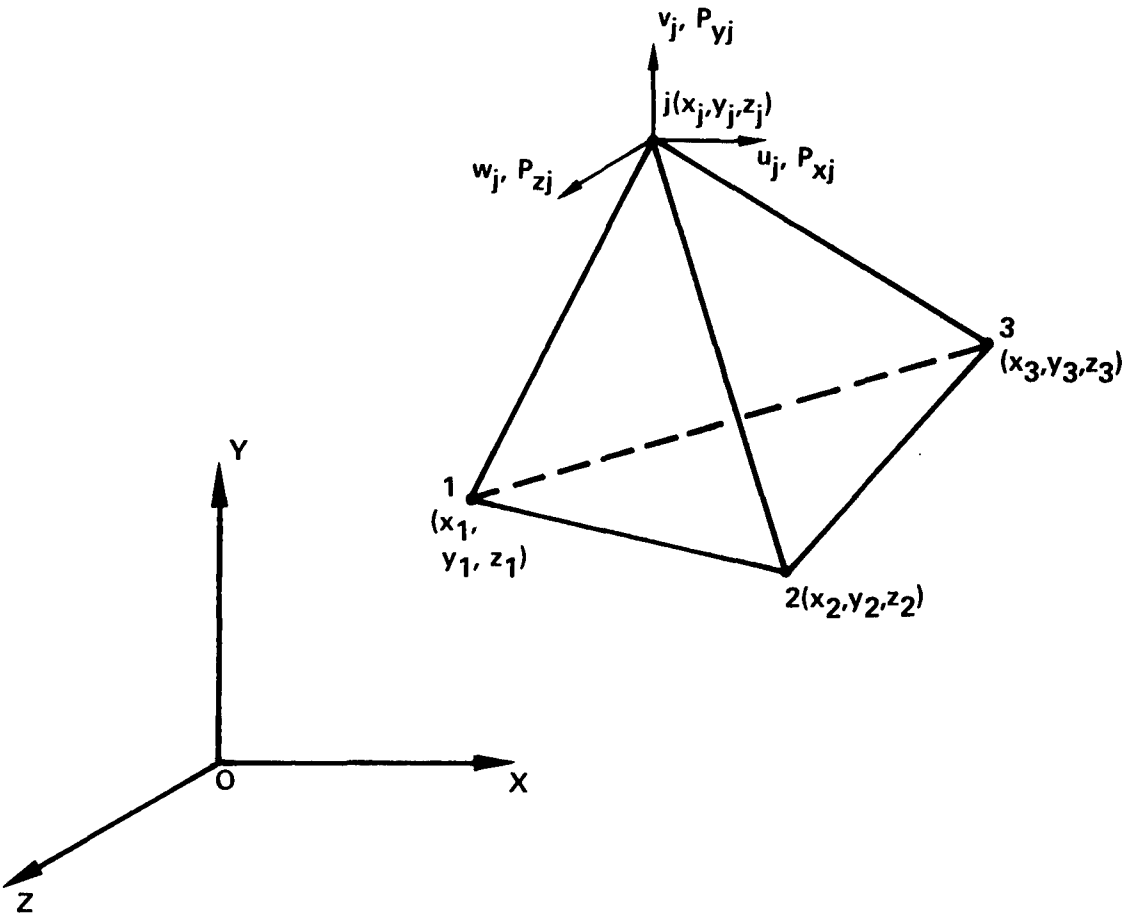

X,Y,Z ARE GLOBAL RECTANGULAR COORDINATES

$$\left\{ \bar{P}_j = \begin{matrix} P_{xj} \\ P_{yj} \\ P_{zj} \end{matrix} \right\}$$ A NODAL FORCE VECTOR AT NODE j

$$\left\{ \bar{U}_j = \begin{matrix} u_j \\ v_j \\ w_j \end{matrix} \right\}$$ A DISPLACEMENT VECTOR AT NODE j

Figure 3.1 Tetrahedron, a solid element and rectangular coordinate system

3.2.1 The Isoparametric Displacement Field

Consider the general family of elements with six faces, the hexahedron family. The use of an appropriate natural coordinate system greatly simplifies the formulation of the element stiffness matrix for some very complex members of this family. These coordinate lines are generally curved in space and follow only the interface topology of an individual element. As shown in Fig. 3.2 (and later in Fig. 3.3) for instance, ξ, η, ζ are natural coordinates; each coordinate axis is associated with a pair of opposing faces which are given the coordinate values of ± 1. In their local reference frame, the elements take on the image of a 2 by 2 by 2 cube, whereas in the real cartesian coordinate system (x, y, z), they can be any arbitrarily warped, six-sided solids.

We begin with the linear hexahedron that has the eight corner nodes shown in Fig. 3.2 and introduce a polynomial expansion of the displacement component in rectangular cartesian coordinates

$$u = u(x, y, z)$$
$$= q_{11} + q_{12}x + q_{13}y + q_{14}z + q_{15}xy + q_{16}yz + q_{17}zx + q_{18}xyz$$

or

$$u = [\phi_i(x, y, z)]\,\{q_{1i}\} \qquad i = 1, 2, \ldots, 8 \tag{3.1}$$

It will be demonstrated (Section 3.2.4) that the criteria of convergence are satisfied. Without losing generality, we can consider an element in the form of a rectangular parallelopiped with the origin located at centroid and the coordinate planes as planes of symmetry. By evaluating nodal displacement parameters at the appropriate coordinates, i.e., $u_i = u(x_i, y_i, z_i)$, etc., we can assemble the nodal displacement vector, for instance, $\{u_i\} = [A_{ij}]\,\{q_{1i}\}$, etc. From Eq. (2.15), we obtain by identity

$$u = N_1 u_1 + N_2 u_2 + \ldots\ldots + N_8 u_8$$
$$= \sum_{i=1}^{8} N_i u_i \tag{3.2}$$

and

$$N_i = \frac{1}{8}(1 + x_i x)(1 + y_i y)(1 + z_i z) \qquad i = 1, \ldots\ldots, 8 \tag{3.3}$$

where $x_i = \pm 1$, $y_i = \pm 1$, and $z_i = \pm 1$ are coordinate values at node i.
Here, $N_i(x, y, z)$ is known as the shape function, or interpolation function, such that it takes on unit value at the indexing node (i) and is zero at all other nodes. These interpolation functions are readily developed simply by writing them as the product of the equations of the lines or surfaces through all the remaining nodes. This can frequently be done by direct inspection.

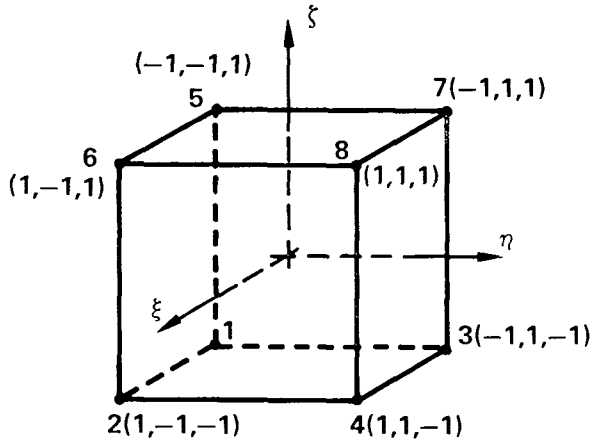

Figure 3.2a Local coordinates

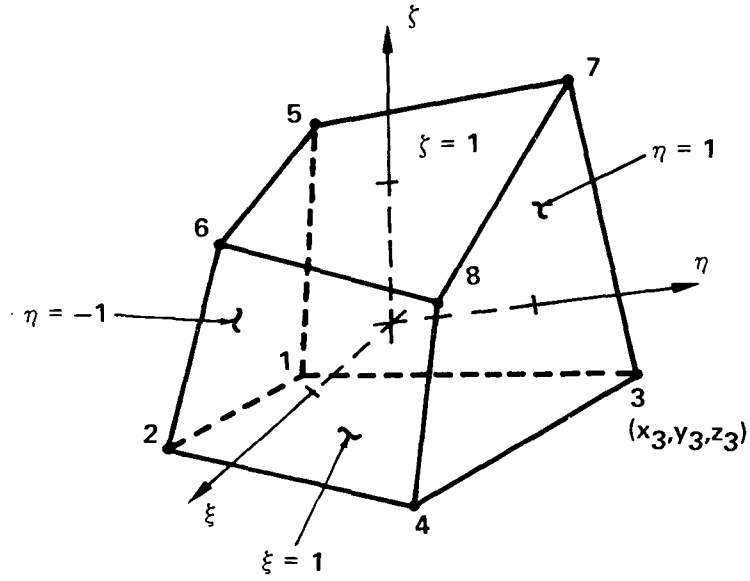

Figure 3.2b Cartesian coordinates

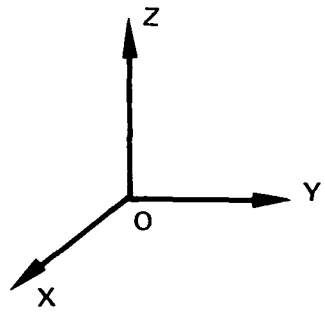

Figure 3.2 An eight-node generalized hexahedron

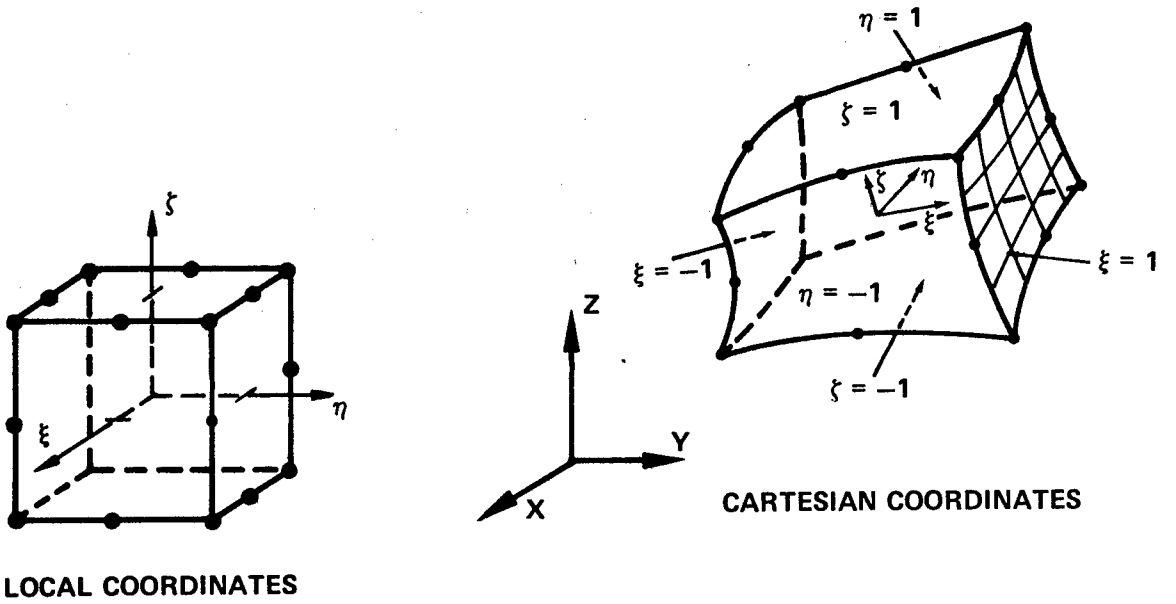

Figure 3.3a Quadratic element (20 nodes)

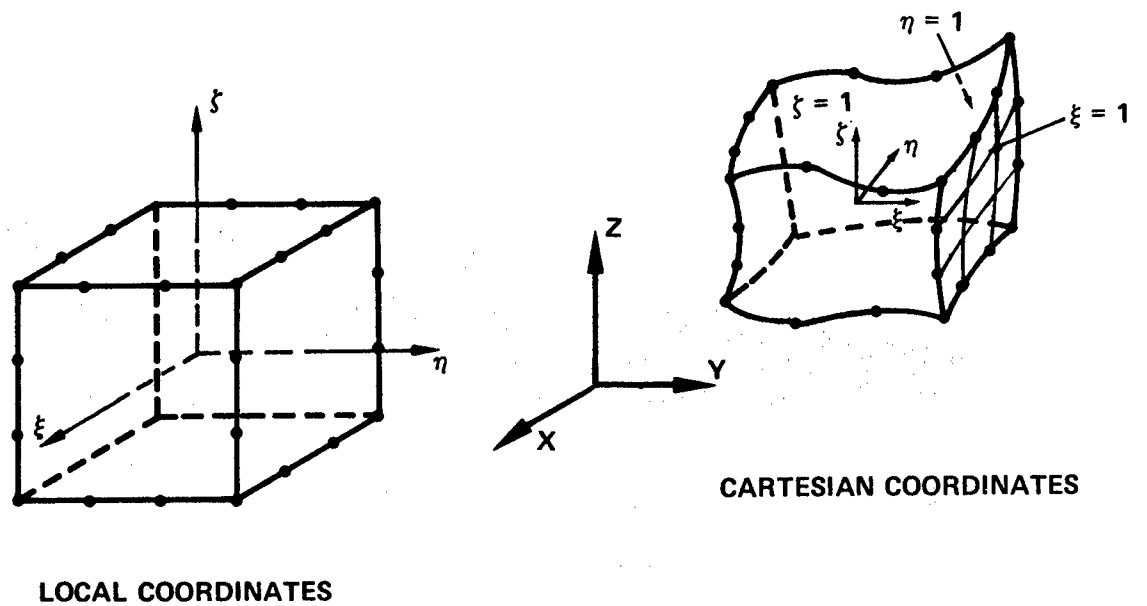

Figure 3.3b Cubic element (32 nodes)

Figure 3.3 Refined curved hexahedron

Proceeding in the same fashion, we can define other displacement components v and w as

$$\left.\begin{aligned} v &= v(x, y, z) \\ &= \sum_{i=1}^{8} N_i v_i \end{aligned}\right\}$$

and

$$\left.\begin{aligned} w &= \sum_{i=1}^{8} N_i w_i \qquad i = 1, 2, \ldots\ldots, 8 \end{aligned}\right\} \tag{3.4}$$

where the shape function N_i takes on the same form, Eq. (3.3).

As mentioned earlier, an element of prismatic shape has rather limited appeal in dealing with practical problems. This geometric constraint can be relaxed by a suitable coordinate transformation commonly known as mapping. Consider, for instance, an element of Fig. 3.2a being distorted geometrically to a shape shown in Fig. 3.2b. In other words, map the element into x, y, z-coordinate space such that a typical node i moves to a position (x_i, y_i, z_i). A relation of the forms

$$\left.\begin{aligned} x &= \sum_i N_i x_i \\ y &= \sum_i N_i y_i \\ z &= \sum_i N_i z_i \qquad i = 1, 2, \ldots, n \end{aligned}\right\} \tag{3.5}$$

(where n = NNPE, the number of nodes per element) gives $x = x(\xi, \eta, \zeta), \ldots$ and can be used to define the mapping. Here, the shape functions

$$\begin{aligned} N_i &= N_i(\xi, \eta, \zeta) \\ &= \frac{1}{8}(1 + \xi_i \xi)(1 + \eta_i \eta)(1 + \zeta_i \zeta) \end{aligned} \tag{3.6}$$

are written in terms of the local dimensionless coordinates ξ, η, and ζ. Following the nodal ordering number as given in Fig. 3.2a, we have the local nodal coordinates

$$\begin{aligned} (\xi_i, \eta_i, \zeta_i) = &(-1, -1, -1), (\ 1, -1, -1), \\ &(-1,\ \ 1, -1), (\ 1,\ \ 1, -1), \\ &(-1, -1,\ \ 1), (\ 1, -1,\ \ 1), \\ &(-1,\ \ 1,\ \ 1), (\ 1,\ \ 1,\ \ 1), \\ &\text{for } i = 1, 2, \ldots, 8 \end{aligned}$$

The displacements u, v, w can be interpolated in the same manner; hence $u = u(\xi, \eta, \zeta)$, etc. Again, we write

$$\left.\begin{aligned} u &= \sum_i N_i u_i \\ v &= \sum_i N_i v_i \\ w &= \sum_i N_i w_i \qquad i = 1, \ldots, n \end{aligned}\right\} \tag{3.7}$$

The shape functions $N_i(\xi_i, \eta_i, \zeta_i)$ used here are identical to those employed in the coordinate definition and in such cases the formulation has been termed "isoparametric" (Zienkiewicz et al., 1969). With the position and the displacement of a material point in an element space defined, a family of isoparametric elements can be formed routinely.

3.2.2 Numerical Calculation of Stiffness Matrix

Consider an element stiffness matrix, Eq. (2.11),

$$[K_e] = \iiint_{\substack{\text{volume of} \\ \text{element}}} [B]^T [D] [B] \, dx \, dy \, dz$$

To integrate it, we need to evaluate the integrand $[B]^T[D][B] = G(x, y, z)$ in terms of independent space variables (x, y, z). The algebraic expression of G involves the strain matrix $[B]$ which is derived from the definition of strain and consists of appropriate first derivatives of the displacements. For a solid element, we have

$$\{\epsilon\} = \begin{Bmatrix} \epsilon_x \\ \epsilon_y \\ \epsilon_z \\ \gamma_{xy} \\ \gamma_{yz} \\ \gamma_{zx} \end{Bmatrix} = \begin{bmatrix} \dfrac{\partial N_i}{\partial x} & 0 & 0 \\ 0 & \dfrac{\partial N_i}{\partial y} & 0 \\ 0 & 0 & \dfrac{\partial N_i}{\partial z} \\ \dfrac{\partial N_i}{\partial y} & \dfrac{\partial N_i}{\partial x} & 0 \\ 0 & \dfrac{\partial N_i}{\partial z} & \dfrac{\partial N_i}{\partial y} \\ \dfrac{\partial N_i}{\partial z} & 0 & \dfrac{\partial N_i}{\partial x} \end{bmatrix} \begin{Bmatrix} u_i \\ v_i \\ w_i \end{Bmatrix} \qquad i = 1, 2, \ldots, \text{NNPE} \tag{3.8}$$

$$= \underset{6 \times 24}{[B]} \quad \underset{24 \times 1}{\{U^a\}} \qquad \text{for NNPE} = 8$$

It is clear then the expression G is algebraicly complex and its integration presents a formidable task since the shape functions $N_i = N_i(\xi, \eta, \zeta)$ are established in local rather than global coordinates. In order to proceed further, it is desirable to introduce an auxiliary expression $g(\xi, \eta, \zeta)$ in terms of local coordinates (ξ, η, ζ).

The Jacobian of the transformation is defined as $J = \partial(x, y, z)/\partial(\xi, \eta, \zeta)$ and the matrix is

$$[J] = \begin{bmatrix} \frac{\partial x}{\partial \xi} & \frac{\partial y}{\partial \xi} & \frac{\partial z}{\partial \xi} \\ \frac{\partial x}{\partial \eta} & \frac{\partial y}{\partial \eta} & \frac{\partial z}{\partial \eta} \\ \frac{\partial x}{\partial \zeta} & \frac{\partial y}{\partial \zeta} & \frac{\partial z}{\partial \zeta} \end{bmatrix} \tag{3.9}$$

$$= \begin{bmatrix} \frac{\partial N_1}{\partial \xi} & \frac{\partial N_2}{\partial \xi} & \cdots & \frac{\partial N_8}{\partial \xi} \\ \frac{\partial N_1}{\partial \eta} & \frac{\partial N_2}{\partial \eta} & \cdots & \frac{\partial N_8}{\partial \eta} \\ \frac{\partial N_1}{\partial \zeta} & \frac{\partial N_2}{\partial \zeta} & \cdots & \frac{\partial N_8}{\partial \zeta} \end{bmatrix} \begin{bmatrix} x_1 & y_1 & z_1 \\ x_2 & \cdot & \cdot \\ x_3 & \cdot & \cdot \\ \cdot & \cdot & \cdot \\ \cdot & \cdot & \cdot \\ \cdot & \cdot & \cdot \\ \cdot & \cdot & \cdot \\ x_8 & y_8 & z_8 \end{bmatrix}$$

where
$$\left.\begin{aligned} \frac{\partial N_i}{\partial \xi} &= \frac{\xi_i}{8}(1 + \eta_i \eta)(1 + \zeta_i \zeta) \\ \frac{\partial N_i}{\partial \eta} &= \frac{(1 + \xi_i \xi)}{8}(\eta_i)(1 + \zeta_i \zeta) \\ \frac{\partial N_i}{\partial \zeta} &= (1 + \xi_i \xi)(1 + \eta_i \eta)\frac{\zeta_i}{8}, \quad i = 1, 2, \ldots\ldots, 8 \end{aligned}\right\}$$

Following the standard rule of partial differentiation, for example,

$$\frac{\partial N_i}{\partial x} = \frac{\partial N_i}{\partial \xi}\frac{\partial \xi}{\partial x} + \frac{\partial N_i}{\partial \eta}\frac{\partial \eta}{\partial x} + \frac{\partial N_i}{\partial \zeta}\frac{\partial \zeta}{\partial x}, \text{ etc.,}$$

we have

$$\begin{bmatrix} \frac{\partial N_1}{\partial x} & \frac{\partial N_2}{\partial x} & \cdots\cdots & \frac{\partial N_8}{\partial x} \\ \frac{\partial N_1}{\partial y} & \frac{\partial N_2}{\partial y} & \cdots\cdots & \frac{\partial N_8}{\partial y} \\ \frac{\partial N_1}{\partial z} & \frac{\partial N_2}{\partial z} & \cdots\cdots & \frac{\partial N_8}{\partial z} \end{bmatrix} = [J]^{-1} \begin{bmatrix} \frac{\partial N_1}{\partial \xi} & \frac{\partial N_2}{\partial \xi} & \cdots\cdots & \frac{\partial N_8}{\partial \xi} \\ \frac{\partial N_1}{\partial \eta} & \frac{\partial N_2}{\partial \eta} & \cdots\cdots & \frac{\partial N_8}{\partial \eta} \\ \frac{\partial N_1}{\partial \zeta} & \frac{\partial N_2}{\partial \zeta} & \cdots\cdots & \frac{\partial N_8}{\partial \zeta} \end{bmatrix} \tag{3.10}$$

Now the values of $\partial N_i/\partial \xi$, $\partial N_i/\partial \eta$, $\partial N_i/\partial \zeta$, and matrix $[J]$ can be calculated point by point in an element subregion. The matrix $[B]$ can be readily assembled. The components of strains everywhere within the elastic element are now defined in terms of nodal deflections $\{U^a\}$ as parameters.

The integration in terms of local coordinate variables (ξ, η, ζ) can be executed in a simple format, that is,

$$\begin{aligned} [K_e] &= \iiint_{\text{Vol}} G(x, y, z)\, dx\, dy\, dz \\ &= \int_{-1}^{1}\int_{-1}^{1}\int_{-1}^{1} [B]^T [D] [B] |J|\, d\xi\, d\eta\, d\zeta \end{aligned} \tag{3.11}$$

and

$$g(\xi, \eta, \zeta) = [B]^T [D] [B] |J(\xi, \eta, \zeta)| \tag{3.12}$$

For all practical purposes the integration performed numerically (Hammer, 1959) as a summation of quadratures is a simple matter on a digital computer. Here,

$$[K_e] = \sum_{iz=1}^{NPZ} \sum_{iy=1}^{NPY} \sum_{ix=1}^{NPX} g(\xi_{ix}, \eta_{iy}, \zeta_{iz})\, H_{ix}\, H_{iy}\, H_{iz} \tag{3.13}$$

If the Legendre-Gauss quadrature formula is employed, ξ_{ix}, η_{iy}, ζ_{iz} correspond to the abscissas for the zeros of the Legendre polynomial of degree NPX, . . . etc. NPX, NPY, NPZ are the number of integration points to be used in each linear quadrature space. The values of ξ_{ix} and its weight factors H_{ix} can be found in standard quadrature tables (Stroud and Secrest, 1966).

It is worth noting that the stiffness matrix $[K_e]$ is symmetric and that the strain matrix $[B]$ and the elasticity matrix $[D]$ include many zero terms, or null submatrices. A substantial reduction in arithematic operation is possible by carrying the algebraic processing a little further. First, the strain matrix $[B]$

$$[B]_{6\times 24} = \left[\begin{array}{c|c|c} B_{11} & B_{12} & B_{13} \\ \hline B_{21} & B_{22} & B_{23} \end{array}\right] = \begin{bmatrix} B1 & 0 & 0 \\ 0 & B2 & 0 \\ 0 & 0 & B3 \\ B2 & B1 & 0 \\ 0 & B3 & B2 \\ B3 & 0 & B1 \end{bmatrix} \tag{3.14}$$

can be expressed in terms of submatrices:

$$\left.\begin{aligned} B1\,(8) &= \left[\frac{\partial N_1}{\partial x}, \frac{\partial N_2}{\partial x}, \ldots\ldots, \frac{\partial N_8}{\partial x}\right] \\ B2\,(8) &= \left[\frac{\partial N_1}{\partial y}, \frac{\partial N_2}{\partial y}, \ldots\ldots, \frac{\partial N_8}{\partial y}\right] \\ B3\,(8) &= \left[\frac{\partial N_1}{\partial z}, \frac{\partial N_2}{\partial z}, \ldots\ldots, \frac{\partial N_8}{\partial z}\right] \end{aligned}\right\} \tag{3.15}$$

Second, the elasticity matrix $[D]$ which relates the stresses and strains, Eq. (2.5), can include any anisotropic properties and can be prescribed as a function of spatial distribution, e.g., $D_{ij}(x, y, z)$. The $[D]$ matrix is symmetric and can be written as:

$$[D\,(6,6)] = \begin{bmatrix} D_m & 0 \\ 0 & D_s \end{bmatrix} \tag{3.16}$$

where

$$[D_m] = \begin{bmatrix} D_{11} & D_{12} & D_{13} \\ & D_{22} & D_{23} \\ \text{SYM} & & D_{33} \end{bmatrix}$$

$$[D_s] = \begin{bmatrix} D_{44} & 0 & 0 \\ & D_{55} & 0 \\ \text{SYM} & & D_{66} \end{bmatrix}$$

[0] is a 3 by 3 null matrix. For this study, we shall consider an isotropic material. In that case

$$[D_m] = DK \begin{bmatrix} AA & BB & BB \\ & AA & BB \\ \text{SYM} & & AA \end{bmatrix}, \qquad [D_s] = DK \begin{bmatrix} CC & 0 & 0 \\ & CC & 0 \\ \text{SYM} & & CC \end{bmatrix}$$

where $DK = \dfrac{E}{(1+\nu)(1-2\nu)}$

$AA = 1 - \nu$

$BB = \nu$

$CC = (1-2\nu)/2$

E and ν are the usual elastic constants, Young's modulus and Poisson's ratio, respectively.

At this stage, the calculation of element stiffness matrix can be broken into parts. Terms that contain null factors can be screened, large number of intermediate calculations can be eliminated, and economy in computer time can be realized. For instance:

$$\underset{24\times 24}{[K_e(i,j)]} = \int_{-1}^{1}\int_{-1}^{1}\int_{-1}^{1} \underset{24\times 6}{[B(m,i)]^T} \underset{6\times 6}{[D(m,n)]} \underset{6\times 24}{[B(n,j)]} |J|\, d\xi\, d\eta\, d\zeta \tag{3.17}$$

or

$$[K_e] = \begin{bmatrix} \underset{\sim}{K}(r,s) & \underset{\sim}{K}(r,s+8) & \underset{\sim}{K}(r,s+16) \\ & \underset{\sim}{K}(r+8,s+8) & \underset{\sim}{K}(r+8,s+16) \\ \text{SYMM} & & \underset{\sim}{K}(r+16,s+16) \end{bmatrix} \tag{3.18}$$

$$r, s = 1, 2, \ldots\ldots, 8$$

A typical submatrix, for example, is

$$\underset{\sim}{K}(r,s) = \int_{-1}^{1}\int_{-1}^{1}\int_{-1}^{1} [B_{11}^T D_m B_{11} + B_{21}^T D_s B_{21}] |J|\, d\xi\, d\eta\, d\zeta \tag{3.19}$$

This can be reduced to

$$\int_{-1}^{1}\int_{-1}^{1}\int_{-1}^{1} [B1(r)\, D_{11}\, B1(s) + \{B2(r)\, D_{44}\, B2(s) + B3(r)\, D_{66}\, B3(s)\}] |J|\, d\xi\, d\eta\, d\zeta \tag{3.20}$$

Other submatrices are

$$\int_{-1}^{1}\int_{-1}^{1}\int_{-1}^{1} [B1(r)\, D_{12}\, B2(s) + B2(r)\, D_{44}\, B1(s)] |J|\, d\xi\, d\eta\, d\zeta$$

$$\int_{-1}^{1}\int_{-1}^{1}\int_{-1}^{1} [B1(r)\, D_{13}\, B3(s) + B3(r)\, D_{66}\, B1(s)] |J|\, d\xi\, d\eta\, d\zeta$$

$$\int_{-1}^{1}\int_{-1}^{1}\int_{-1}^{1} [B2(r)\, D_{22}\, B2(s) + B1(r)\, D_{44}\, B1(s) + B3(r)\, D_{55}\, B3(s)] |J|\, d\xi\, d\eta\, d\zeta$$

$$\int_{-1}^{1}\int_{-1}^{1}\int_{-1}^{1} [B2(r)\, D_{23}\, B3(s) + B3(r)\, D_{55}\, B2(s)] |J|\, d\xi\, d\eta\, d\zeta$$

$$\int_{-1}^{1}\int_{-1}^{1}\int_{-1}^{1} [B3(r)\, D_{33}\, B3(s) + B2(r)\, D_{55}\, B2(s) + B1(r)\, D_{66}\, B1(s)] |J|\, d\xi\, d\eta\, d\zeta$$

For submatrices on the diagonal, stiffness coefficients must be computed only for those terms where $s \geq r$, since advantage is taken of the symmetry of the stiffness matrix. Finally the nodal parameters can be regrouped, i.e.,

$$\{U^a\} = \{U_i\}$$

and

$$\{U_i\} = \begin{Bmatrix} u_i \\ v_i \\ w_i \end{Bmatrix} \qquad i = 1, 2, \ldots\ldots, 8$$

to expedite the assembly into the entire structural system matrix $[K]$ of Eq. (2.14).

3.2.3 Higher Order Curved Elements

In earlier developments, the boundary of a finite element was usually thought of as composed of straight edges and its geometric form completely defined by a series of corner nodes. Where an edge is curved, appropriate intermediate nodes must be specified along that edge. One intermediate point will suffice to define the shape of an edge with a simple or constant curvature. Two or more intermediate points will be required to specify the geometry of an edge with a multiple or reversed curvature.

3.2.3.1 Quadratic Curved Element. In most cases, the boundary of a complex structural shape can be closely represented by a sequence of quadratic curves or quadratic surfaces. Therefore many complicated problems can be realistically defined and solved with only a limited number of simple, discrete, curved elements. These curved elements can be readily formulated by using isoparametric concepts (Section 3.2.1). For example, by placing one midside node along each edge of an 8-node hexahedron, we obtain a 20-node element. This 20-node hexahedron is coming into widespread use and is an important tool in three-dimensional analysis (Fig. 3.3a).

For a 20-node hexahedron element with edges capable of displaying simple curvatures, we can write a displacement expansion that contains 12 terms in addition to those required for the 8-node hexahedron (Eq. (3.1)) to ensure compatibility.
Hence,

$$\begin{aligned} u_{20} &= [\phi_i(x, y, z)]\,\{a_i\} \qquad i = 1, 2, \ldots\ldots, 20 \\ &= a_1 + a_2 x + a_3 y + a_4 z + a_5 xy + a_6 yz + a_7 zx + a_8 xyz \\ &\quad + a_9 x^2 + a_{10} y^2 + a_{11} z^2 \\ &\quad + a_{12} x^2 y + a_{13} x^2 z + a_{14} y^2 x + a_{15} y^2 z + a_{16} z^2 y + a_{17} z^2 x \\ &\quad + a_{18} x^2 yz + a_{19} xy^2 z + a_{20} xyz^2 \end{aligned} \tag{3.21}$$

It is seen that the displacement is capable of a quadratic variation along any space variable, and consequently the 20-node element is often called a quadratic element.

Following the example of Section 3.2.1, we obtain immediately the shape functions for the 20-node hexahedron element:

For corner nodes $i = 1$ to 8, $\xi_i = \pm 1$, $\eta_i = \pm 1$, $\zeta_i = \pm 1$

$$N_i = \frac{1}{8}(1 + \xi_i \xi)\,(1 + \eta_i \eta)\,(1 + \zeta_i \zeta)\,(\xi_i \xi + \eta_i \eta + \zeta_i \zeta - 2) \tag{3.22}$$

For midside nodes $i = 9$ to 12, $\xi_i = \pm 1$, $\eta_i = \pm 1$, $\zeta_i = 0$

$$N_i = \frac{1}{4}(1 + \xi_i \xi)\,(1 + \eta_i \eta)\,(1 - \zeta^2)$$

and midside nodes $i = 13$ to 16, $\xi_i = \pm 1$, $\eta_i = 0$, $\zeta_i = \pm 1$

$$N_i = \frac{1}{4}(1 + \xi_i \xi)\,(1 - \eta^2)\,(1 + \zeta_i \zeta) \tag{3.23}$$

and midside nodes $i = 17$ to 20, $\xi_i = 0$, $\eta_i = \pm 1$, $\zeta_i = \pm 1$

$$N_i = \frac{1}{4}(1 - \xi^2)\,(1 + \eta_i \eta)\,(1 + \zeta_i \zeta)$$

The displacements and coordinates definition for the quadratic element follow directly Eq. (3.7) and (3.5) of the previous case. The summation will extend to all 20 nodes, i.e.

$$\begin{cases} u = \sum_i N_i\, u_i \\ v = \sum_i N_i\, v_i \\ w = \sum_i N_i\, w_i \end{cases} \qquad i = 1, 2, \ldots\ldots, 20$$

The calculation of element stiffness matrix follows the procedure outlined in Section 3.2.2. For the quadratic element, matrix $[K_e]$ is of an order of 60×60; a Fortran listing of a subroutine for computing stiffness coefficients for this element is included in the appendix.

3.2.3.2 Cubic Curved Element. By placing two intermediate nodes at the one-third and two-third points along each edge of an 8-node hexahedron, we then obtain a 32-node cubic element, Fig. 3.3. To ensure compatibility, a displacement expansion involving 32 terms can be written:

$$\begin{aligned} u_{32}(x, y, z) = u_{20}(x, y, z) &+ a_{21}x^3 + a_{22}y^3 + a_{23}z^3 \\ &+ a_{24}x^3y + a_{25}x^3z + a_{26}y^3z + a_{27}y^3x + a_{28}z^3x + a_{29}z^3y \\ &+ a_{30}x^3yz + a_{31}xy^3z + a_{32}xyz^3 \end{aligned} \tag{3.24}$$

where the first 20 terms are identical to u_{20} in Eq. (3.21).

The 32 shape functions for the cubic element can be obtained by standard procedure or by inspection (Zienkiewicz, 1971) and the 96×96 element stiffness matrix can be computed in a manner similar to those already described.

3.2.4 Practical Considerations

It is appropriate to note that the isoparametric formulation provides its elements with the quality of compatibility and the requirements of monotonic convergence.

The compatibility condition requires that the displacement along an edge between the adjacent elements be uniquely defined in terms of the displacements of the nodal points along that boundary line at any stage of loading (for example, initial and final). Eq. (3.5) and (3.7) define exactly the displacements and the coordinates along the edge of an element as functions of the nodal displacements and the nodal coordinates, respectively; thus compatibility is ensured.

A general displacement field must allow an element to undergo a rigid-body displacement without introducing strain. The constant terms in the expression for displacement (for example, Eq. (3.1)) satisfy the rigid-body translation while the linear terms satisfy the rigid-body rotation.

A state of constant strain will be represented in an element as its size decreases. This condition is again satisfied by having the complete linear expansion in the displacements (Timoshenko, 1934). The premise is proved.

The property of interelement continuity and the assurance of convergence of the solution are important considerations for element selection. In practice, good element performance invariably requires the exercise of sound judgment in locating a suitable set of nodal coordinates to describe the geometry of the individual elements when a structure is idealized. It is important to keep the element aspect ratio (i.e., the ratio of adjacent edges when an element is proportioned) from becoming excessive. Also it is essential to locate the side nodes of a curved edge close to the center of the edge and to form corner angles well under 180 deg. The rationale will become clear through an evaluation of the computational process. For instance, the numerical integration of an isoparametric element will involve

calculation of the Jacobian of the coordinate transformation, or the functional determinant $|J| = \left|\frac{\partial(x, y, z)}{\partial(\xi, \eta, \zeta)}\right|$. To ensure that the mapping is unique and that there is a one to one correspondence of coordinates (x, y, z) and (ξ, η, ζ), it is necessary that the Jacobian determinant does not change sign in the element space (which implies $|J| \neq 0$).

Now note that

$$|J| = \begin{vmatrix} \frac{\partial x}{\partial \xi} & \frac{\partial y}{\partial \xi} & \frac{\partial z}{\partial \xi} \\ \frac{\partial x}{\partial \eta} & \frac{\partial y}{\partial \eta} & \frac{\partial z}{\partial \eta} \\ \frac{\partial x}{\partial \zeta} & \frac{\partial y}{\partial \zeta} & \frac{\partial z}{\partial \zeta} \end{vmatrix} = \begin{vmatrix} \bar{P}_\xi^T \\ \bar{P}_\eta^T \\ \bar{P}_\zeta^T \end{vmatrix} \tag{3.25}$$

where $\bar{P}_\xi$, $\bar{P}_\eta$, $\bar{P}_\zeta$ are vectors tangent to local coordinate (ξ, η, ζ) lines (Fig. 3.4). From the standard expression

$$\begin{aligned} d\,(\text{Vol}) &= dx\, dy\, dz \\ &= |J|\, d\xi\, d\eta\, d\zeta \end{aligned} \tag{3.26}$$

hence $|J| = \lim \left|\frac{\Delta \text{ Vol } xyz}{\Delta \text{ Vol } \xi\eta\zeta}\right|$. Therefore, the Jacobian provides a quantitative measure by which the admissibility of an element geometry can be evaluated. This is a useful guide in selecting the appropriate structural idealization for element application. (Since $|J| = \bar{P}_\xi \cdot \bar{P}_\eta \times \bar{P}_\zeta$, the Jacobian is viewed as a scalar triple product, and numerically it equals the volume of a parallelopiped with opposing sides parallel to the vector triplet $\bar{P}_\xi$, $\bar{P}_\eta$, $\bar{P}_\zeta$.)

3.3 Specialization

3.3.1 Load Matrix for a Prescribed Pressure

It is often a tedious task to calculate the load on the surface of a complex structure due to a distributed pressure. The difficulty arises from the lack of a simple practical means to describe a design surface. However, with the evolution associated with the isoparametric curved element formulation, such a surface can be numerically defined and load calculation evaluated.

In a finite element system, the layout of the element mesh pattern that represents a structure depends on the manner in which the loads are to be carried. As a rule, loads are prescribed only at the nodal points and in the directions corresponding to displacement components defined in the global coordinates X, Y, and Z. Sometimes "statically equivalent" loads are used as an expedient computation. For correct solutions especially when the details of local stress distribution are desired, the load calculations should follow the procedure outlined in Section 2.2.1. An example is given here.

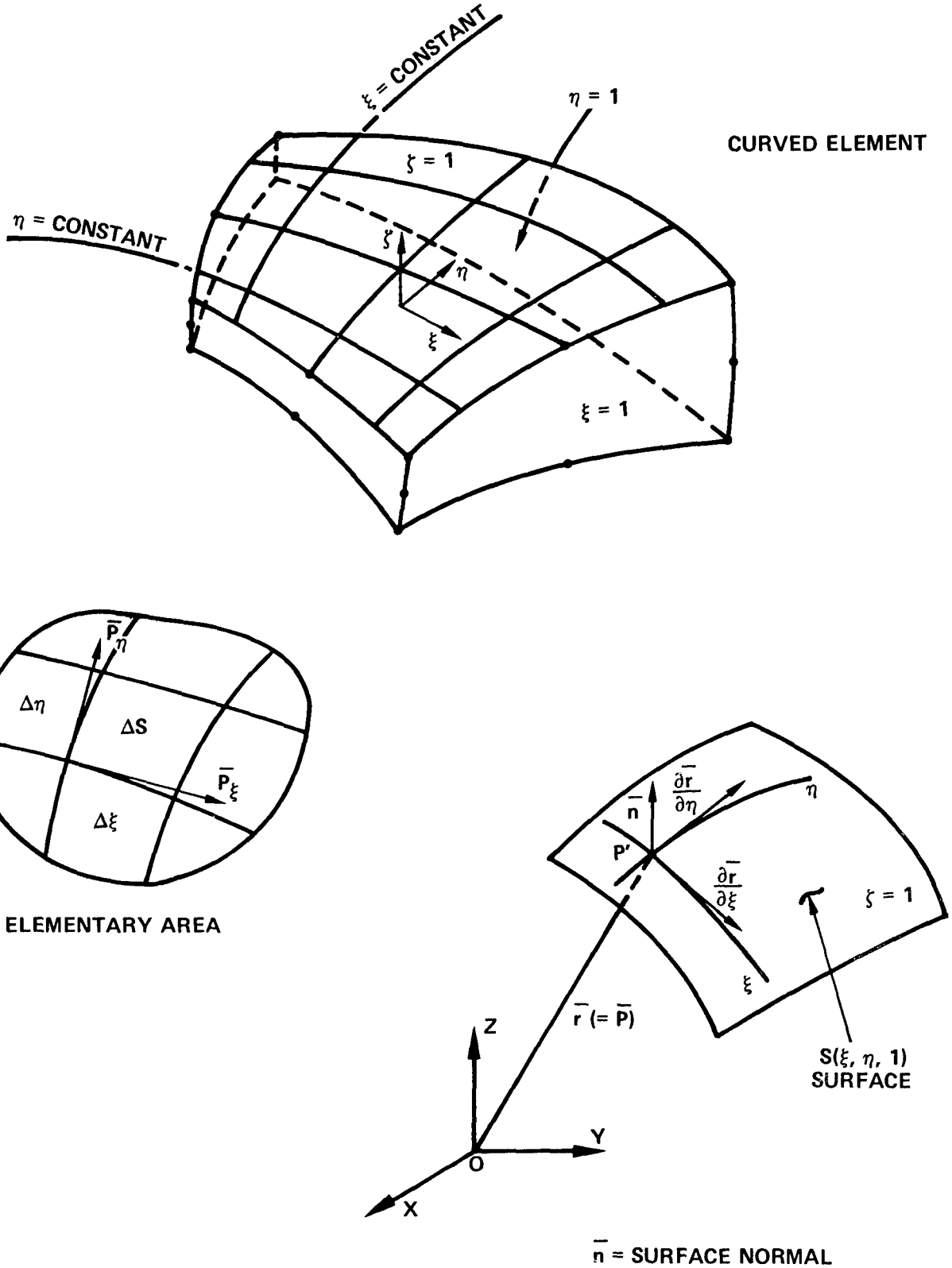

Figure 3.4 Curved element representation of a complex surface

Consider the general case of a fluid pressure distribution

$$\bar{P} = - q(x, y, z) \cdot \hat{n} \tag{3.27}$$

where $q(x, y, z)$ is a scalar factor that describes the variation in spatial pressure and $\hat{n}$ is the external surface normal. In case of hydrostatic pressure, $q(x, y, z)$ reduces to $q(z)$. From Eq. (2.12), the equivalent loading vector at the ith node is

$$\{F(I)\} = \begin{Bmatrix} F_x(I) \\ F_y(I) \\ F_z(I) \end{Bmatrix} = \int_D N(I) \{P\} \, ds \tag{3.28}$$

where $N(I)$ is the shape function for node i and ds is the differential area of a given surface region (D) for which the pressure has been specified.

Since the position of any point in an element body is defined by the coordinate equation (Eq. (3.5)), points on any surface area can be readily obtained. For instance, by setting $\zeta = \pm 1$, we obtain the surface equations in a parametric form for the top and the bottom faces, respectively.

$$\begin{aligned} X &= \sum_i N_i X_i = X(\xi, \eta) \\ Y &= \sum_i N_i Y_i = Y(\xi, \eta) \\ Z &= \sum_i N_i Z_i = Z(\xi, \eta) \end{aligned} \tag{3.29}$$

The summation extends to all nodes on a given surface. Nodal numbers for a given (top) face and corresponding shape functions are shown in the following nodal number labeling scheme.

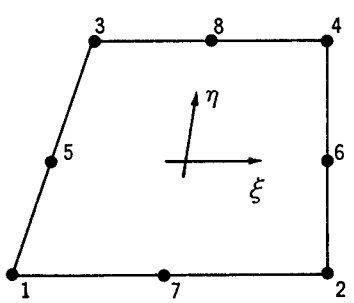

Quadratic Element

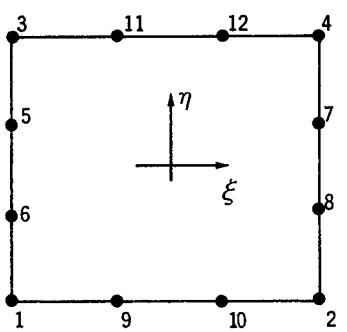

Cubic Element

For the quadratic element:

Corner nodes 1, 2, 3, 4 $\xi_i = \mp 1,\ \eta_i = \mp 1.$

$$N_i = \frac{1}{4}(1 + \xi_i \xi)(1 + \eta_i \eta)(\xi_i \xi + \eta_i \eta - 1)$$

Midside nodes 5, 6 $\xi_i = \mp 1,\ \eta_i = 0.$

$$N_i = \frac{1}{2}(1 + \xi_i \xi)(1 - \eta^2)$$

Midside nodes 7, 8 $\xi_i = 0,\ \eta_i = \mp 1.$

$$N_i = \frac{1}{2}(1 - \xi^2)(1 + \eta_i \eta)$$

(3.30)

For the cubic element:

Corner nodes 1, 2, 3, 4 $\xi_i = \mp 1,\ \eta_i = \mp 1.$

$$N_i = \frac{1}{32}(1 + \xi_i \xi)(1 + \eta_i \eta)[9(\xi^2 + \eta^2) - 10]$$

Side nodes 5, 6, 7, 8 $\eta_i = \mp \frac{1}{3},\ \xi_i = \mp 1.$

$$N_i = \frac{9}{32}(1 + \xi_i \xi)(1 - \eta^2)(1 + 9\,\eta_i \eta)$$

Side nodes 9, 10, 11, 12 $\xi_i = \mp \frac{1}{3},\ \eta_i = \mp 1$

$$N_i = \frac{9}{32}(1 - \xi^2)(1 + 9\,\xi_i \xi)(1 + \eta_i \eta)$$

(3.31)

With the surface defined in curvilinear coordinates, i.e., $S(\xi, \eta)$ in Eq. (3.29), its normal vector can be expressed by

$$\bar{n} = n_x \hat{i} + n_y \hat{j} + n_z \hat{k} = \bar{P}_\xi \times \bar{P}_\eta \tag{3.32}$$

$$= \begin{vmatrix} \hat{i} & \hat{j} & \hat{k} \\ \dfrac{\partial x}{\partial \xi} & \dfrac{\partial y}{\partial \xi} & \dfrac{\partial z}{\partial \xi} \\ \dfrac{\partial x}{\partial \eta} & \dfrac{\partial y}{\partial \eta} & \dfrac{\partial z}{\partial \eta} \end{vmatrix}$$

where $\bar{P}_\xi$ and $\bar{P}_\eta$ are vectors tangent to the surface and in the directions of the ξ- and η-coordinate lines, respectively (Fig. 3.4). An elementary area of the surface is given by

$$\Delta \bar{S} = \bar{P}_\xi \, \Delta \xi \times \bar{P}_\eta \, \Delta \eta$$

The surface area of a region D is

$$S = \lim_{\substack{\Delta\xi \to \epsilon \\ \Delta\eta \to \epsilon}} \sum |\bar{P}_\xi \times \bar{P}_\eta| \, \Delta \xi \, \Delta \eta$$

The area of one complete face of an element can be found conveniently by a numerical integration process; we have

$$\begin{aligned} S &= \int_{-1}^{1} \int_{-1}^{1} |\bar{n}| \, d\xi \, d\eta \\ &= \sum_{i=1}^{NPT} \sum_{j=1}^{NPT} |\bar{n}| \cdot H_i(\xi) \cdot H_j(\eta) \quad i, j = 1, 2, \ldots, NPT \end{aligned} \tag{3.33}$$

For a relatively smooth surface, such as the surface of a cylinder or a skewed propeller blade, a three-point integration rule gives adequate accuracy (i.e., for $NPT = 3$, the error range is 0.03 to 0.12 percent). Hence the numerical integration provides an effective way to compute a complex surface area as well as its projections and other surface characteristics.

Now the nodal load components for any node (I) due to a pressure loading on a face of the element can be expressed as

$$\bar{F}(I) = \int_{-1}^{1} \int_{-1}^{1} N(I) \, \{p\} \, |\bar{n}| \, d\xi \, d\eta \tag{3.34}$$

Expressed in quadrature format,

$$\left.\begin{aligned} F_x(I) &= \sum_i \sum_j q_{ij} \cdot N(I) \cdot n_x \cdot H_i(\xi) \cdot H_j(\eta) \\ F_y(I) &= \sum_i \sum_j q_{ij} \cdot N(I) \cdot n_y \cdot H_i(\xi) \cdot H_j(\eta) \\ F_z(I) &= \sum_i \sum_j q_{ij} \cdot N(I) \cdot n_z \cdot H_i(\xi) \cdot H_j(\eta) \end{aligned}\right\} \tag{3.35}$$

The distributed load q_{ij} must be evaluated in a pointwise manner at each integration point $i, j = 1, 2, \ldots, NPT$. As before, these are the numbers of Gaussian integration points along the ξ- and η-coordinate lines, respectively. The final load vector $\{p\}$ is obtained by summing up individual contributions from all elements attached to these nodes or the network of nodes (see Section 2.2.2).

3.3.2 Stresses on an Arbitrary Surface

For obvious reasons, it is conventional to give experimental stress data along certain well-defined reference frames tangent to the surface area of interest. Expression of the stresses in a global coordinate system generally does not give a clear picture of the surface situation for a structure of arbitrary shape. The stress calculation should therefore be put into a format that allows numerical results to be readily assessed, interpreted, and/or compared to experimental values or other known results.

In the process of computing stiffness coefficient matrix $[K]$, values of strain and stress are computed at each Gaussian quadrature point. These values are expressed in terms of nodal displacement parameters (u_i, v_i, w_i), with reference to the global coordinate (x, y, z) system. As evaluated, these strain values are stored on tape. Once the equations of the structure system are solved and nodal displacements become known, stresses and strains can be obtained by direct substitution into Eq. (2.4) and (2.6). For design purposes, these results are sufficient to describe the response of an elastic body in many practical applications.

For structures of complex shapes, stresses at points other than those quardrature points may be desirable. This will require additional calculations at the designated locations where stress evaluation is sought. Matrix $[B]$, shown in Eq. (3.8), should be used for this purpose. The corresponding process outlined in Section 3.2.2 must be repeated. Once again, there is a need to define the surface orientations from which a set of local coordinates can be chosen so that the computed stresses can be of value for immediate, meaningful interpretations.

We begin with the definition of unit normal

$$\hat{n} = \frac{\bar{n}}{|\bar{n}|} \tag{3.36}$$

where $\bar{n} = \bar{P}_\xi \times \bar{P}_\eta$ is given in Eq. (3.32). Now let $\hat{P}_\eta$ be the unit tangent vector which is along an η-coordinate line and $\hat{P}_\eta = \bar{P}_\eta / |\bar{P}_\eta|$. Then

$$\hat{T} = \hat{P}_\eta \times \hat{n} \tag{3.37}$$

$\hat{T}$ will be the third unit vector, completing a right-handed orthogonal triad scribed in the body or attached to a surface. The triad $(\hat{T}, \hat{P}_\eta, \hat{n})$ can be considered as a local reference frame (x', y', z'). See Fig. 3.5 and 3.6. Hence, the matrix

$$\begin{aligned}[\hat{T}, \hat{P}_\eta, \hat{n}] &= [\hat{e}_1, \hat{e}_2, \hat{e}_3] \\ &= [\theta]\end{aligned} \tag{3.38}$$

where $\hat{e}_1, \hat{e}_2, \hat{e}_3$ are unit vectors in directions of local rectangular coordinates (x', y', z'). $[\theta]$ is also known as the direction cosines matrix. $[\hat{T}, \hat{P}_\eta, \hat{n}]$ can be expressed in terms of traditional directional cosine symbols (ℓ, m, n), namely

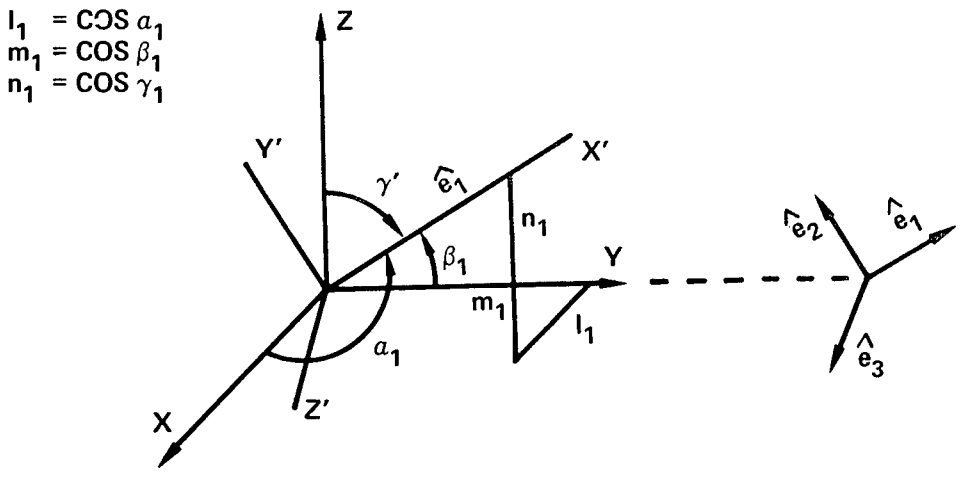

Figure 3.5 Rotation of reference frame

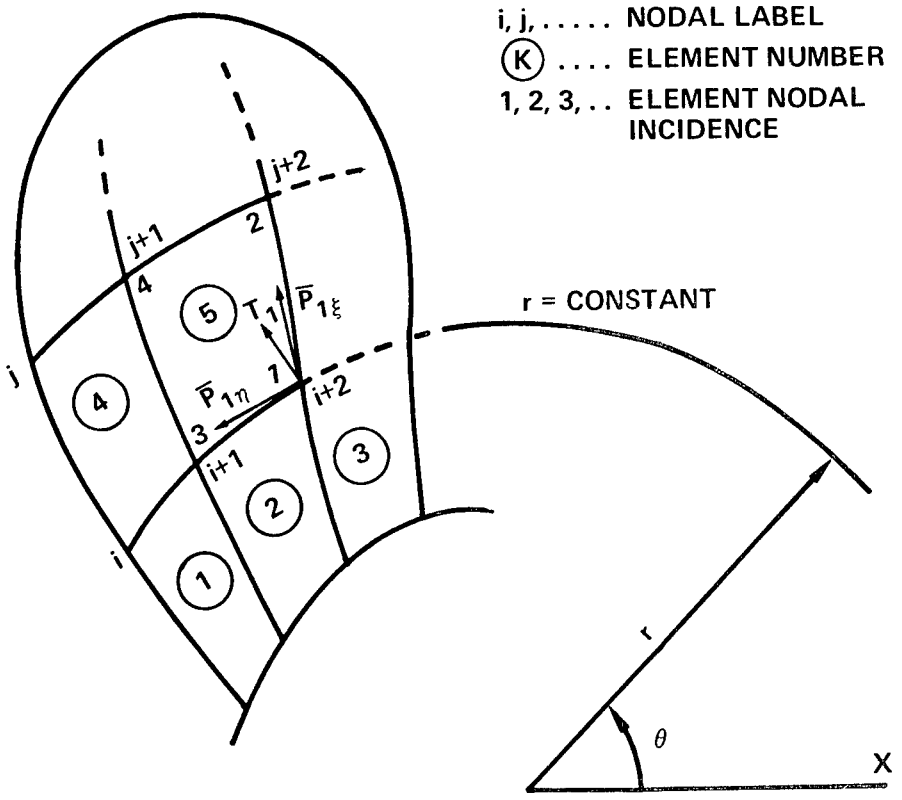

Figure 3.6 Element nodal incidence and local reference frame

$$\left.\begin{aligned} \hat{T} &= \ell_1 \hat{i} + m_1 \hat{j} + n_1 \hat{k} \\ \hat{P}_\eta &= \ell_2 \hat{i} + m_2 \hat{j} + n_2 \hat{k} \\ \hat{n} &= \ell_3 \hat{i} + m_3 \hat{j} + n_3 \hat{k} \end{aligned}\right\} \tag{3.39}$$

Let (u', v', w') be the displacement components along the local cartesian coordinates (x', y', z'). They can be obtained from displacements (u, v, w), which are referenced to the global cartesian coordinates, by a single transformation:

$$\begin{Bmatrix} u' \\ v' \\ w' \end{Bmatrix} = [R] \begin{Bmatrix} u \\ v \\ w \end{Bmatrix} \tag{3.40}$$

where $[R]$ is the rotation matrix

$$[R] = \begin{bmatrix} \ell_1 & m_1 & n_1 \\ \ell_2 & m_2 & n_2 \\ \ell_3 & m_3 & n_3 \end{bmatrix} = [\theta]^T$$

Following the standard rule of differentiation (see Eq. (3.10)) displacement derivatives can be written with respect to local coordinates (x', y', z'):

$$\begin{bmatrix} \frac{\partial u}{\partial x'} & \frac{\partial v}{\partial x'} & \frac{\partial w}{\partial x'} \\ \frac{\partial u}{\partial y'} & \frac{\partial v}{\partial y'} & \frac{\partial w}{\partial y'} \\ \frac{\partial u}{\partial z'} & \frac{\partial v}{\partial z'} & \frac{\partial w}{\partial z'} \end{bmatrix} = \begin{bmatrix} \frac{\partial x}{\partial x'} & \frac{\partial y}{\partial x'} & \frac{\partial z}{\partial x'} \\ \frac{\partial x}{\partial y'} & \frac{\partial y}{\partial y'} & \frac{\partial z}{\partial y'} \\ \frac{\partial x}{\partial z'} & \frac{\partial y}{\partial z'} & \frac{\partial z}{\partial z'} \end{bmatrix} \begin{bmatrix} \frac{\partial u}{\partial x} & \frac{\partial v}{\partial x} & \frac{\partial w}{\partial x} \\ \frac{\partial u}{\partial y} & \frac{\partial v}{\partial y} & \frac{\partial w}{\partial y} \\ \frac{\partial u}{\partial z} & \frac{\partial v}{\partial z} & \frac{\partial w}{\partial z} \end{bmatrix}$$

$$= [R] \begin{Bmatrix} \frac{\partial}{\partial x} \\ \frac{\partial}{\partial y} \\ \frac{\partial}{\partial z} \end{Bmatrix} [u, v, w] \tag{3.41}$$

By substituting local displacements (u', v', w') in place of (u, v, w) in Eq. (3.41), we can arrive at a convenient form of the expression to calculate local strain components from strains given in global coordinates:

$$[\epsilon'] = \begin{bmatrix} \frac{\partial u'}{\partial x'} & \frac{\partial v'}{\partial x'} & \frac{\partial w'}{\partial x'} \\ \frac{\partial u'}{\partial y'} & \frac{\partial v'}{\partial y'} & \frac{\partial w'}{\partial y'} \\ \frac{\partial u'}{\partial z'} & \frac{\partial v'}{\partial z'} & \frac{\partial w'}{\partial z'} \end{bmatrix}$$

$$= [R] \begin{bmatrix} \frac{\partial u}{\partial x} & \frac{\partial v}{\partial x} & \frac{\partial w}{\partial x} \\ \frac{\partial u}{\partial y} & \frac{\partial v}{\partial y} & \frac{\partial w}{\partial y} \\ \frac{\partial u}{\partial z} & \frac{\partial v}{\partial z} & \frac{\partial w}{\partial z} \end{bmatrix} [R]^T \qquad (3.42)$$

Stress components computed in the global coordinate system can be transformed to locally oriented stresses $[\sigma']$ by a similar expression, that is,

$$[\sigma'] = \begin{bmatrix} \sigma'_x & \tau'_{xy} & \tau'_{xz} \\ \tau'_{xy} & \sigma'_y & \tau'_{yz} \\ \tau'_{xz} & \tau'_{yz} & \sigma'_z \end{bmatrix}$$

$$= [R]\,[\sigma]\,[R]^T \qquad (3.43)$$

Once the element mesh and labeled element nodal numbers are laid out over the idealization of a structure, the element incidences must be suitably ordered (Fig. 3.6) such that one curvilinear coordinate, η for instance, will be placed on a designated coordinate surface. When the surface normal vector is computed, another orthogonal surface tangent will complete a right-handed triad. This combination will furnish a set of local rectangular axes and form the basis of a rotation matrix. These data enable the stresses to be calculated over an arbitrarily shaped body along any prescribed orientation.

3.3.3 Applications to Plates and Shells

The solid isoparametric finite elements outlined here are based on a general three-dimensional solution. Such elements have demonstrated broad applicability for problems in structural mechanics. Where the element thickness is decreased to the proportion of a medium thick plate (or a thin shell), a specialized formulation is permissible to achieve greater economy and effectiveness (Ahmad et al., 1965, 1970 and Pawsey, 1970). Some well-known approximation will be utilized in the computations of stiffness coefficients $[K_e]$, e.g., as advocated in classical plate theory (Timoshenko and Woinowsky-Krieger, 1959 and Flugge, 1960) such that lines perpendicular to the middle surface remain straight under loading and strains along these lines can be ignored in the energy summation.

We begin with the element geometry. Pairs of points i_{top} and i_{bottom}, each with given cartesian coordinates, prescribe the shape of an element (see Fig. 3.7) $i = 1, 2, \ldots,$ NNPE where NNPE is the number of nodes per element. Let ξ, η be the two curvilinear coordinates in the middle surface of the shell and ζ a linear coordinate in the thickness direction. As before, ξ, η, and ζ vary between -1 and $+1$ on the respective faces of the element. The cartesian coordinates (x, y, z) of any point of the shell can be defined by interpolation on the coordinates at nodal points i; hence

$$\begin{Bmatrix} x \\ y \\ z \end{Bmatrix} = \sum_{i=1}^{n} N_i \frac{(1+\zeta)}{2} \begin{Bmatrix} x_i \\ y_i \\ z_i \end{Bmatrix}_{\text{top}} + \sum_{i=1}^{n} N_i \frac{(1-\zeta)}{2} \begin{Bmatrix} x_i \\ y_i \\ z_i \end{Bmatrix}_{\text{bottom}} \tag{3.44}$$

Here $N_i = N_i(\xi, \eta)$ are surface shape functions of the type given by Eq. (3.30). Once again, parabolic, cubic, etc. (or of any specific order) shape functions can be adopted for the middle surface of a shell element.

By introducing a nodal vector $\bar{V}_{3i}$ that connects the pairs of nodes i_{top} and i_{bottom}, we can rewrite the relationship between the cartesian and curvilinear coordinates in terms of the midsurface coordinates and the vector $\bar{V}_{3i}$.

$$\begin{Bmatrix} x \\ y \\ z \end{Bmatrix} = \sum_{i=1}^{n} N_i \begin{Bmatrix} x_i \\ y_i \\ z_i \end{Bmatrix}_{\text{mid}} + \sum_{i=1}^{n} N_i \frac{\zeta}{2} \bar{V}_{3i} \tag{3.45}$$

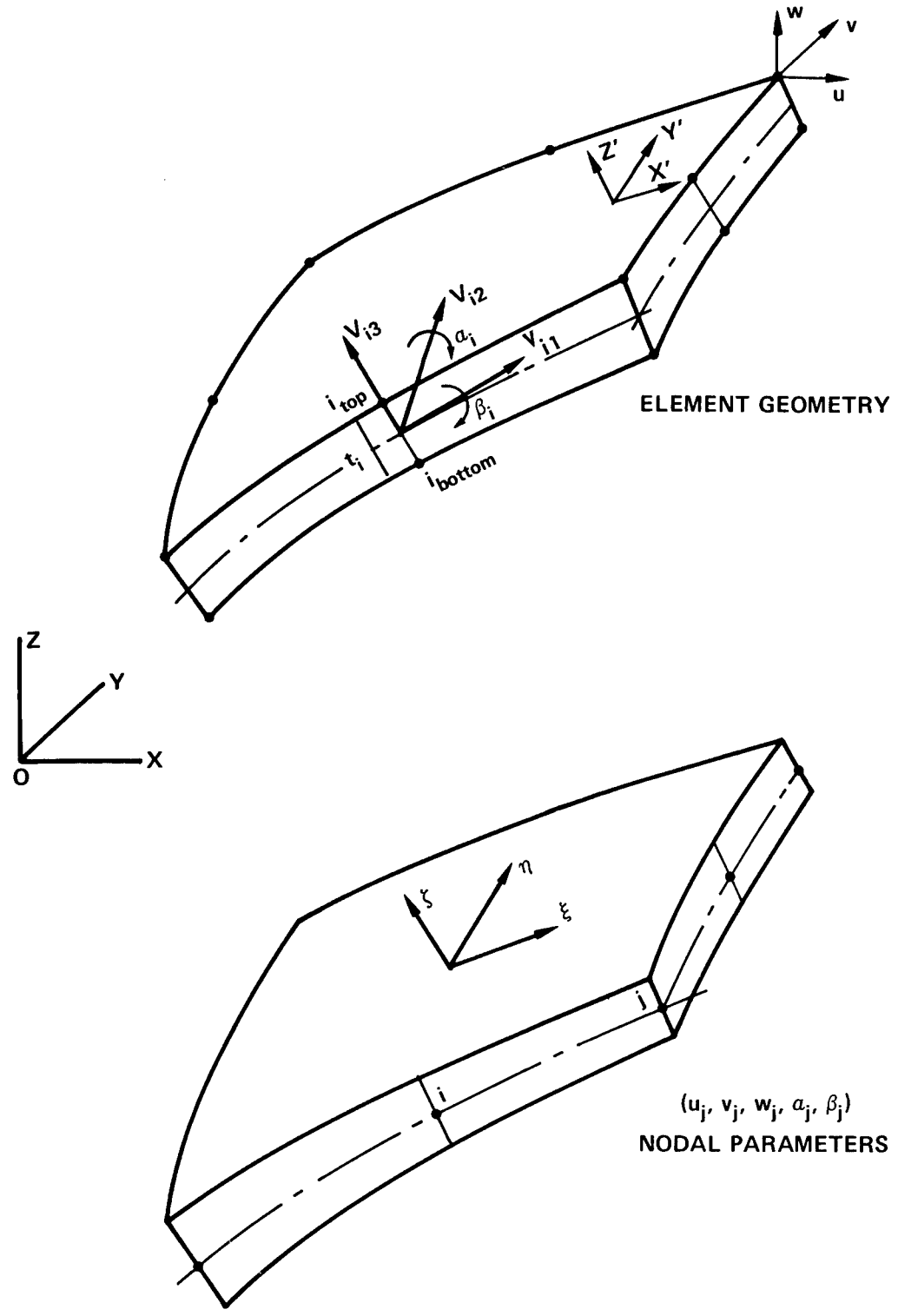

Figure 3.7 A quadric curved shell element

where

$$\bar{V}_{3i} = \begin{Bmatrix} x_i \\ y_i \\ z_i \end{Bmatrix}_{\text{top}} - \begin{Bmatrix} x_i \\ y_i \\ z_i \end{Bmatrix}_{\text{bottom}} \tag{3.46}$$

$$i = 1, 2, \ldots, \text{NNPE } (=n)$$

Now the displacement pattern has to be assumed for the element. Since the strains in the direction normal to the midsurface are assumed to be negligible, the displacement vector $\bar{r}$ throughout the element will be taken to be completely defined by the midsurface nodal displacement $\bar{r}_{mi}$ and two rotations $(\bar{\alpha}, \bar{\beta})$ of the nodal normal $\bar{V}_{3i}$ about axes orthogonal to it. If two such orthogonal directions are given by unit vectors $\hat{V}_{2i}$ and $\hat{V}_{1i}$, with corresponding scalor rotations α_i and β_i, we can write

$$\bar{r} = \sum_{i=1}^{n} N_i \left\{ \bar{r}_{mi} + \zeta \frac{t_i}{2} (\bar{\alpha}_i + \bar{\beta}_i) \times \bar{V}_{3i} \right\} \tag{3.47}$$

where

$$\bar{r} = \begin{Bmatrix} u \\ v \\ w \end{Bmatrix} = u\hat{i} + v\hat{j} + w\hat{k}$$

$$\bar{r}_{mi} = u_i \hat{i} + v_i \hat{j} + w_i \hat{k} \tag{3.48}$$

and

$$\left.\begin{aligned} \hat{V}_{1i} &= \hat{i} \times \hat{V}_{3i} \\ \hat{V}_{2i} &= \hat{V}_{3i} \times \hat{V}_{1i} \end{aligned}\right\} \tag{3.49}$$

$$\left.\begin{aligned} \bar{\alpha}_i &= \alpha_i \hat{V}_{2i} \\ \bar{\beta}_i &= \beta_i \hat{V}_{1i} \end{aligned}\right\} \tag{3.50}$$

$$i = 1, 2, \ldots, \text{NNPE } (=n)$$

Here u, v, and w are displacements in the directions of global x, y, and z axes, and u_i, v_i, and w_i are displacements at the midsurface node i. At each node, we now have the five basic degrees of freedom:

$$\{U_{is}\} = \begin{Bmatrix} u_i \\ v_i \\ w_i \\ \alpha_i \\ \beta_i \end{Bmatrix} \tag{3.51}$$

From the basic shell assumptions, the strain components are essential in directions of tangential orthogonal axes related to the surface ζ = constant. The strains to be used in the element approach must be converted to this same reference system. At a point on this surface, take z' in the direction of surface normal $\bar{n}$, Eq. (3.32). We can establish a set of local orthogonal axes x', y', and z'. One simple scheme is given by Eq. (3.49). The strain components of interest are

$$\{\epsilon'\} = \begin{Bmatrix} \epsilon_{x'} \\ \epsilon_{y'} \\ \gamma_{x'y'} \\ \gamma_{x'z'} \\ \gamma_{y'z'} \end{Bmatrix} = \begin{Bmatrix} \dfrac{\partial u'}{\partial x'} \\ \dfrac{\partial v'}{\partial y'} \\ \dfrac{\partial u'}{\partial y'} + \dfrac{\partial u'}{\partial x'} \\ \dfrac{\partial u'}{\partial z'} + \dfrac{\partial w'}{\partial x'} \\ \dfrac{\partial v'}{\partial z'} + \dfrac{\partial w'}{\partial y'} \end{Bmatrix}$$

or

$$\{\epsilon'\} = [B'] \{U_s^a\} \tag{3.52}$$

The stresses corresponding to these strains are defined with the aid of the elasticity matrix $[D']$. We have

$$\{\sigma\} = \begin{Bmatrix} \sigma_{x'} \\ \sigma_{y'} \\ \tau_{x'y'} \\ \tau_{x'z'} \\ \tau_{y'z'} \end{Bmatrix} = [D'] \{\epsilon'\} \tag{3.53}$$

where

$$[D'] = \begin{bmatrix} D'_m & 0 \\ 0 & D'_s \end{bmatrix} = \frac{E}{(1-\nu^2)} \begin{bmatrix} 1 & \nu & 0 & 0 & 0 \\ & 1 & 0 & 0 & 0 \\ & & \frac{1-\nu}{2} & 0 & 0 \\ & & & \frac{1-\nu}{2k} & 0 \\ \text{SYM} & & & & \frac{1-\nu}{2k} \end{bmatrix} \tag{3.54}$$

The 5×5 matrix $[D']$ is defined for an isotropic material. E and ν are Young's modulus and Poisson's ratio, respectively. The factor k (= 1.2) included in the last two shear terms is intended to improve the shear displacement approximation (Ahmad, 1970). It is seen that because of the displacement assumption, the shear strain is approximately constant through the thickness, whereas in reality the shear distribution is approximately parabolic. The value $k = 1.2$ is the ratio of relevant strain energies.

The next step is the calculation of the element stiffness matrix

$$[K_e] = \int_{-1}^{1} \int_{-1}^{1} \int_{-1}^{1} [B']^T [D'] [B'] |J| \, d\xi \, d\eta \, d\zeta \tag{3.55}$$

By definition, $\{\epsilon'\} = [B'] \{U_s^a\}$. Matrix $[B']$ relates the local displacement derivatives to the nodal parameters. The calculation of $[B']$ involves three steps:

a. Compute global displacement derivatives for a set of curvilinear coordinates in the manner shown by Eq. (3.10).

b. Transform these derivatives (i.e., the strain components expressed in global coordinates) to local displacement derivatives by Eq. (3.42). Here, the direction cosine matrix $[\theta]$ can be constructed by a process given by Eq. (3.49) with unit vector $\hat{V}_3$ parallel to z'-axis which is in the direction of surface normal $\bar{n}$.

c. Assemble the local displacement derivatives to form the strain vector $\{\epsilon'\}$ in terms of nodal parameter vector $\{U_s^a\}$ given by Eq. (3.52).

Now the whole integral of Eq. (3.55) can be expressed as an explicit function of the curvilinear coordinates. After carrying out some operations at the submatrix level, simplifications and saving in numerical processing can be achieved. A numerical integration will allow the properties of the element to be evaluated.

3.4 Implementation

3.4.1 Introduction to Solution Methods

In the displacement method of finite element analysis, the problem eventually reduces to the solution of a set of linear simultaneous equations that express the load-displacement or equilibrium relation for the structure. The displacement boundary conditions can be readily imposed by deleting the appropriate nodal parameters (corresponding to nodal degrees of freedom) from Eq. (2.14). After reduction—which, in effect, removes the rigid-body mode—we have

$$[K_r]\,\underline{U} = \underline{P} \tag{3.56}$$

where $[K_r]$ is the nonsingular structure-stiffness matrix,

$\underline{U}$ is a vector of unknown nodal parameters (displacements), and

$\underline{P}$ is a vector of applied load.

Once Eq. (3.56) is solved, the global displacement parameters $\underline{U}$ become known. The desired stress and strain at any point within any element can be found immediately by substituting the nodal displacements in Eq. (2.4) and (2.5) in turn.

In practical application, a sizable number of finite elements is required for the representation of structural design problems. Consequently, an extensive network of nodes evolves and the size of the stiffness matrix which corresponds to the number of unknown nodal variables is often overwhelming (not infrequently several thousand degrees of freedom arise). A large portion of the total computer time required to solve a given problem is generally consumed in solving the set of linear equations (Eq. (3.56)). Here, the method of solution can have a significant bearing on the computational efficiency which is measured in terms of demand on core size. At times, the core requirement may dictate the applicability of the finite element method.

It is of prime interest, then, to select a solution algorithm which takes into account the symmetric, positive definite and banded nature of stiffness matrix $[K_r]$. Further the Gauss elimination is known to be numerically stable, irrespective of the order in which the equations, Eq. (3.56), are eliminated (pivot search is not necessary) and therefore the full advantage of symmetry can be realized. The elimination of a row S (which represents an equilibrium equation in nodal variable U_s) leads to a modification of the coefficients in the remaining rows according to the formulas

$$\left.\begin{aligned} k_{ij}^{*} &= k_{ij} - k_{is}\left(\frac{k_{sj}}{k_{ss}}\right) \\ P_i^{*} &= P_i - k_{is}\left(\frac{P_s}{k_{ss}}\right) \end{aligned}\right\} \tag{3.57}$$

Stiffness coefficients k_{ij}, k_{is} $(= k_{si})$, . . etc. represent the sum of individual element contributions. It does not matter in which order the summation is made and, further, they need not be fully summed except those in row S currently being eliminated. This process affects a triangular array immediately below the row that is being eliminated. It can be carried out by retaining in the core only the triangle of coefficients which moves diagonally downward as the elimination proceeds; see Fig. 3.8.

As depicted by a coarse or a fine mesh, the finite element idealization of a structure frequently takes the form of a simply connected region. In these cases, the stiffness matrix can always be arranged in a nicely banded form by labeling the unknown parameters U_i in a suitable order. In the case of a closed ring that represents a multiply connected region, the band can be large despite high sparsity. It is also true that the bandwidth of the individual equations tends to be large in three-dimensional problems where large solid elements with intermediate nodes along their edges are used. In addition, one has to operate on many zero terms within the band, and this adds to the cost of solving equations by a band algorithm. For these and many other cases as well, the "frontal" technique (see Section 3.42) requires less storage and arithmetic than the best Gaussian banded algorithm (Melosh and Bamford, 1969 and Irons, 1970). The frontal solution algorithm is employed for this study, and is described in the next section.

3.4.2 Frontal Technique

Most of the inefficiency in data processing keyed to matrix bandedness can be avoided by applying the frontal technique. It is based on the principle implied by the very nature of Gauss elimination, Eq. (3.57). Frontal processing takes advantage of the fact that nonzero elements in a column of the decomposition (inside the triangular portion of the array affected by row operations) cannot occur in any row prior to the occurrence of a nonzero element (i.e., the stiffness coefficient $k_{is} = k_{si} \neq 0$) in the column of the stiffness matrix. In this approach, the first appearance during decomposition of an element in a column of $[K_r]$ causes the addition of that column to the wavefront which is the "front of active variables." Data that must be readily available on core include only the coefficients of the equations on the wavefront. A variable becomes "active" on its first appearance and is eliminated immediately after its last. Hence, if a variable x_s is ready for elimination, there must be no subsequent elements that contain x . (It was implied previously that k_{si}, k_{sj}, ... , P_s in Eq. (3.57) must be fully summed.) Thus the size of the "front" is smaller than or, at worst, equal to the bandwidth of the equations. In effect, this eliminates a good number of zeroes from the process of computation, and it saves substantially on core requirement.

Fig. 3.9 illustrates an application of the wavefront method. The associated graph, representing a portion of a ship structure, explains the name "wavefront," i.e., equation solving is visualized as progressing like a wave over the structure. At any given time in the analysis, the wavefront includes the total number of active degrees of freedom.

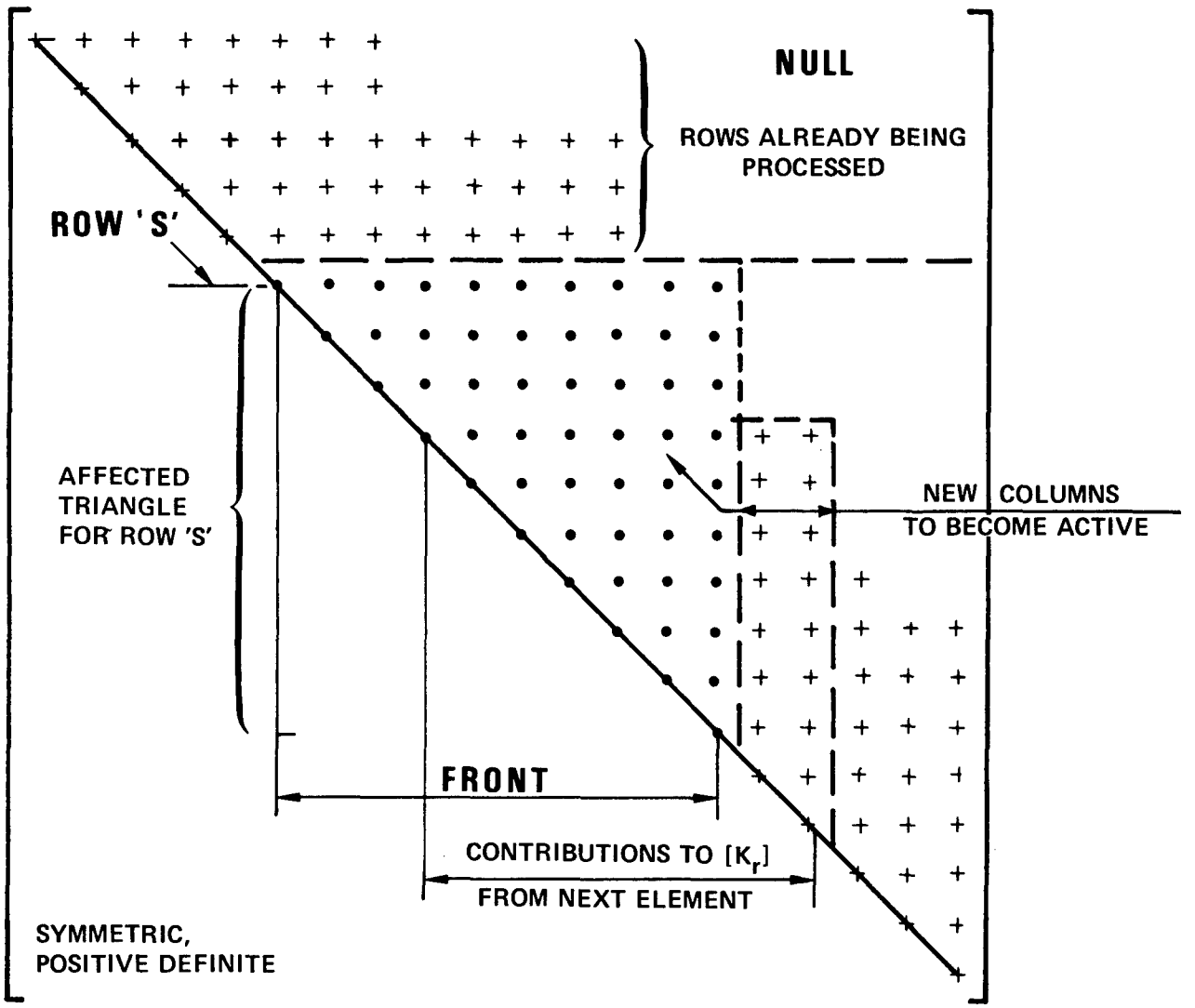

Figure 3.8 Stiffness matrix of a structural system (solution by the Gauss frontal technique)

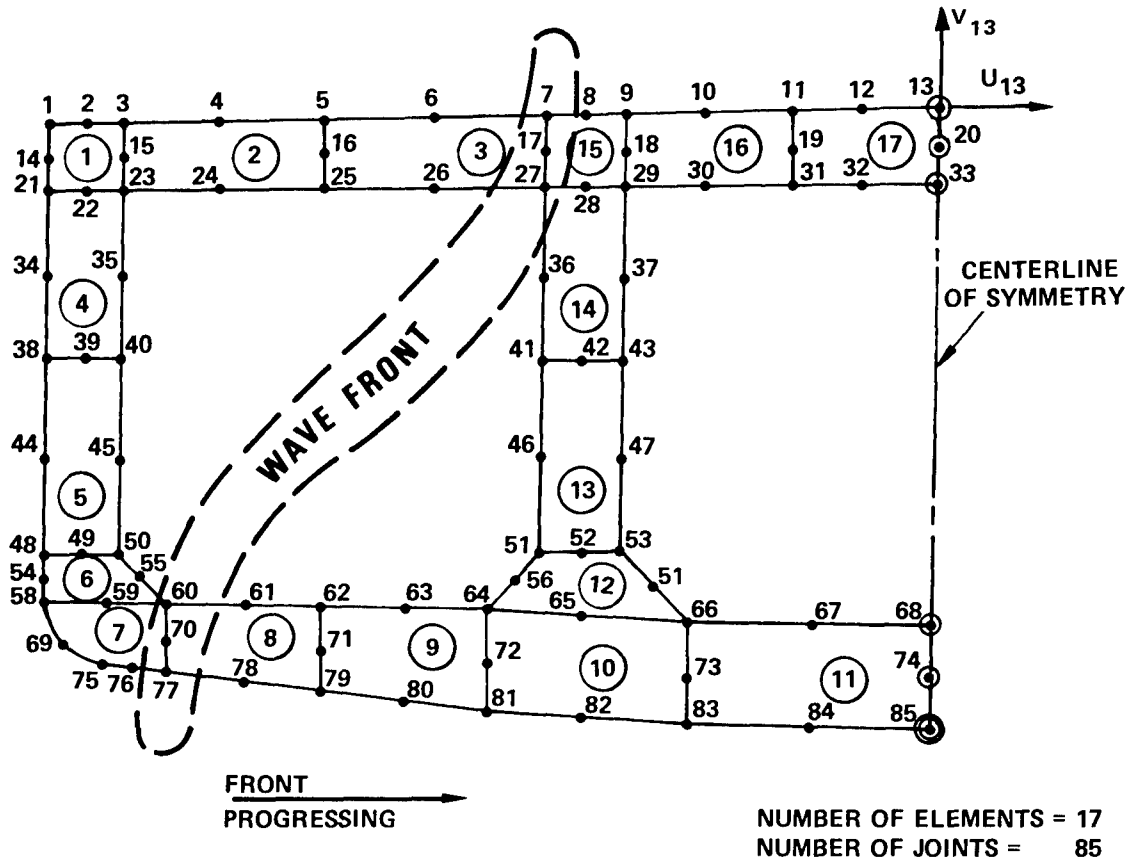

Figure 3.9 Frontal processing of a finite element idealization of the cross frame of a ship

These are associated with partially processed degrees of freedom (or nodal variables). For example, Fig. 3.9 shows a situation just before element ⑧ is introduced.* If there is only one equation per joint, joints 7, 17, 27, and 60, 70, 77 (representing active nodal variables) currently constitute the wavefront. Joints 1, 2, 3, 4, 5, 6, 14, 15, 16, 21, 22, 23, 24, and 25, etc. (which lie to the left (back) of the dotted line) have been fully processed and are no longer considered active. At the next step, element ⑧ introduces the new active variables 61, 62, 71, 78, and 79. As elements are being processed one after another, the front moves forward across the structure.

Further we observe that:

a. The order of element sequence is critical in frontal solution, just as the node numbering is critical in a band algorithm, although the best order is not always unique.

b. Ordering of the nodes is irrelevant to the frontal technique. The node numbers are merely unique labels that relate the degrees of freedom for element and structure. They have no effect on the order of elimination. Here, when a given mesh is changed by adding or deleting nodes, the frontal data are little changed, but a band algorithm may require extensive node renumbering in order to preserve a small bandwidth. This can be extremely valuable in design application when a mesh is to be modified locally for a rerun.

c. The size of front and hence the storage requirements for a given problem can be assessed from the mesh pattern such as given in Fig. 3.9. For example, before element ⑧ is introduced, there are six active variables: 7, 17, 27, 60, 70, 77; immediately after the stiffness coefficient generated by element ⑧ has been added in, the list of active variables increases to 11.

3.5 Evaluation of Numerical Results

The preceding sections have described the formulation of solid finite elements for the three-dimensional analysis of a general elastic body and a method for its implementation. The performance of these elements in the representation of an elastic structure will now be evaluated. Some preliminary computations were conducted with these elements using examples given in Chapter 9 of Zienkiewicz (1970) and favorable numerical results were obtained. Additional problems are included here and solutions for such basic structural components as beams, plates, and shells are presented to verify the behavior of individual elements and to examine the adequacy of the finite element models. A special example will be given in Chapter 4 to demonstrate the effectiveness of the procedure in solving the difficult problem of marine propeller blades.

*Element ⑮ has not yet been introduced.

3.5.1 Prismatic Beams

3.5.1.1 A Cantilever Beam. Timoshenko (1934) treated a prismatic bar subjected to pure bending as a problem of elasticity in three dimensions. Consider the bar bent in one of its principal planes (x-z) by a couple M at one end and held fixed at the other. Take the origin of the coordinates at the centroid of the cross section, i.e., point 0 (Fig. 3.10). The displacement components as predicted by the theoretical solution are:

$$\begin{cases} u = \dfrac{1}{2R}\,[z^2 - \nu\,(x^2 - y^2)] \\ v = \nu\,\dfrac{xy}{R} \\ w = -\,\dfrac{xz}{R} \end{cases}$$

and $\dfrac{1}{R} = \dfrac{M}{EI}$ is the curvature of the deflected bar. After deformation, points on a plane cross section will remain on that plane, but the cross-sectional shape will change. The sides of the cross section become inclined and the top and bottom edges are bent into parabolic curves as shown by the dotted lines in Section A-A of Fig. 3.10.

An aluminum cantilever beam having a cross section of 0.5- by 0.6875-in. thick and a length of 11.0 in. was bent by an end couple of 4.10 in.-lb. Surface displacements were measured by using holographic interferometry (Dhir and Sikora, 1972). Three-dimensional displacement components (u, v, w) for the top face along the front edge were obtained; see Fig. 3.10. This experiment was conducted as a preliminary process to evaluate the quality of measurements obtainable by holography. In this case, the measured data indicate that the beam appeared to be distorted locally near the support; the investigators had difficulty in simulating the fixed-end condition for the slender beam.

The cantilever beam is represented by four 20-node (quadric) hexahedron elements with a total length of 11 in. The finite element model is completely fixed at one end and bent at the other by an end couple produced by two equal and opposite forces ($=\pm 5.9636$ lb) applied to the top and bottom midside node. Computed displacements u and v are almost exact; they are within 0.1 percent of the correct solution. Computed stresses are good and are generally within 0.5 percent of the exact solution except at points near the concentrated applied forces.

3.5.1.2 A Simply Supported Beam. The purpose of the current example is to assess the effect of mesh pattern (as it relates to the element aspect ratio) on the behavior of the finite element model. A simply supported rectangular beam 40 in. long and with a 0.6 by 6.0 in. cross section is represented by four quadric elements (Table 3.1).

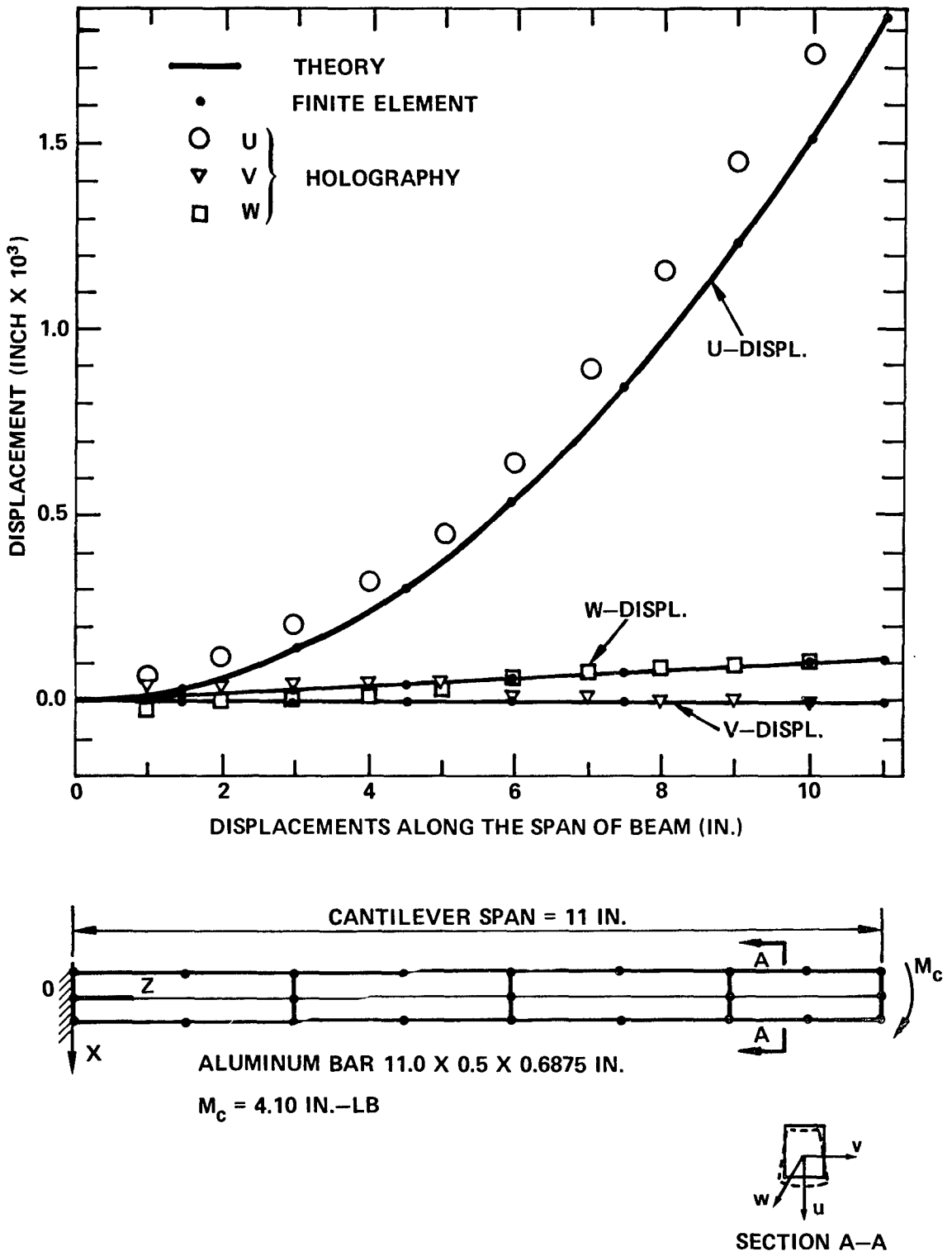

Figure 3.10 Pure bending of a prismatic bar

TABLE 3.1 RESULTS OF ANALYSIS OF A SIMPLY SUPPORTED BEAM

DISCRETE MODEL B1

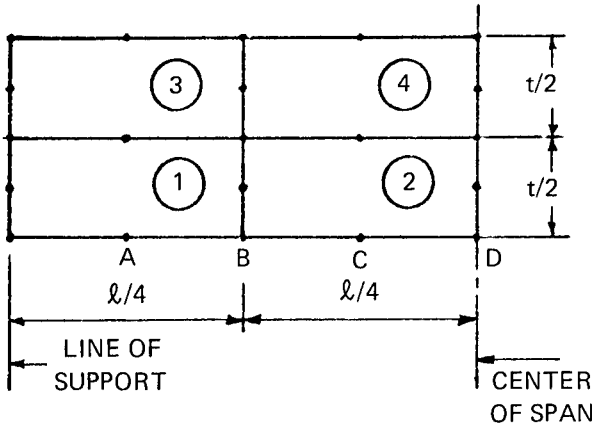

DISCRETE MODEL B2

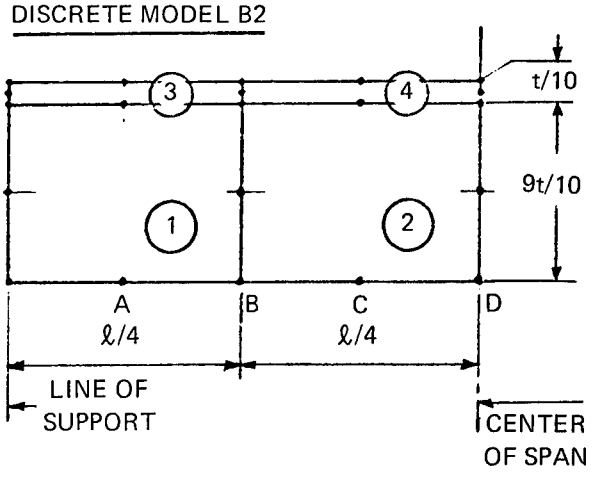

SPAN ℓ = 40 IN.
THICKNESS t = 6 IN.
WIDTH b = 0.6 IN.
CENTER POINT LOAD P = 10,000 LB

POISSON RATIO ν = 0.30
YOUNG'S MODULUS E = 30,000,000 PSI
BENDING STRESS σ PSI

	Vertical Deflection at Section in.				Stresses at Section C psi	
	A	B	C	D	σ_{top}	σ_{bottom}
Discrete Model B1	0.0156	0.0292	0.0390	0.0427	− 20,590	21,030
Discrete Model B2	0.0155	0.0290	0.0388	0.0425	− 20,820	21,040
Beam Theory	0.0151	0.0283	0.0376	0.0412	− 20,830	20,830
Theory of Elasticity	0.0158	0.0298	0.0398	0.0440	− 20,720	20,890

These elements are of uniform size in discrete model B1 while they are of nonuniform size in discrete model B2. The beam is loaded at midspan by a concentrated force P. Vertical deflections and normal stresses are obtained from the discrete element models. The response of discrete model B2 with its nonuniform mesh size appears to be slightly stiffer. Theoretical solutions (listed in Table 3.1) are obtained (a) by using elementary beam theory in which the effect of shear stresses is neglected and (b) by elastic theory (Timoshenko 1934) in which the beam is treated as a two-dimensional problem. Numerical results obtained by both finite element calculations are acceptable from an engineering standpoint.

3.5.2 Plate Bending

When the thickness of an elastic body is small compared to its other dimensions, it is called a plate. A flat plate is classified as thin or medium thick according to its span to thickness ratio (ℓ/t) whether, this ratio is greater or less than 40. When a medium thick plate ($5 \geq \ell/t \geq 40$) is bent with small deflection—small in the sense that the plate deflection is small compared with its thickness—the classical plate theory (i.e., the Kirchoff assumption) holds. Then, the laterally loaded plate can be treated as a two-dimensional problem.

The 20-node hexahedron elements are used to model a plate structure with varying mesh fineness (Fig. 3.11). Here the analysis is for a simply supported square plate with a 40-in. span and a 1-in. thickness subjected to a concentrated center load. This is a severe bending test because the situation is singular at the loading point (the solution for stresses at this point is not bounded).

The center deflection under concentrated load obtained from finite element calculations is plotted against mesh size in Fig. 3.12. Note the rapid convergence of the deflection. For a mesh size $N = 4$ ($\ell/t = 5$), the calculated deflection is within 1.5 percent of the exact solution. Numerical results for some well-known plate bending elements are also shown in Fig. 3.12 for comparison purposes. These results are taken from the Nastran Theoretical Manual (1969).

The dotted lines in Fig. 3.13 indicate the distribution of bending moments M_x and M_y along the centerline of the square plate computed from the finite element model. The theoretical results (Timoshenko, 1959) are for a concentrated load P applied over a circular area of 0.05-a radius.

For general plate bending analysis, the application of the specialized element given in Section 3.3.3 is preferred because of its efficiency and ensuing economy. Although the solid element is not intended to be used for plate bending problems, it did behave well as a plate when molded to the geometry of a plate. The element did yield results which converged rapidly to the exact solution.

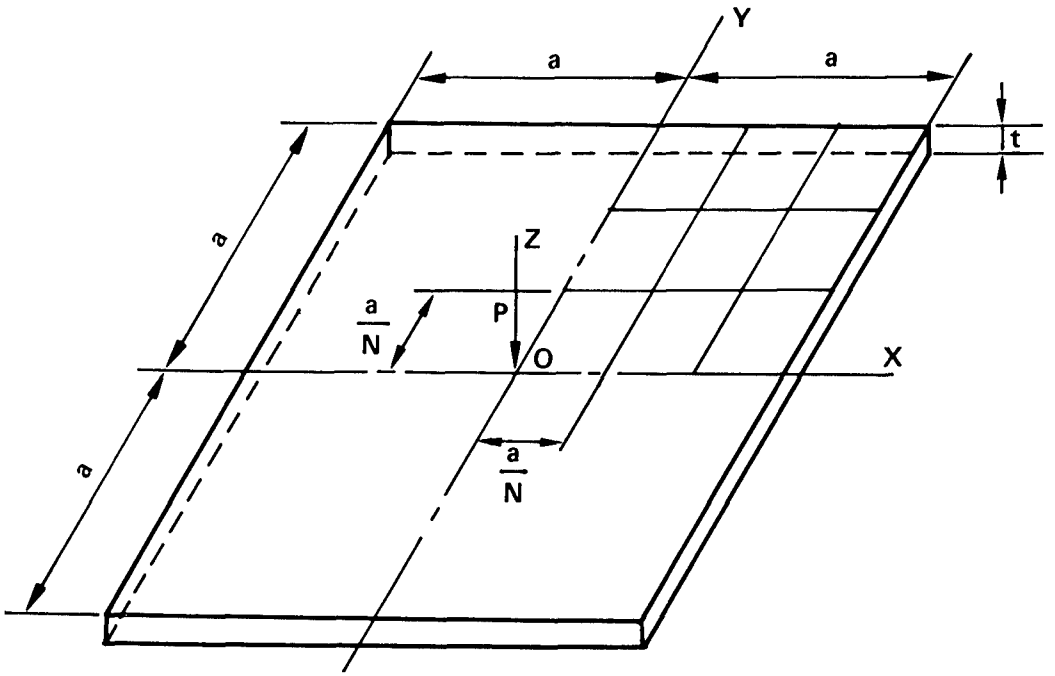

Figure 3.11a A simply supported square plate under center load

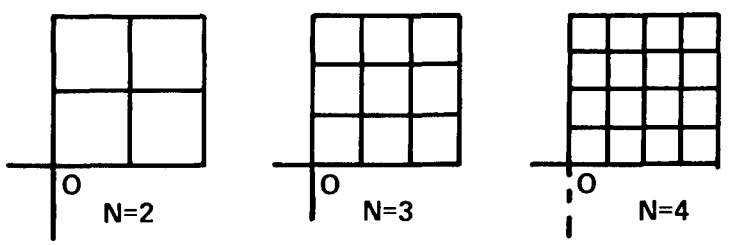

Figure 3.11b Element mesh used on the analyzed quadrant of the plate

Figure 3.11 Plate bending sample problem (example 3.1)

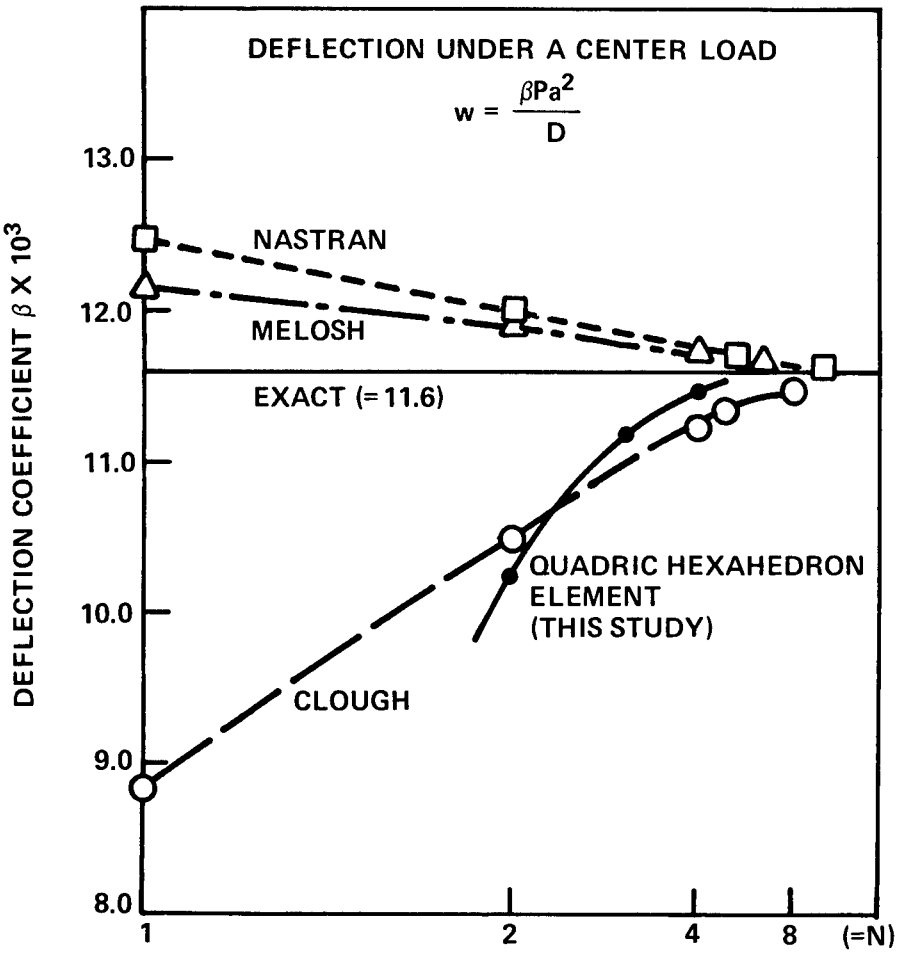

Figure 3.12 Convergence of center deflection of a square plate with mesh refinement (example 3.1)

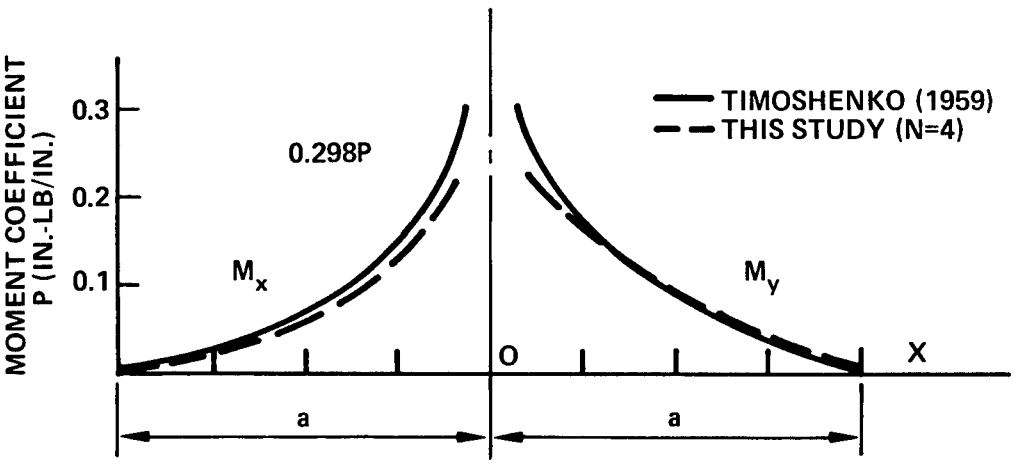

Figure 3.13 Distribution of bending moments along a center line of a square plate (example 3.1)

3.5.3 Thick-Walled Cylinder

The subject of this analysis is a section of cylindrical wall 12-in. long with an outside diameter of 20 in. The wall is 2-in. thick and its outer surface is under a uniformly distributed pressure. The problem is that of an axisymmetric solid and the situation is two-dimensional. In this case, a quadrant of the thick-walled cylinder is considered and each time either two or three 20-node hexahedron elements are used to model the curved shell.

Displacements are computed for all nodal joints in global coordinates XYZ. Stresses are computed at integration points as well as on the curved surfaces, including both interior and exterior. The stresses are expressed in global coordinates and also in local curvilinear coordinates (ξ, η, ζ). A two-element representation of the curved shell is illustrated in Table 3.2. Also given there are computed stresses, the radial component σ_r, and the tangential component σ_θ along a typical section. Numerical results obtained from the three-dimensional finite element solution are in good agreement with the theoretical solution (Timoshenko, 1934). The computed stresses are generally closer to the exact solution at the integration points than at other points, e.g., on the surfaces.

This example provides a way to verify certain subprograms used to define surface characteristics, local axis orientations, and stress transformations for an arbitrary shaped body. These subprograms are designed to enable immediate interpretation of finite element solutions where a complex structural configuration is considered (see Section 4.4).

3.5.4 Stiffened Plates

In the case of a simple beam having a longitudinal plane of symmetry with external forces also acting in this plane, bending will take place in the same plane. Elementary beam theory assumes that a transverse section of the beam that is originally plane remains plane and normal to the longitudinal fibers of the beam after bending. Direct measurement shows that the beam theory gives very accurate results for the deflection of beams and the strains of longitudinal fibers. The results of finite element calculation for a beam of rectangular section (Table 3.1) also confirm the validity of the elementary theory of bending.

Now consider a T-beam which, in essence, is a rectangular beam with projected flanges. When a T-beam has the proportions of an ordinary structural shape as found in a standard handbook, its behavior under simple bending can still be predicted by ordinary beam theory. However, when the flanges of a beam are extended further, the transverse stress distribution is no longer uniform across the width of the flange. It is known that parts of the flange at a distance from the web do not take their full share in resisting bending. This phenomenon is called "shear lag." A beam of this type is less stiff than predicted by elementary beam theory.

The configuration of a beam with very wide flanges becomes that of a stiffened plate. Plates that are stiffened transversely and/or longitudinally are important components in the hull structure of ships. The plate which serves as load bearer also acts as the flange of

TABLE 3.2 RESULTS OF STRESS CALCULATIONS FOR A THICK-WALLED CYLINDER

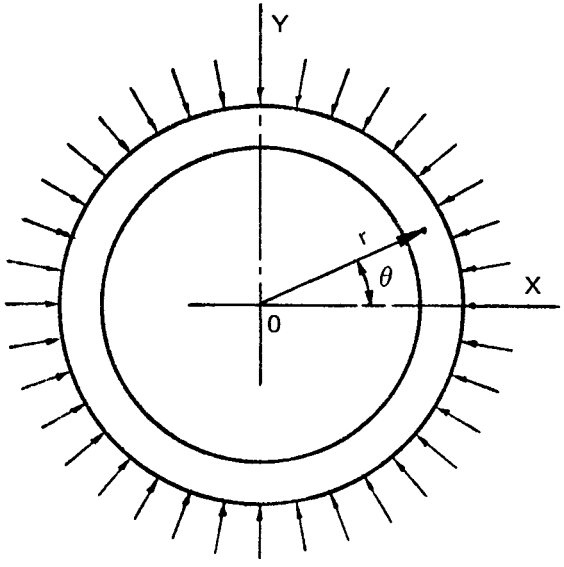

CYLINDRICAL WALL SUBJECTED TO UNIFORMLY DISTRIBUTED EXTERIOR PRESSURE

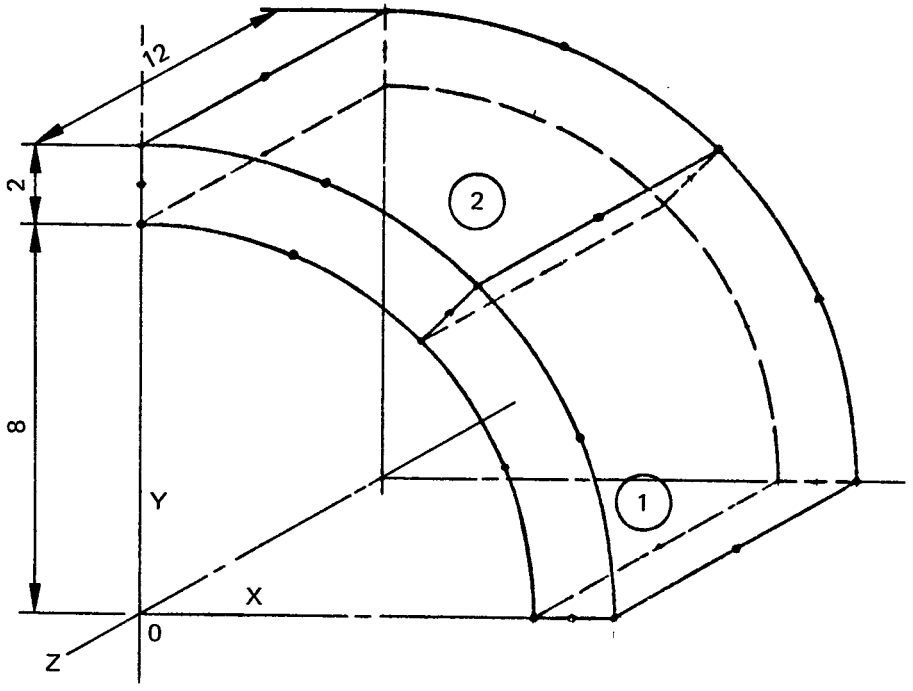

CURVED HEXAHEDRON ELEMENT REPRESENTATION FOR A QUADRANT OF CYLINDRICAL WALL

Radial Distance r (in.)	Finite Element Solution		Theoretical Solution	
	σ_r (psi)	σ_θ (psi)	σ_r (psi)	σ_θ (psi)
8.00	0.10	5.59	0.00	5.55
8.225	0.19	5.42	0.17	5.39
9.000	0.54	4.96	0.58	4.97
9.775	0.94	4.64	0.92	4.64
10.00	1.08	4.58	1.00	4.58

the stiffener. There are numerous approximate methods for analyzing these plates. Most frequently, they are based on idealization of the system into a grid (or network) of beams or into an equivalent orthotropic plate. These methods require an estimate on the effective width of the plate and the torsional rigidity of the composite. Thus they demand considerable engineering judgment and interpretation and are not completely reliable.

Important progress has been made in recent years on finite element analysis of eccentrically stiffened plates and shells (Mehrain, 1967; Kohnke, 1969; and Chu, 1970). The stiffened plates are represented by a composite of beams and plates (one- and two-dimensional elements, respectively). Actually, at or near the interface of the plate and its stiffener, an accurate solution of their structural behavior would require a three-dimensional analysis. The improved hexahedron element is utilized here to analyze the intricate stress distribution of stiffened plates.

Fig. 3.14 indicates a general scheme used to analyze a laterally loaded stiffened plate. The plate with a stiffener on one side is taken as a simply supported plate beam carrying a center load P. Because of symmetry, a half span of the beam is idealized and twelve 20-node hexahedron elements are used for its representation. At each end, vertical supports are provided for both flange and web plates. Five different flange versus stiffener aspect ratios are used as parameters (plate beams CX2 through CX6) to assess the effect of flange width on the structural behavior of these stiffened plates. As the flange of a beam is progressingly widened (e.g., plate beam CX3), the maximum center deflections calculated by the finite element representation are found to increase at a greater rate than those obtained by the elementary beam formula. In other words, because of shear lag, each incremental flange material is engaged in a lesser capacity than has been assumed.

Fig. 3.15 depicts the distribution of longitudinal stresses (σ_y) on a transverse section of plate beam CX3. Stresses are generally higher in the parts of flange near the stiffener and especially in the vicinity of the concentrated load. Similar patterns of stress distribution with varying degree of stress gradient are found in each beam that has projected flanges. Stress distribution across the web plate differs somewhat from the linear variation assumed in the elementary theory of bending. The neutral axis at these cross sections of the beam does not pass through the geometric centroid (Fig. 3.15). Such behavior was more pronounced for a plate beam such as CX3 with its deeper web plate ($S = 6$ in.) than for the others, for example, CX4.

Fig. 3.15 also shows the distribution of typical transverse stresses (σ_x) along the flange plate. They indicate some local bending of the flange in the transverse direction near the concentrated force. Additional stress data of interest are given in Table 3.3. These stresses were obtained at the Gaussian integration points (used to form the stiffness matrix of the isoparametric element). Stresses computed at such points have been shown to be generally of high accuracy. Stresses for other locations in the plate beam can be found by interpolation.

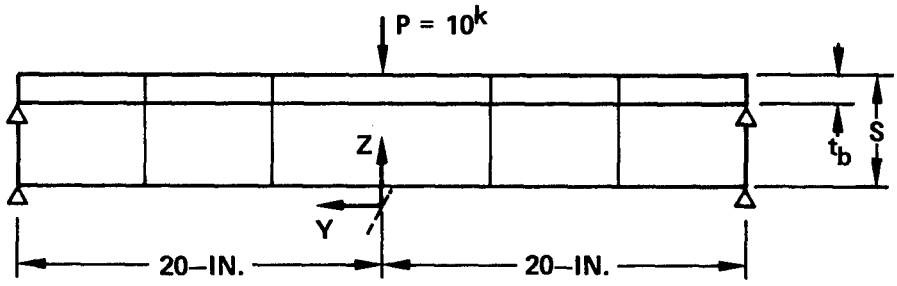

A SIMPLY SUPPORTED PLATE BEAM

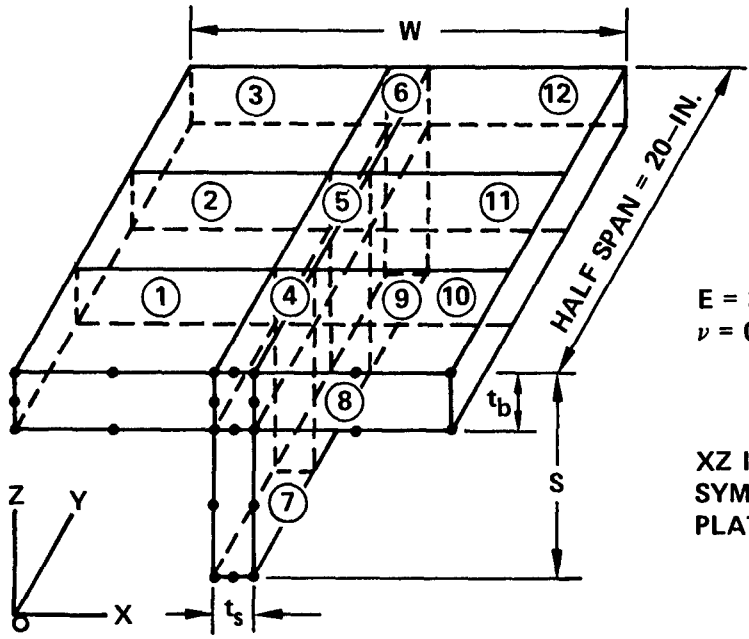

E = 30,000 KSI
ν = 0.30

XZ IS THE PLANE OF SYMMETRY OF PLATE BEAM

A FINITE ELEMENT REPRESENTATION

PLATE BEAM MARK	BEAM PARAMETER				CENTER DEFLECTION (IN.)	
	w	t_b	s	t_s	FINITE ELEMENT	BEAM THEORY
CX1	0.6	0.6	6.0	0.6	0.0425	0.0412
CX2	6.0	0.6	6.0	0.6	0.0214	0.0191
CX3	12.0	0.6	6.0	0.6	0.0185	0.0158
CX4	1.8	0.6	3.0	0.6	0.213	0.210
CX5	6.0	0.6	3.0	0.6	0.147	0.142
CX6	12.00	0.6	3.0	0.6	0.129	0.123

PARAMETERS OF BEAM CROSS SECTION AND COMPUTED DEFLECTIONS

Figure 3.14 Stiffened plate sample problem (example 3.2)

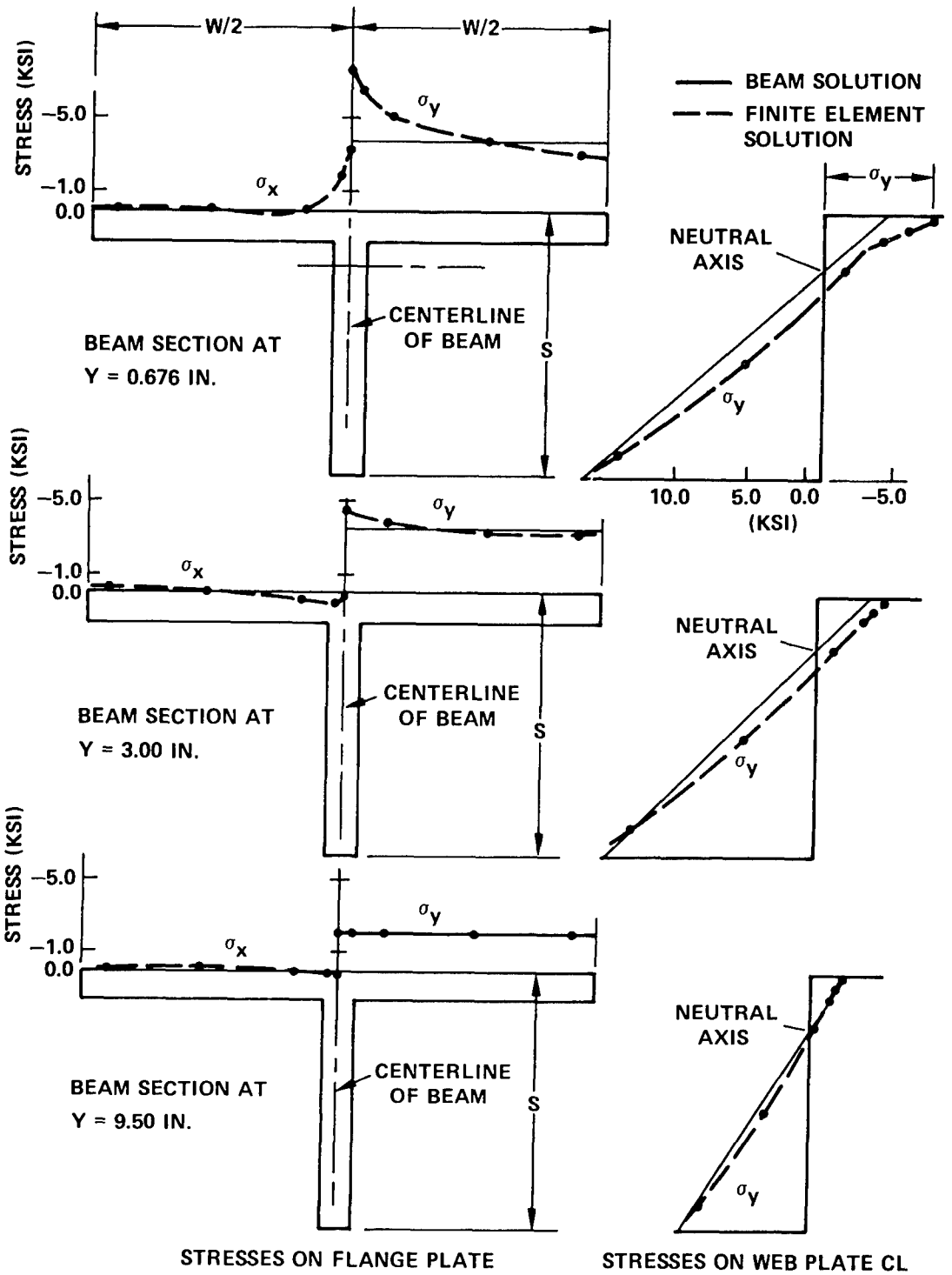

Figure 3.15 Distribution of normal stresses in a plate beam (example 3.2)

TABLE 3.3 LONGITUDINAL STRESSES (σ_y) IN A STIFFENED PLATE (EXAMPLE 3.2)

Table 3.3a Plate beam CX2

Y	σ_y (psi)								
(in.)	A1	A2	A3	B1	B2	B3	C1	C2	C3
0.676	−6252	−5103	−3479	− 6795	−5417	−3525	−7768	−6215	− 4127
3.000	−5989	−4945	−3529	− 5845	−4817	−3450	−5959	−5000	− 3755
5.324	−5557	−4471	−3074	− 5267	−4442	−3411	−5063	−4555	− 3961
9.500	−3683	−3180	−2547	− 3725	−3201	−2537	−3748	−3199	− 2498
16.500	−1155	− 979	− 752	− 1214	−1039	− 814	−1255	−1082	− 863
	D1	D2	D3	E1	E2	E3	F1	F2	F3
0.676	−9161	−6841	−4624	−10247	−7926	−5705	−2533	5995	18193
3.000	−6093	−5051	−4045	− 6575	−5528	−4519	−2225	5486	16420
5.324	−4773	−4496	−4048	− 4646	−4367	−3916	−2135	4687	14265
9.500	−3757	−3232	−2466	− 3639	−3113	−2347	−1126	3541	9634
16.500	−1200	−1050	− 854	− 1230	−1079	− 882	− 387	1203	3182

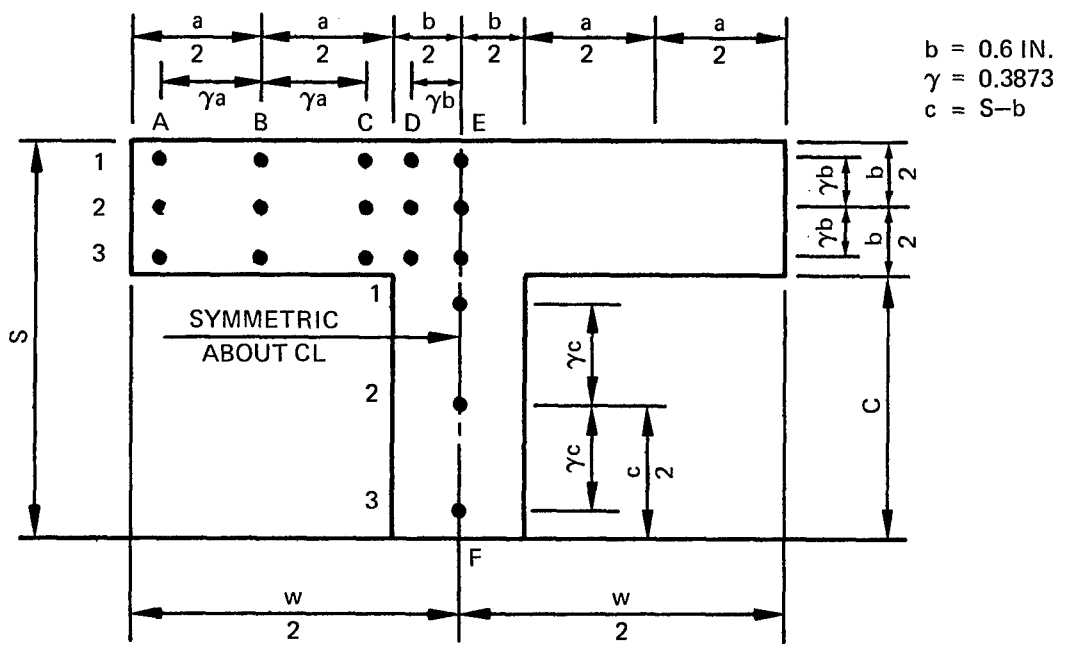

POSITION OF INTEGRATION POINTS USED IN STRESS TABULATION

Table 3.3b Plate beam CX3

Y	σ_y (psi)								
(in.)	A1	A2	A3	B1	B2	B3	C1	C2	C3
0.676	−3267	−2335	−1374	−3979	−2855	−1713	−5092	−3791	− 2480
3.000	−3428	−2378	−1311	−3487	−2511	−1531	−3878	−2995	− 2119
5.324	−3454	−2267	−1076	−3158	−2311	−1473	−3124	−2641	− 2177
9.500	−2015	−1629	−1244	−2151	−1717	−1283	−2268	−1803	− 1338
16.500	− 522	− 369	− 218	− 729	− 586	− 444	− 805	− 670	− 537
	D1	D2	D3	E1	E2	E3	F1	F2	F3
0.676	−6733	−4610	−2802	−7851	−5731	−3925	−1290	+5261	14095
3.000	−4173	−3260	−2491	−4656	−3745	−2980	−1004	4775	12740
5.324	−2771	−2668	−2541	−2619	−2519	−2393	−1045	4024	11155
9.500	−2265	−1872	−1455	−2130	−1736	−1317	− 299	3157	7605
16.500	− 713	− 587	− 445	− 747	− 621	− 479	− 84	1107	2505

Table 3.3c Plate beam CX4

Y	σ_y (psi)								
(in.)	A1	A2	A3	B1	B2	B3	C1	C2	C3
0.676	−48270	−37590	−26240	−48610	−37800	−26415	−49440	−38595	−27255
3.000	−43650	−34230	−24500	−43315	−33880	−24220	−43200	−33840	−24330
5.324	−39980	−30840	−21740	−40005	−30960	−22030	−39965	−31100	−22435
9.500	−21720	−21230	−15420	−27150	−21320	−15550	−27130	−21340	−15590
16.500	− 9105	− 7235	− 5325	− 9110	− 7207	− 5277	− 9160	− 7225	− 5270
	D1	D2	D3	E1	E2	E3	F1	F2	F3
0.676	−50570	−38710	−27930	−51640	−39780	−29005	−12830	+28290	70310
3.000	−43655	−33720	−24340	−44135	−34210	−24830	−11605	25560	63520
5.324	−39870	−31220	−22580	−39765	−31120	−22490	−10430	22850	56830
9.500	−26980	−21315	−15520	−26860	−21195	−15400	− 7100	16000	38930
16.500	− 9136	− 7210	− 5315	− 9162	− 7236	− 5343	− 2400	5389	13220

Table 3.3d Plate beam CX 5

Y	σ_y (psi)								
(in.)	A1	A2	A3	B1	B2	B3	C1	C2	C3
0.676	−18990	−11890	−4678	−19970	−12480	−4912	−21430	−13650	− 5854
3.000	−18160	−11120	−4005	−18240	−11220	−4189	−18680	−11820	− 4985
5.324	−17340	−10110	−2875	−17060	−10300	−3573	−17060	−10880	− 4788
9.500	−11110	− 7214	−3338	−11150	− 7246	−3347	−11165	− 7225	− 3284
16.500	− 3494	− 2229	− 963	− 3651	− 2371	−1094	− 3780	− 2493	− 1212
	D1	D2	D3	E1	E2	E3	F1	F2	F3
0.676	−23300	−14550	−6405	−24480	−15740	−7608	3672	31575	60930
3.000	−18720	−11970	−5518	−19255	−12515	−6070	3264	28630	55050
5.324	−16770	−11000	−5217	−16655	−10895	−5118	3011	25750	49160
9.500	−11200	− 7256	−3243	−11070	− 7123	−3108	2466	18135	33610
16.500	− 3653	− 2411	−1162	− 3687	− 2445	−1196	824	6105	11365

Table 3.3e Plate beam CX6

Y	σ_y (psi)								
(in.)	A1	A2	A3	B1	B2	B3	C1	C2	C3
0.676	−11410	−5070	1312	−12670	− 6115	461	−14560	− 7812	− 1070
3.000	−11550	−4975	1625	−11840	− 5470	906	−12750	− 6619	− 512
5.324	−11580	−4742	2110	−11230	− 5015	1183	−11510	− 5965	− 464
9.500	− 6985	−3453	77	− 7115	− 3641	− 167	− 7194	− 3776	− 354
16.500	− 1936	− 781	371	− 2351	− 1243	− 139	− 2517	− 1444	− 379
	D1	D2	D3	E1	E2	E3	F1	F2	F3
0.676	−17150	−9085	−1510	−18270	−10320	−2770	7100	31300	57310
3.000	−13360	−7155	−1157	−13900	− 7720	−1740	6500	28450	51670
5.324	−11400	−6279	−1159	−11280	− 6173	−1070	6020	25725	46180
9.500	− 7185	−3829	− 442	− 7055	− 3693	− 301	4514	18140	31640
16.500	− 2322	−1220	− 86	− 2364	− 1263	− 130	1573	6189	10650

CHAPTER 4

SPECIAL CLASS OF STRUCTURAL PROBLEMS

4.1 Introduction to Propeller Blades

Marine propeller blades present a special class of structural problems for which no generally satisfactory solution is presently available.

Screw propellers have been and remain the principal device used to move a ship. Despite their importance, there is little or no realistic approach by means of which an accurate evaluation of propeller stresses can be obtained. The problem lies in the difficulty of describing a blade design in simple mathematical terms. Until recently, existing methods applicable to screw propellers have relied heavily on practical experience and semitheoretical considerations. They provide a criterion of stress rather than the actual surface stresses.

In the past, analytical methods for predicting blade stresses have been developed by using "beam" theory or "shell" theory. The use of elementary beam theory was first proposed by Taylor (1933) who treated a blade as a cantilever attached to the propeller hub and recommended that stresses be calculated for cylindrical blade sections with the neutral axis parallel to the nose-to-tail (pitch) line* of the expanded section. Cantiliver beam theories have yielded reasonable estimates of stresses at certain selected points of relatively straight and narrow blades. Some modified forms of beam theory have been proposed (Rosengh, 1937; Hancock, 1942; Schoenherr, 1963; and McCarthy and Brock, 1969) for wide-bladed propellers with blade width to length ratios of about 1. The shell theory approach was first proposed by Cohen (1955) who treated a simplified propeller blade model as a helicoidal shell with variable thickness and infinite width. However, where this approach was applied to the problem of a shell of finite width, it was impossible to produce a solution to satisfy the boundary conditions. Later studies included those of Conolly (1961) and others (General Applied Science Laboratory, 1963 and Atkinson, 1968). Shell-type theories that incorporate broad assumptions do not appear to offer tangible improvement; moreover, they are rather involved for routine design purposes. Analytical methods that attempt to predict blade stresses on the basis of conventional mechanics have not been eminently successful.

Considerable effects have been devoted to measuring blade strains on both model and prototype propeller blades (Connolly, 1961; Wereldsma, 1965; McCarthy and Brock, 1969; and Boswell, 1969). In certain cases, good agreement was obtained between beam theory and measured data. However because of the large number of factors involved, care must be taken in drawing general conclusions from limited measurements.

---

*See Comstock (1967) for propeller terminology.

The trend in shipbuilding to full afterbodies for mammoth tankers and bulk carriers and to higher speeds for modern naval vessels has been accompanied by large irregularities and fluctuations in the wakes of such ships. As a result, the propeller experiences increased dynamic excitation and generates severe vibratory forces on the hull and propulsion system.

Propeller-induced vibration is one of the main problems associated with ship propulsion employing the screw propeller. The thrust derived from blade-lift force is unsteady when the blades rotate in a nonuniform velocity field behind the ship. The interaction of these unsteady forces with the hull and appendages causes the excitation of the ship by the propellers. Blade skew, high blade area ratios (i.e., wider blades), and a larger number of blades per shaft have all been tried in an attempt to reduce vibration. These innovations of propeller geometry drastically alter blade displacement patterns (Dhir and Sikora, 1971, 1972) and render the standard methods (i.e., beam theory) invalid. If blade design is to have a sound and rational basis, then an effective analytical method is clearly required so that suitable blade strength and stiffness can be determined for a specified ship-operation task.

The finite element procedure outlined in Chapter 3 will now be used to analyze a screw propeller in its more general form, that of a highly skewed propeller. The computed results will then be compared with measured displacements and stresses derived from measured strain under steady pressure loading. This study will provide the basis for further extending the procedure until it is eventually able to take unsteady stressing due to dynamic effects and fatigue behavior into account.

4.2 The Geometry of Skewed Propellers

When properly designed, skewed propeller can be used not only to significantly reduce propeller-induced vibrations but also to improve blade performance against cavitation, etc. (Cummings et al., 1972).

The general characteristics of screw propellers and their typical design process can be found in standard sources (Comstock, 1967). A propeller is usually described by a set of architectural drawings that show various views of the blade and a table that gives detailed dimensions of blade sections including pitch angles, camber ordinates, thickness ordinates, and chord lengths. These are useful input for propeller manufacturers. Application of the finite element procedure, however, requires analytical specification of the blade geometry, i.e., the definition of a suitable set of coordinate systems.

The highly skewed propeller is a recent innovation and its geometry is more involved. The skewed blade illustrated conceptually in Fig. 4.1 is shown in Fig. 4.2 as a projection on the XY plane. Two right-handed coordinate systems share the common $Z\,(=z)$ axis (coinciding with the centerline of the shaft). The common Z-axis is taken positive downstream from the propeller. One of the systems is the global rectangular coordinates (X, Y, Z), a ship-fixed frame of reference whose origin lies on the shaft centerline at a convenient longitudinal

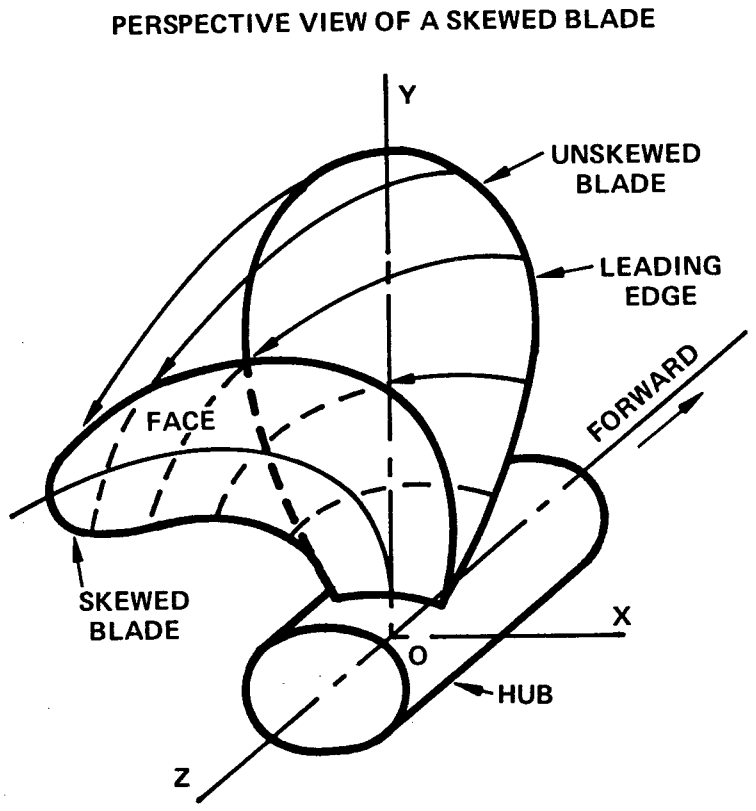

Figure 4.1 Global coordinate system used in definition of skewed propeller

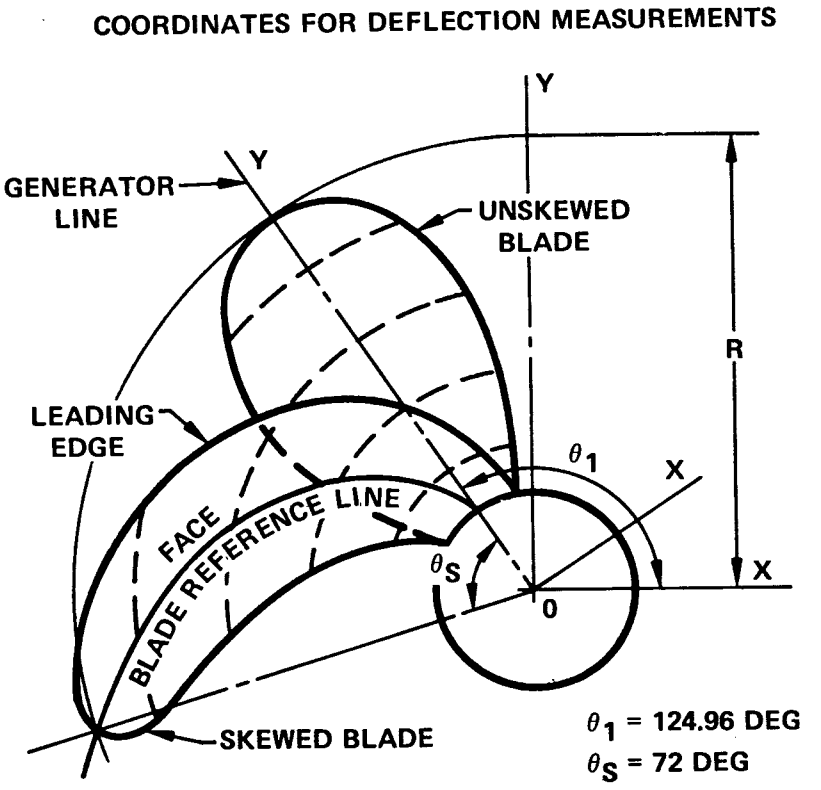

Figure 4.2 *XY*-plane projection of a propeller blade (looking forward)

location. The other is the local rectangular coordinates (x, y, Z) attached to the rotating propeller. The y-axis for this system passes through the midchord of a blade root section. The y-axis is tangent to the blade reference line and is also known as the generator line of the blade. The angular displacement of the generator line θ is measured in the XY-plane from the global axis OX, positive in a counterclockwise direction. The skew angle θ_S is the projected angle of the blade measured from the generator line oy.

Fig. 4.3 provides a pictorial view of the basic parameters that will provide a complete description of the blade geometry. The blade section, which lies on a cylindrical surface of radius ρ (usually expressed as percentage of blade tip radius R), is shown in Fig. 4.4 in developed view and with more details. The blade section has a reference line (also known as the geometric pitch line) which makes an angle ϕ_p with the xy-plane. The geometric pitch line usually lies along the nose-tail line (curved line CDE in Fig. 4.3).* This line joins the the leading point and the trailing point of the blade section cut by the cylinder (ρ = constant).

Another important baseline is the blade reference line which is defined as the line through an approximate "datum" point at each radius ($\rho \leq R$). This datum point is usually on the nose-tail line and will generally be the midchord point (Fig. 4.4).

On the cylindrical surface (ρ = constant), a coordinate system (ξ_1, ξ_2, ρ) is defined. The variable ξ_1 is measured from the datum point along the nose-tail line positive in the downstream direction (i.e. toward trailing edge). ξ_2 is normal to the ξ_1-line and points in the upstream direction (Fig. 4.3). The system is left-handed to permit blade section geometry to be specified in the conventional two-dimensional orientation such that positive camber is in the positive ξ_2-direction. Finally, the blade-section profile ordinates (see Fig. 4.4) $E_U = (Ec + Et)$ and $E_L = (Ec - Et)$ for $-0.5c \leq \xi_1 \leq 0.5c$ can be expressed in terms of the camberline function $E_c\,(\xi_1, \rho)$ and thickness function $E_t\,(\xi_1, \rho)$.

"Rake" and "skew" have been implemented frequently in modern propeller designs. They represent certain specialized departures from orthodox blade geometry in the fore- and-aft and transverse projected views, respectively. Unfortunately use of the terms has different meanings for different people. Therefore there is a need to have precise definitions of skew and rake because they are essential to a valid structural analysis.

Skew is defined as the sucessive "transverse displacement" of the blade sections along their respective pitch helices. A skew angle is a projected angle in the (transverse) XY-plane between a radial line (generator line, Fig. 4.2) from the centerline of the propeller hub through midchord of the blade root section and a radial line through midchord of the blade section in question. Each section of the blade has a different skew angle; the skew angle θ_s of the tip section is commonly used as the measure of the skew of the blade. Rake $\mathcal{R}$ is

---

*Space curve CDE is also known as pitch helix which is generated as the blade rotates; ϕ_p is the pitch angle.

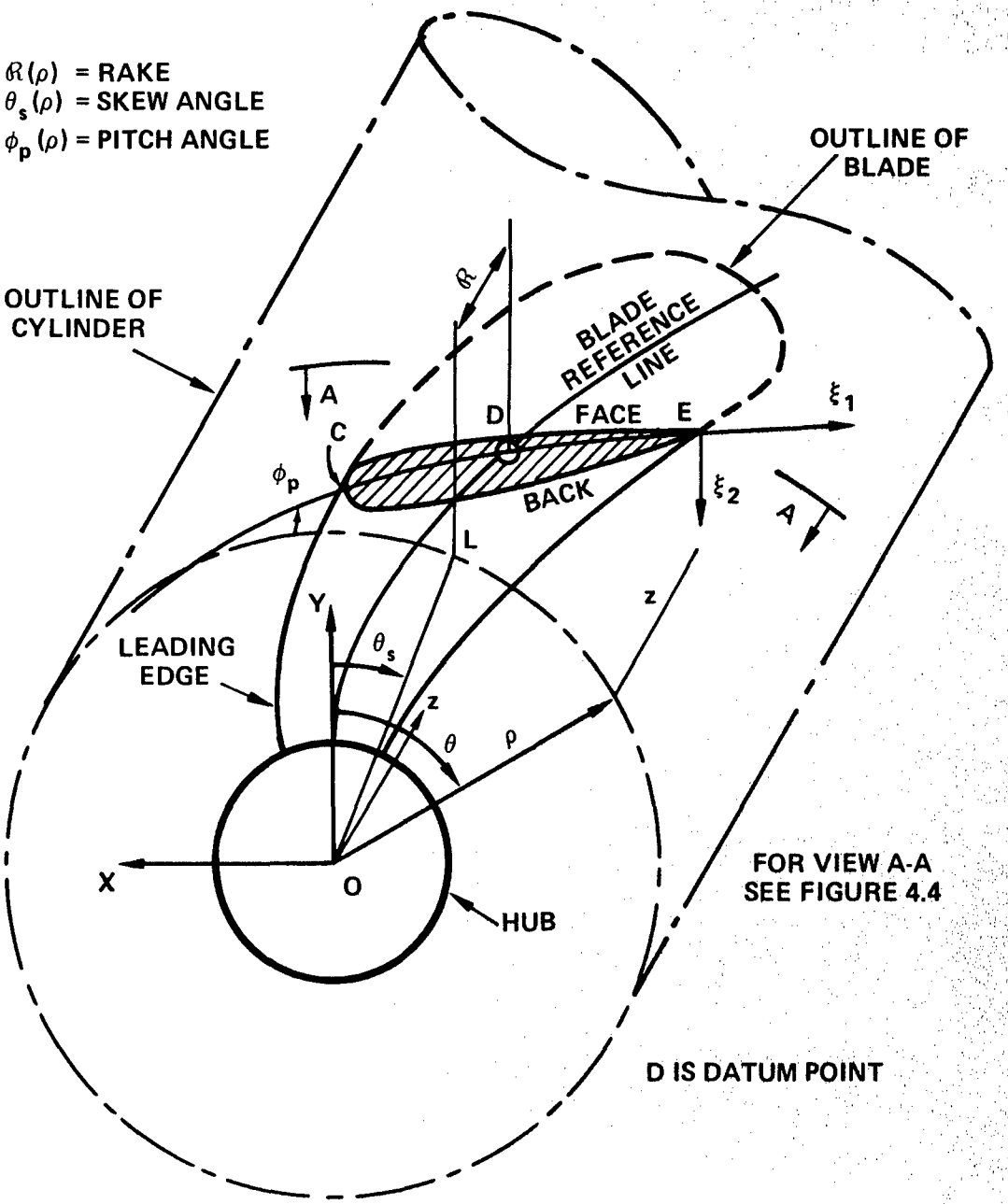

LINE CDE IS THE NOSE-TAIL LINE LOCATED ON A CYLINDRICAL SURFACE OF RADIUS ρ
(THE BLADE IS CUT BY A CYLINDRICAL SURFACE CONCENTRIC TO THE PROPELLER AXIS, LOOKING AFT)

Figure 4.3 Local blade coordinate system (x, y, Z) and (ρ, θ, Z)

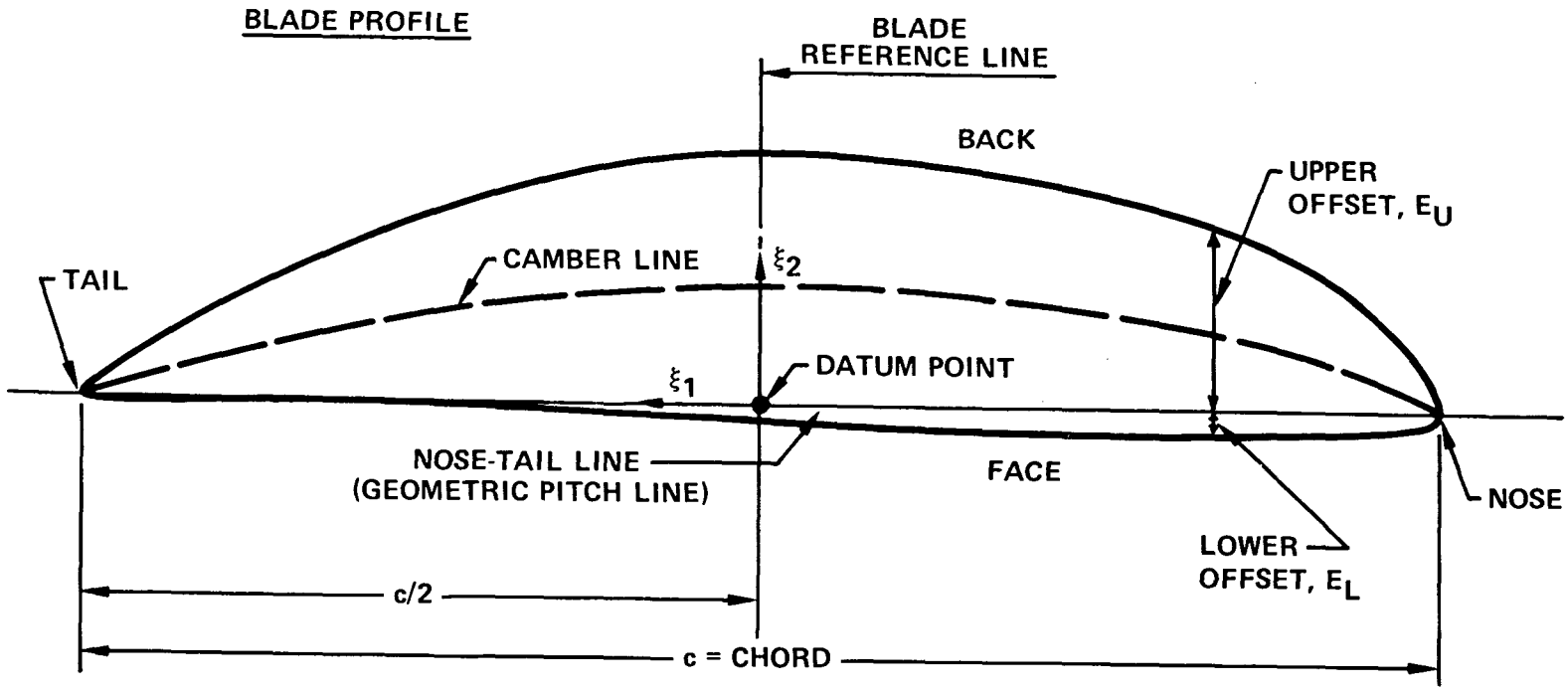

Figure 4.4 Developed view of cylindrical blade section

defined as the successive longitudinal "displacement" forward or aft of the blade sections from the radial reference line (Fig. 4.3). These definitions of rake and the skew allow the datum points along a blade reference line to be described analytically by $(\rho, \theta(\rho), \mathcal{R}(\rho))$ with respect to the local cylindrical coordinates (ρ, θ, z). Hence the blade section profile and complete blade surface can be constructed.

4.3 Experimental Data

Dhir and Sikora (1971) used holographic interferometry to predict the static deflections of a highly skewed marine propeller blade model. The aluminum blade model (Fig. 4.5) was loaded on one side by a specially designed pressure chamber under controlled air pressure (Boswell, 1969 and McCarthy and Brock, 1969). Applied pressure ranged from 0.032 to 0.192 psi. This holographic technique uses laser as the light source and is capable of measuring the displacement components of complex surfaces with a resolution of about 10 μ in.

The three-dimensional displacements were derived from fringe patterns formed in the holographic interferogram (Fig. 4.6). The interferometric fringes on an object were related to optical path differences, and the double exposure technique was used in its formation (in this case, air pressure was applied to the blade after the first exposure was made). Dark and light fringes represent contours of constant spatial blade displacements. As the applied pressure increases on the propeller blade, the fringe pattern remains essentially unchanged but the number of interference lines increases. The appropriate displacement components can be expressed as a linear combination of the "number" of fringes. This number is counted from the (fixed) hub to the point of interest (obtained through certain designated observation points on the hologram plate) and is multiplied by the wavelength of light used (λ = 5145 $\mathring{A}$; see Dhir and Sikora (1971, 1972) for a detailed description). Refined displacement data are obtained by applying the least-square approximation technique.

The fringe pattern of the hologram indicates that the contours of constant displacement line cross the circular lines which correspond to blade sections of constant radii at various angles. It is concluded that the deflections of the blade do not follow those predicted by the conventional method based on "beam" theory.

Strain measurements on a highly skewed model propeller blade were first made by Boswell (1969). The blade model of 2014 aluminum was similar to that shown in Fig. 4.5 except that it had a skew of 120 deg. Strain-gage rosettes were placed along cylindrical blade sections, five each at the 30-, 50-, and 70-percent radii and three at the 90-percent radius. The rosettes were so oriented that both tangential and radial strains were measured. For every gage located on the blade face, there was a corresponding gage on the blade back.

The blade was subjected to air pressure loading by using the technique described previously. The strain distribution was found to be radically different from that previously measured on unskewed blades. The high principal stresses occurred in a relatively narrow band which extended from near the trailing edge at the blade root to near the leading edge at the 90-percent radius.

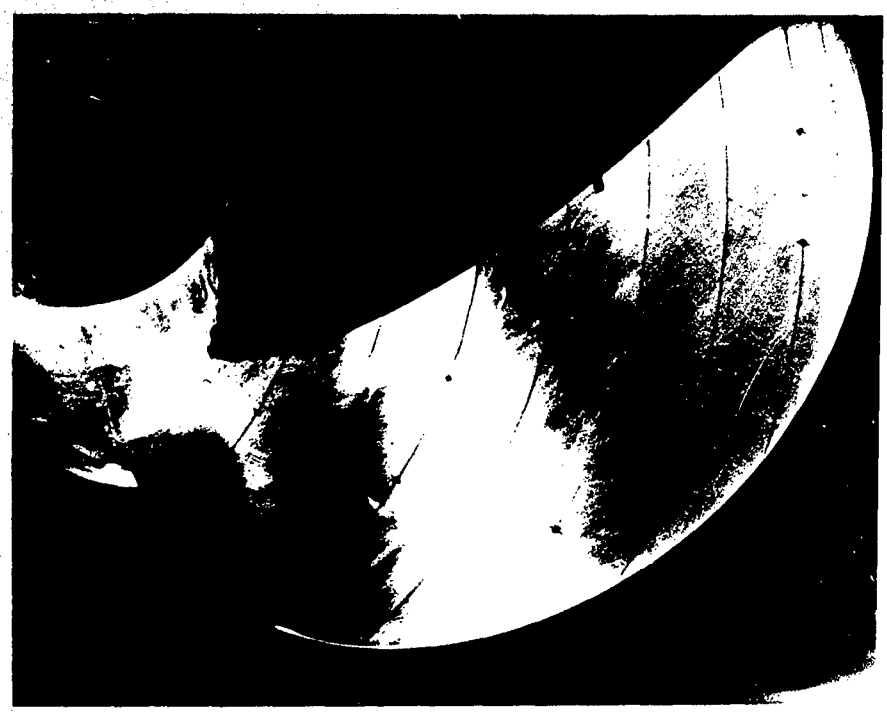

Figure 4.5 Aluminum blade model (looking forward)

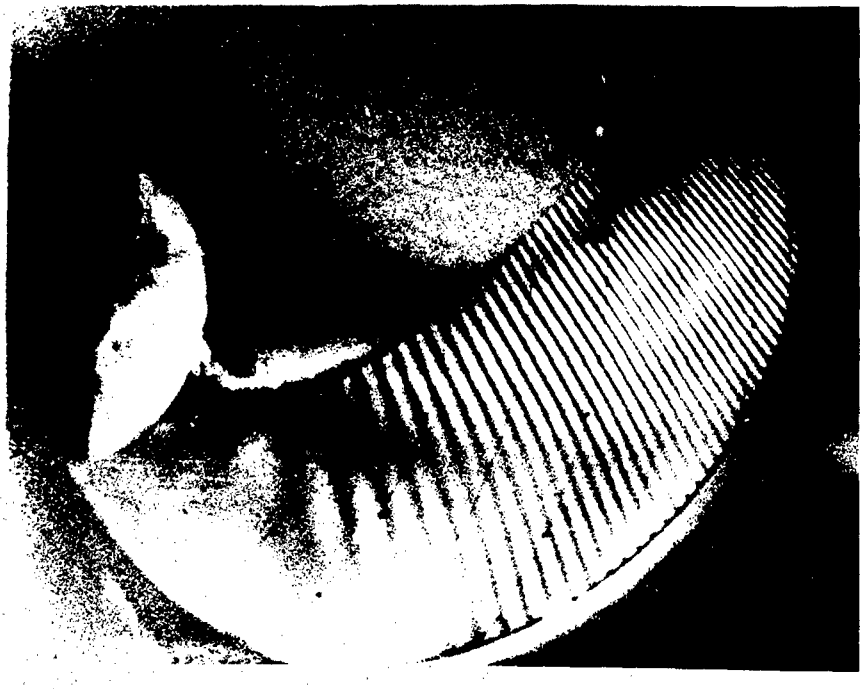

Figure 4.6 Interferometric fringe patterns of blade model with applied pressure (= 0.098 psi)

To obtain an experimental assessment of the effect of skew on blade stress distributions, Cumming et al. (1972) conducted further tests on a series of one-blade versions of propellers with various degrees of skew. These propellers were made of the same material and tested under the same loading conditions. Stress data for a blade with 72-deg skew were obtained for comparison with the present study.

4.4 Finite Element Analyses

The three-dimensional curved elements described in Chapter 3 are used here to predict static deflections and stresses for a highly skewed propeller blade. The blade model is subjected to a uniformly distributed pressure applied on its back surface, and its root section is assumed to be completely fixed. This loading is not the anticipated service load distribution but was selected to match the experimental conditions. Nonuniform loading represents no problem to the program and the influence of load distribution on stresses can be investigated.

The propeller blade used in the current analysis is one in a series of skewed, research model propellers that form part of a larger study undertaken to determine the blade strength and other performance characteristics of highly skewed propellers. Each propeller consists of five equally spaced 1/23-scale propeller blade models attached to a cylindrical hub (Fig. 4.7). The version selected for this study (Fig. 4.5) is a single-blade model of 2014 aluminum with a tip radius of 6 in. and a skew angle of 72 deg.

The geometry of the propeller blade has been shown to be rather involved (Section 4.2). Application of the finite element method requires precise coordinate definition of hundreds of discrete points that cover the complete top and bottom surfaces of the blade. A sizable effort is therefore involved in the calculation of coordinate data. Existing computer programs, e.g., Brockett (1972), and other data generation routines are designed to furnish the pertinent geometric description of a propeller blade. Nevertheless it is the responsibility of the user to discern the validity of his input.

The coordinate data for this analysis were obtained from the geometric output generated by a numerical machine* from input of blade section parameters. As seen from its plotted projection (Fig. 4.8), the coordinate data are for a blade situated in a position 144 deg ahead of the blade shown on Fig. 4.2. The geometric data have been checked visually and by graphical means; however, rigorous error analysis has not been attempted.

Discrete point locations on the blade surfaces were chosen for the element mesh network. Figure 4.9 shows that these points were along 20-, 30-, 40-, 50-, 60-, 70-, 80-, and 90-percent blade radius, etc. They are those points for which blade section geometries were given and for which displacement as well as strain measurements were made. It is only natural that these points are adopted in the formation of the element mesh.

---

*A numerically controlled machine used for model cutting.

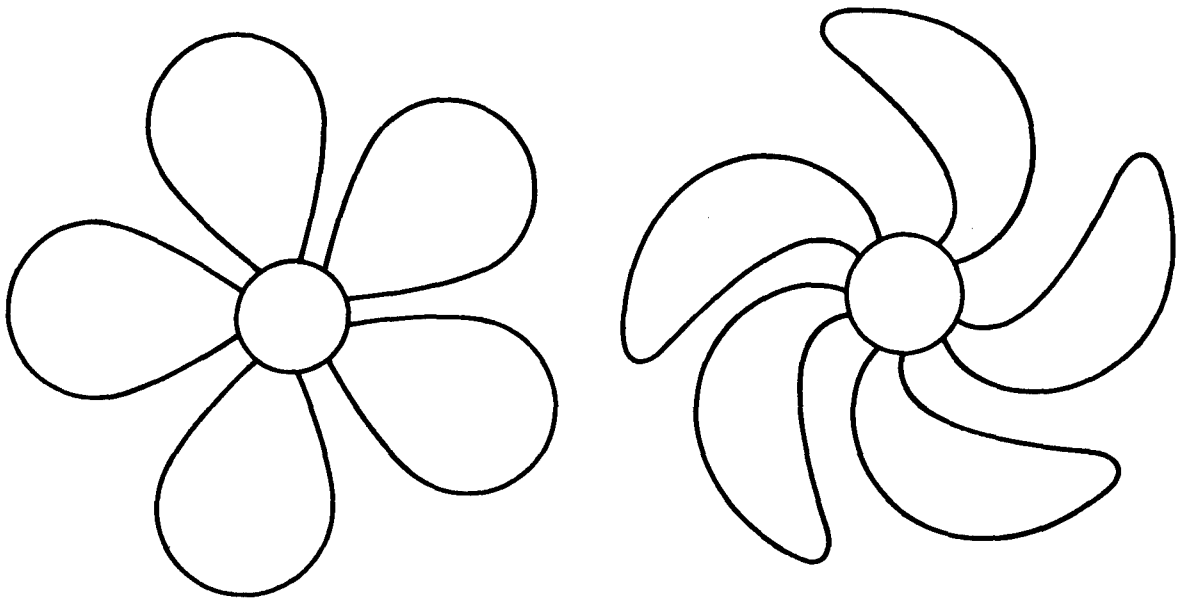

Figure 4.7 Projected view of two 5-bladed model propellers (model propeller series, part I)

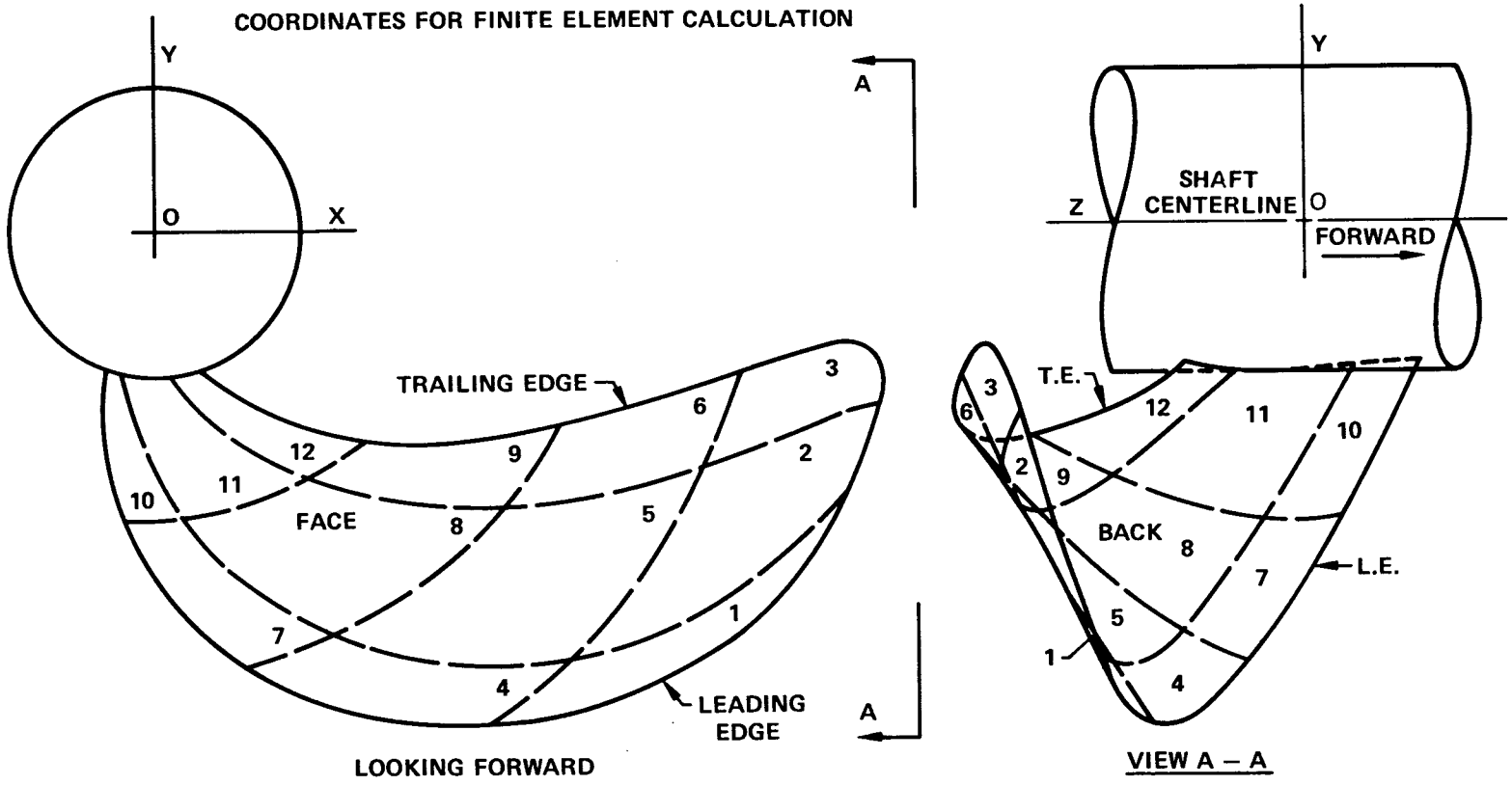

Figure 4.8 *XY*- and *YZ*-projections of a highly skewed propeller blade

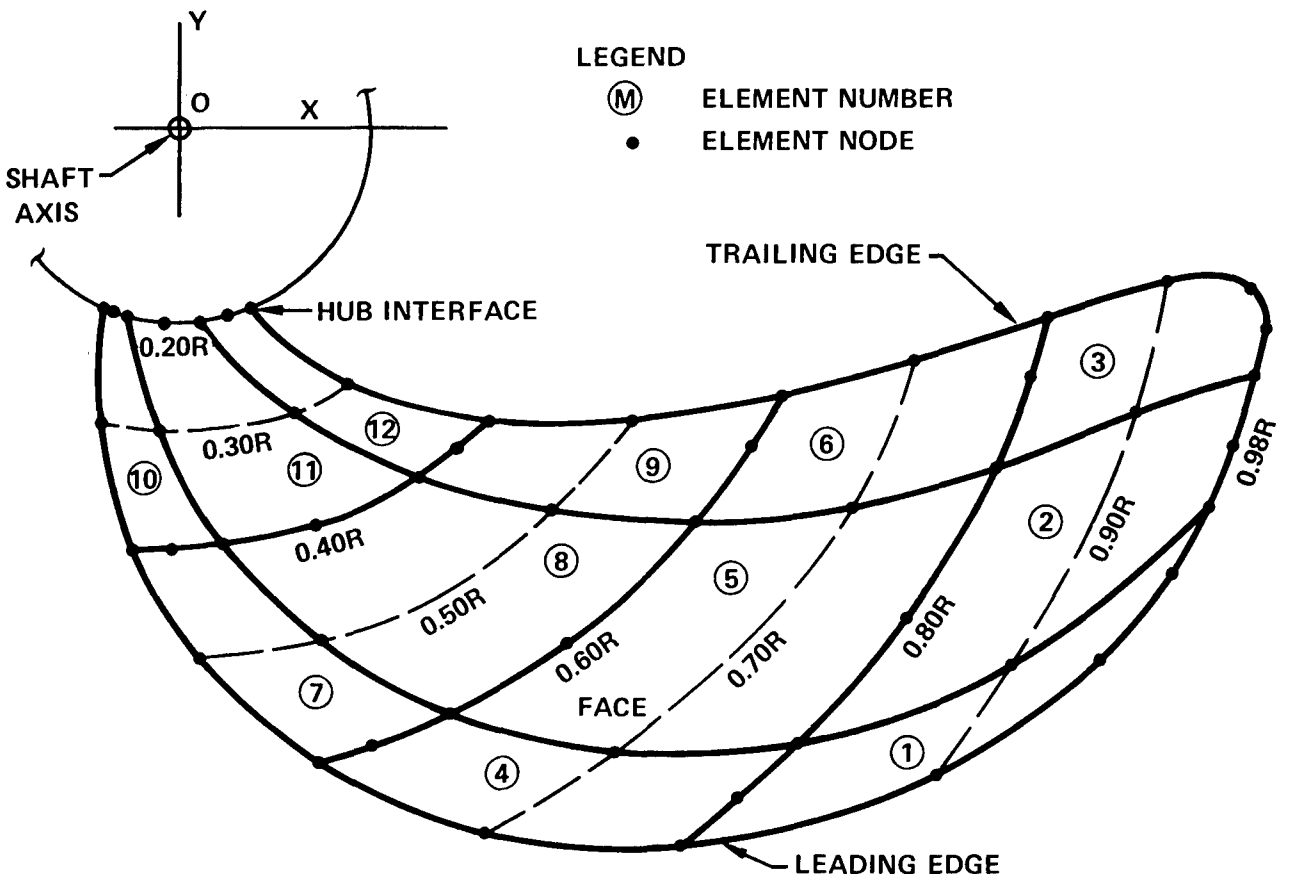

Figure 4.9 Curved solid element representation of a 72-degree skewed propeller blade

Three elements were used to span the chordwise dimension, and four elements were used to cross from the blade root to its tip. Available coordinate data and element shapes into which the blade was discretized were taken into consideration. This arrangement allowed a direct comparison of computed and measured deflections and immediate interpretation of the stress calculation.

To a large extent, the effectiveness of a finite element analysis depends on the appropriate element arrangement or mesh pattern which is used to represent a given structure. The maximum number of elements is generally dictated by considerations of accuracy and cost. The accuracy of the computed results increases as the number of elements increases, provided the resulting elements are not so numerous as to exceed computer size limitation or the number of computations are so large that round-off errors become a dominant factor. On the other hand, as the number of elements increases, the cost of input preparation and computation processing also increases. Obviously a compromise is required for these two competing considerations. There is no easy way to attain an optimal mesh; nevertheless, numerical instability or distortion of element performance can always be avoided by the discreet exercise of good engineering judgment. (Some basic rules for element mesh layout were described in Section 3.2.4.)

After element meshes were generated and nodes labeled, the elements were numbered in succession such that the maximum front width (see Section 3.4.2) was optimized. In the finite element method, each element is defined by a series of nodes to which it is connected and its orientation (with reference to local axes) is determined by the numbering sequence of the nodes defined in the incidence table. The first two numbered nodes serve to fix the direction of element axis-ξ. The element axis-η is taken in the direction of a line from the first to the third numbered node. The ζ-axis is obviously the remainder that completes the right-handed element axis system. In the case of propeller blades, nodes can be placed along a cylindrical surface so that the direction of local element axes ξ and η will respectively correspond to the radial and tangential axes of the cylindrical coordinates.

Note that the experimentally determined blade displacements were measured with respect to the global coordinates (X, Y, Z) when the blade was oriented in the position shown in Fig. 4.2, where $\theta_1 = 124.96$ deg. The finite elements coordinates obtained from the numerical machine provided a blade with the projection shown in Fig. 4.9, i.e., θ_1 was approximately 269 deg. Finite element calculations gave displacement components u and v that were 144 deg out of phase ($\Delta\theta_1$) with reference to measured displacements; accordingly, the element displacements were transformed so that they could be compared on the same scale (Fig. 4.10).

Computed displacements were obtained along the cylindrical blade section at 30-, 40-, 50-, 60-, 70-, 80-, and 90-percent radii in addition to points near the blade tip. Measured deflections by holographic interferometry are available at 50-, 70-, and 90-percent radii on blade face; these are plotted on Fig. 4.10.

Figure 4.10 Computed and measured displacements of a 72-degree skewed propeller

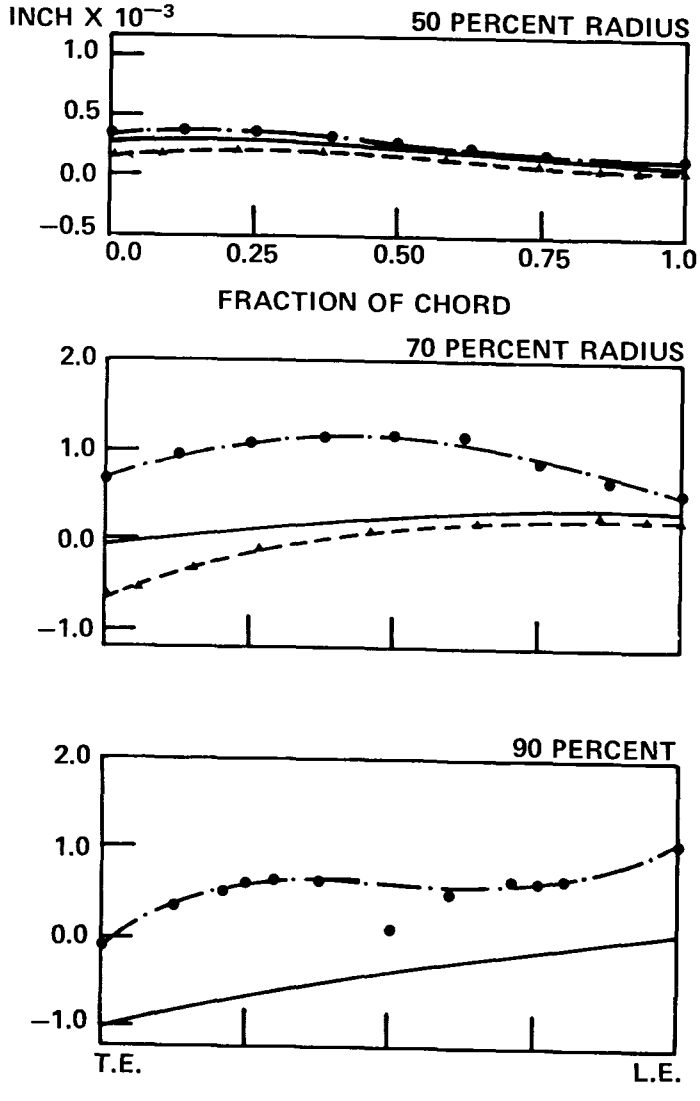

Figure 4.10a Displacement U

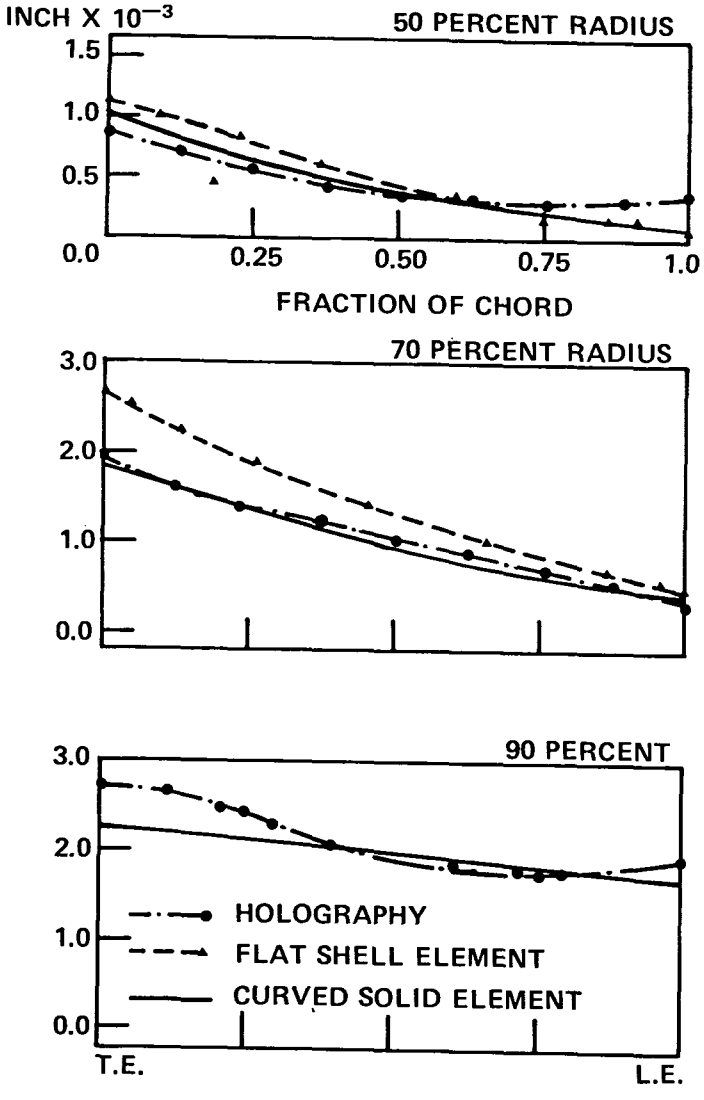

Figure 4.10b Displacement V

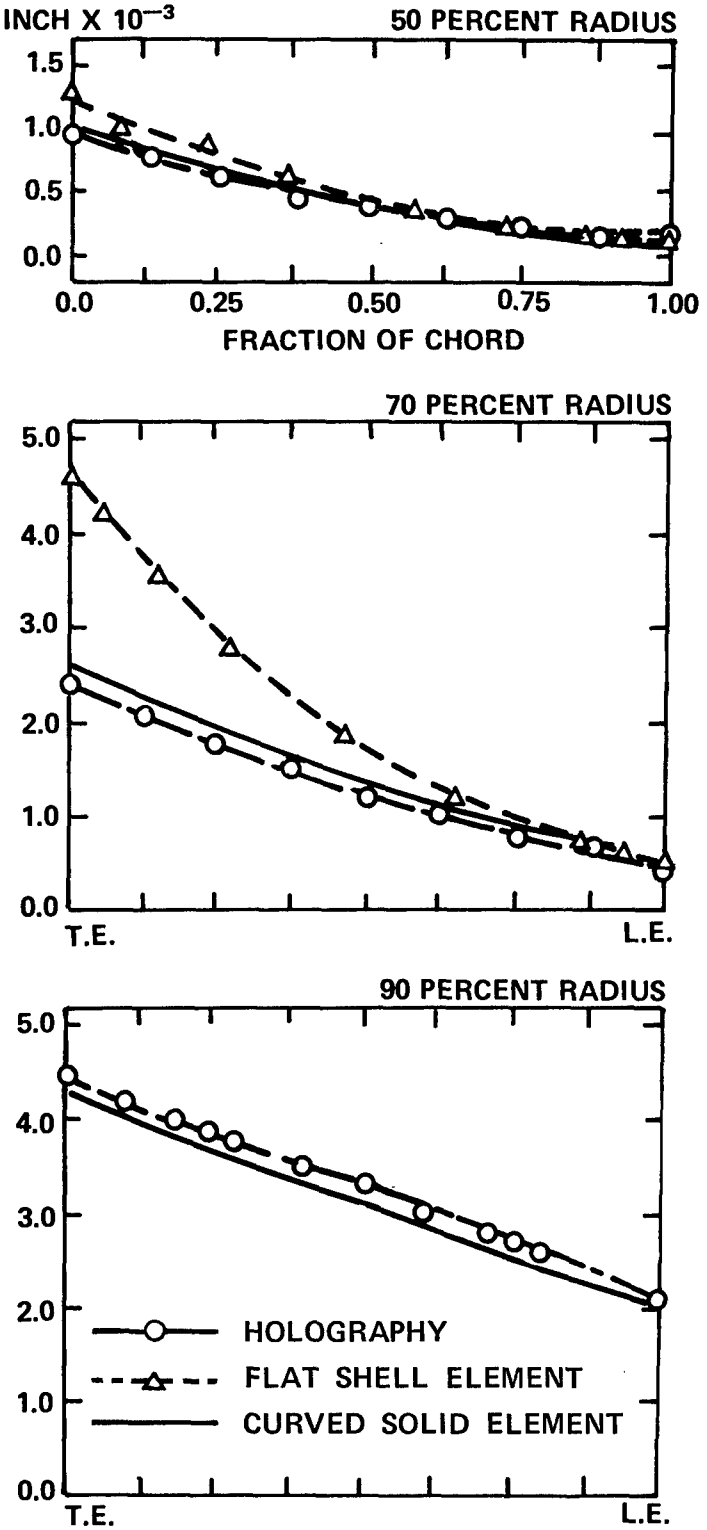

Figure 4.10c Displacement W

Computed stresses in global coordinates at interior points as well as surface points are given along cylindrical blade sections. Stress outputs are available at 30-, 50-, 70-, and 90-percent radii and at many intermediate points. Stress transformation is applied so that there is an option to print out stresses in local cylindrical coordinates. Stresses in most areas are obtainable by interpolation. Computed stresses are plotted on Fig. 4.11 together with stresses calculated from experimentally obtained strain data.

4.5 Discussion of Results

Fig. 4.10 shows that blade displacement component w (parallel to the centerline of the propeller shaft) was generally higher near the trailing edge than near the leading edge for various blade radii. This was also visible from the interferometric fringes (Fig. 4.6) representing displacement contours. This indicates that displacements for a skewed propeller are no longer parallel to the cylindrical blade sections. Clearly this is a case for which the assumption made by the conventional method of blade design is not valid. Further it is noted that the values for u and v are appreciably larger than the displacements that can be accounted for by beam theory. A new approach is needed to predict the elastic behavior of a skewed blade.

Genalis (1972) treated the skewed blade as a thin shell and idealized it as an assemblage of discrete, flat, triangular elements; see Fig. 4.12. Because of the complexity of blade profiles and blade surface curvatures (such as described previously in Figs. 4.3 and 4.7), a large number (about 270) of these shell elements is required in order to achieve a reasonable approximation to the geometry of a skewed blade. Thus a substantial effort is required for input preparations including all coordinates and load data. (It is conceivable here that the chance for input error is increased because of the huge amount of complex input data involved.) Furthermore, the proportions of the elements in the region near the hub are well beyond the limits of medium thick plate or thin shell theory from which such elements are derived. Computed displacements were given for the shell solution along cylindrical sections at 50- and 70-percent radii (Fig. 4.10).* The discrepancy of the numerical results as obtained from the flat thin shell element solution, from the isoparametric finite element, and from the experimental methods can be attributed (a) to the geometric mismatch introduced by using a flat shell element approximation for this highly curved blade of varying thickness and (b) to the breakdown in the suitability of thin shell theory in the region near the hub. (Furthermore, some inaccuracy may be attributable to rounding errors developed during the solution process.) The error accumulation evident in the thin shell element values at the 70-percent radius was even more pronounced at 90-percent radius.

*Any inaccuracy of input data will almost inevitably show up in the numerical results. The reliability of computed values may be increased if an appropriate algorithm is available to screen or to smooth input. The tolerance in the fabrication of the blade model was said to be within 5 percent.

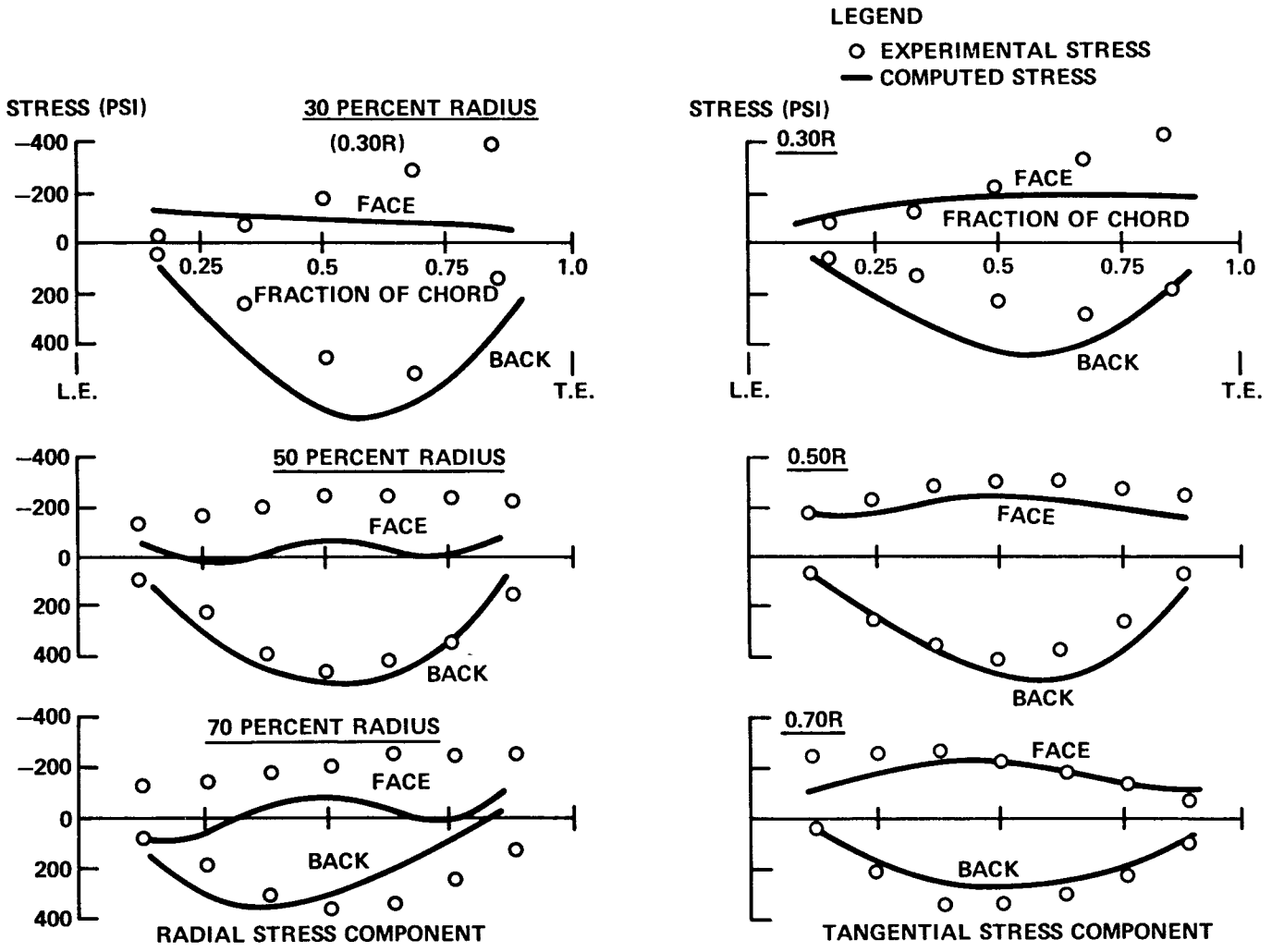

Figure 4.11 Stresses of a 72-degree skewed propeller

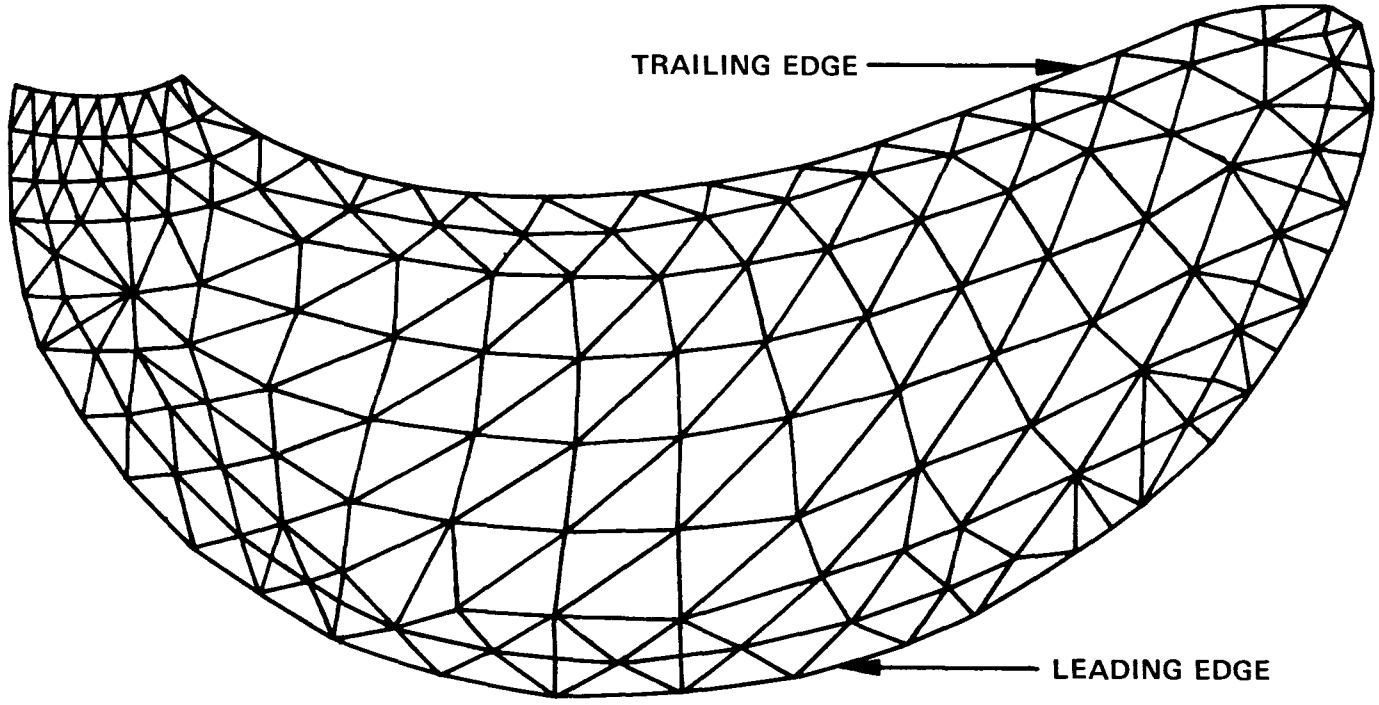

Figure 4.12 Flat shell element representation of a 72-degree skewed propeller blade

The changing profiles of the successive sections from blade root to tip indicate that the skewed blade has a more complicated geometry than an ordinary shell. The blade is treated in this study as a solid continuum of general shape. It is represented by 12 curved, three-dimensional elements which are capable of fitting smoothly in any complex surface. Use of these isoparametric elements gives a marked improvement in the numerical results (Fig. 4.10). Note that the computed displacements agree well with holographic measurements, especially in displacement component w, which is by far the dominant factor of the total blade displacement.

The largest disagreement between the displacements, which are solved for directly by the two procedures (experimental and isoparametric finite element) is in the horizontal displacement normal to the shaft axis. Possible causes for such a discrepancy might be slippage of the test specimen at the support bolts in the hub and mismatch of the isoparametric propeller surface with that of the test specimen. However, since the differences do not show up in the other displacements, the latter explanation seems unlikely. Furthermore, support slippage (i.e., a difference between the ideal clamped condition of the finite element method and the fixity achieved in the test) also seems unlikely because of the low pressures involved. If movement did occur, it would have to be rigid-body movement normal to the axis of the shaft rather than the more likely rotation or tipping. The final possibilities are errors in reading and/or possible binding of the blade model on the pressure seal.

The stress distribution of highly skewed propellers is expected to be unsymmetric and different from that of an unskewed blade. The maximum radial and tangential stresses are located away from midchord and toward the trailing edge in the main body of the skewed blade. The magnitude and distribution of stresses along the cylindrical chords of the blade varies with blade skew. Computed stresses were obtained from the same element mesh (Fig. 4.8) and were shown together with experimental stresses in Fig. 4.11. No calculated stress was given by the shell element program (Genalis, 1972).

A finer mesh would have given a closer approximation to the true stress distribution since convergence is assured with the compatible elements used in the current study.

In some of the experiments, difficulties were encountered in providing a precise fit between the test pressure chamber and the propeller blade; thus free movement of the blade edge was not always obtained. (It was also noticed in the course of stress evaluation for a series of test propellers with varying degree of skews that maximum stresses and blade skews did not increase in direct proportion.) It is desirable therefore to implement a comprehensive test program to enhance the reliability of experimental results. The stress agreement shown in Fig. 4.11 was much better on the back or loaded face than on the front face, and the agreement was better for tangential than for the radial stress. However, since the stresses are one step removed from direct measurement the agreement is not out of line even with these differences. Since the near tip region of the blade is a sensitive region, a higher density of elements in that

region seems desirable. Coupled with the comprehensive test program, this should assist in resolving the differences and provide an accurate delineation of the stresses.

The present procedure can generate an estimated complete stress field for the propeller and thus provide a detailed account of the stress distribution throughout the elastic body. This is of great practical value for a structure of unconventional configuration where conventional methods offer little guidance as to the pattern of stress distribution for a structure like a skewed propeller. A development that utilizes three-dimensional curved elements is probably the most effective analytical method currently available and is capable of representing both the complex blade geometry and load distributions with ease and validity.

CHAPTER 5

CONCLUSIONS AND RECOMMENDATIONS

The rational approach established herein represents the first step in a general solution of the propeller strength problem. A finite element displacement model is utilized to predict the behavior of an elastic body of arbitrary shape under static loads. Compatible solid elements in their general form are adopted. This formulation bypasses the constraints of simplifying assumptions and allows a closer approximation to the true structural configuration than is possible by most other approaches, for instance, by classical plate or shell theories. Solutions are subsequently obtained for displacements and internal stresses.

The numerical results obtained by the refined curved elements described in Chapter 3 are distinctly superior to those obtainable with commonly available simple triangular or rectangular finite elements. The displacements obtained for a complex structure under prescribed loading had a good degree of precision even with the relatively coarse mesh employed. This study confirms the findings of Clough (1969), Zienkiewicz (1971), etc. that significant improvements in element performance are obtainable when higher order displacement functions are employed in the element formulation.

For structures loaded so that a steep stress gradient prevails, stress predictions can always be improved by using progressingly finer element meshes. The element presented in this study showed a rapid rate of convergence as the mesh was refined.

The mapping technique, which is based on the application of the shape function as described in Chapter 3, provides an expedient way to describe the geometry of a general continuous surface. Load computations for a prescribed pressure distribution are therefore conducted in a routine manner.

The method developed in this study is particularly valuable to structures with arbitrary configurations such as skewed or unsymmetric geometry. Large savings in labor and computing costs are possible when the flat-plate or shell-element representation of a complex skewed body is replaced by curved elements. The present development offers perhaps the only realistic solution available for many difficult structural problems of a three-dimensional nature, such as a highly skewed propeller. The method now permits rapid solutions for structures with varying degrees of skew, camber, and loading.

Among other significant applications, the present procedure can provide stress calculations at the root section of a propeller blade joining the hub, at the complicated intersection of cylindrical walls such as a piping joint, and at the delicate interface area of a sandwich construction. Further extension of the analysis may include considerations of anisotropic material properties as well as the nonlinear or plastic behavior of materials (Gupta, 1971).

The current method provides a general and realistic solution to the structural problem of a propeller under static loads, and eventually a procedure can be evolved for the complete

solution of propeller strength under all possible service loads. Inasmuch as a propeller blade experiences varying vibratory forces in addition to the "nearly steady" thrust that is always present during ship operation, a dynamic analysis that includes an investigation of fatigue behavior of the complex ship component is naturally of prime significance.

It is recommended that the current procedure be extended to incorporate a mass matrix of the propeller blade and an auxiliary matrix to account for the effect of "added mass" of the fluid medium surrounding the blade. When a pressure-time relation for a propeller is prescribed, a complete dynamic response can be obtained by using a time increment numerical technique. The effect of damping may also be incorporated.

A sound propeller design is extremely important to the successful operation of a ship and has a significant bearing on its performance. It is worth noting that improved design methods including a dynamic analysis are being vigorously pursued by Norwegian and Japanese ship builders. To remain competitive, U.S. ship builders must take advantage of new technologies and be instrumental in their development.

ACKNOWLEDGMENT

The author expresses his thanks to staff members of the Department of Civil Engineering and of the Department of Computer Science at the University of Illinois, Urbana-Champaign, for helpful discussions throughout the course of the investigation. In particular, he is indebted to Dr. W. Schnobrich under whose direction the doctoral dissertation was prepared. Messrs S. Bakhrebah and K. Hirchert were of invaluable help in the development of the computational algorithm.

The Advanced Ship Division of the Department of Structural Mechanics, NSRDC, provided the funding for the study. Members of the Propulsor Technology Branch (Code 1544) and the Advanced Ship Division (Code 173) offered useful experimental information on propeller strength. The author is grateful to Messrs A. B. Stavovy and R. G. Allen and to Dr. J. C. Adamchak for their continued interest and support.

APPENDIX

EXAMPLE OF FORTRAN PROGRAM FOR NUMERICAL CALCULATION OF AN ELEMENT STIFFNESS MATRIX

An outline of the process is described in Section 3.2.2.

```
                              LIST
      SUBROUTINE STIFFB(XYZ,E,GNU,EK)
       COMMON /VAB7/ INTGER,ND,NPT,NPTS,NPZ
       COMMON /BLAV/GM(3,5),PX(3),PY(3),Q
C     SUBROUTINE TO CALCULATE THE STIFFNESS MATRIX SK FOR ISO-PARAMETRIC
C
C     SK=INTEGRAL PHI DV
C     WHERE PHI= B T X D X B
C
C          X... 0... 0...       X...=VECTOR OF PARTIALS OF N(I)
C          0... Y... 0...            WITH RESPECT TO X
C     B=   0... 0... Z...       Y...=VECTOR OF PARTIALS OF N(I)
C          Y... X... 0...            WITH RESPECT TO Y
C          0... Z... Y...       Z...=VECTOR OF PARTIALS OF N(I)
C          Z... 0... X...            WITH RESPECT TO Z
C                               0...=0 VECTOR
C     NOTE THAT THIS MATRIX MULTIPLICATION HAS BEEN DONE ALGEBRAICALLY
C     PRIOR TO CODING.
C
       REAL    CHI(20,3),CHIX(20),CHIY(20),CHIZ(20)
       EQUIVALENCE (CHIX(1),CHI(1,1)),(CHIY(1),CHI(1,2)),(CHIZ(1),CHI(1,3
      X))
       REAL    JAC(3,3),DETJ,J11,J12,J13,J21,J22,J23,J31,J32,J33
       EQUIVALENCE (JAC(1,1),J11),(JAC(1,2),J12),(JAC(1,3),J13),(JAC(2,1)
      X,J21),(JAC(2,2),J22),(JAC(2,3),J23),(JAC(3,1),J31),(JAC(3,2),J32),
      X(JAC(3,3),J33)
       DIMENSION EK(60,60),SK(60,60),XYZ(20,3)
       DIMENSION A(36),H(36),ISWK(60),TZ(3,3),S(13)
C     EQUIVALENCES ABOVE ARE LOGICALLY NECESSARY
C     EQUIVALENCES BELOW ARE USED ONLY TO CONSERVE SPACE
       EQUIVALENCE (S(1),JAC(1,1)),(S(1),S1),(S(2),S2),(S(3),S3),(S(4),S1
      XXXP1),(S(5),S1YYP1),(S(6),S2YYP1),(S(7),S2ZZP1),(S(7),S3ZZP1),(S(8
      X),ZZ),(S(10),CHIXI),(S(11),CHIYI),(S(12),CHIZI),(S(13),DETJ),(S(10
      X),SUM),(S(10),CON)
C
C      GAUSSIAN QUADRATURE CONSTANTS
       DATA A/
      1 0.00000 00000 0000, -0.57735 02691 8963,  0.57735 02691 8963,
      3-0.77459 66692 4148,  0.00000 00000 0000,  0.77459 66692 4148,
      4-0.86113 63115 9405, -0.33998 10435 8486,  0.33998 10435 8486,
      4 0.86113 63115 9405, -0.90617 98459 3866, -0.53846 93101 0568,
      5 0.00000 00000 0000,  0.53846 93101 0568,  0.90617 98459 3866,
      6-0.93246 95142 0315, -0.66120 93864 6627, -0.23861 91860 8320,
      6 0.23861 91860 8320,  0.66120 93864 6627,  0.93246 95142 0315,
      7-0.94910 79123 4276, -0.74153 11855 9939, -0.40584 51513 7740,
      7 0.00000 00000 0000,  0.40584 51513 7740,  0.74153 11855 9939,
      7 0.94910 79123 4276, -0.96028 98564 9754, -0.79666 64774 1363,
      8-0.52553 24099 1633, -0.18343 46424 9565,  0.18343 46424 9565,
      8 0.52553 24099 1633,  0.79666 64774 1363,  0.96028 98564 9754/
       DATA H/
      1 2.00000 00000 0000,  1.00000 00000 0000,  1.00000 00000 0000,
      3 0.55555 55555 5556,  0.88888 88888 8889,  0.55555 55555 5556,
      4 0.34785 48451 3745,  0.65214 51548 6255,  0.65214 51548 6255,
      4 0.34785 48451 3745,  0.23692 68850 5619,  0.47862 86704 9937,
      5 0.56888 88888 8889,  0.47862 86704 9937,  0.23692 68850 5619,
      6 0.17132 44923 7917,  0.36076 15730 4814,  0.46791 39345 7269,
      6 0.46791 39345 7269,  0.36076 15730 4814,  0.17132 44923 7917,
      7 0.12948 49661 6887,  0.27970 53914 8923,  0.38183 00505 0512,
      7 0.41795 91836 7347,  0.38183 00505 0512,  0.27970 53914 8928,
      7 0.12948 49661 6887,  0.10122 85362 9038,  0.22238 10344 5337,
      8 0.31370 66458 7789,  0.36268 37833 7836,  0.36268 37833 7836,
      8 0.31370 66458 7789,  0.22238 10344 5337,  0.10122 85362 9038/
C      SIZE CONSTANTS
```

```
      DATA      NPTS/20/,LNPTS/40/,KSIZE/60/,KSIZEM/59/
C     CHECK NPT AND CORRECT IF NECESSARY
      IF(NPT.GT.8)NPT=8
      IF(NPT.LT.1)NPT=1
      IPT=NPT*(NPT-1)/2
      IPZ= NPZ*(NPZ-1)/2
C     ZERO MATRIX
      CALL ZEROZ(GM,15)
      CALL ZEROZ(SK,3600)
      AA=1.-GNU
      BB=GNU
      CC=(1.-2.*GNU)/2.
      DK=E/((1.+GNU)*(1.-2.*GNU))
      NPZ1= NPZ+1
      NPZ2= NPZ+2
C     LOOPS OVER XX,YY, AND ZZ FOR GAUSSIAN QUADRATURE OVER VOLUME
      DO 20 IXX=1,NPT
      XX=A(IXX+IPT)
      HXX=H(IXX+IPT)
      DO 20 IYY=1,NPT
      YY=A(IYY+IPT)
      HXXHYY=H(X*H(IYY+IPT)
      DO 22 IZZ=1,NPZ2
      ZZ= A(IZZ+IPZ)
      IF(IZZ.EQ.NPZ1) ZZ=-1.0
      IF(IZZ.EQ.NPZ2) ZZ=1.0
C     CALCULATE PARTIALS OF N(I) WITH RESPECT TO XX, YY, AND ZZ
      DO 30 I=1,2
      S1=2*I-3
      S1XXP1=S1*XX+1.
      S1YYP1=S1*YY+1.
      DO 30 J=1,2
      S2=2*J-3
      JP=2*(J-1)+I
       S2YYP1=S2*YY+1.
      S2ZZP1=S2*ZZ+1.
      CHIX(JP+8)=S1*0.25*S2YYP1*(1.-ZZ**2)
      CHIY(JP+8)=S2*0.25*S1XXP1*(1.-ZZ**2)
      CHIZ(JP+8)=-0.5*ZZ*S1XXP1*S2YYP1
      CHIX(JP+12)=S1*0.25*S2ZZP1*(1.-YY**2)
      CHIY(JP+12)=-0.5*YY*S1XXP1*S2ZZP1
      CHIZ(JP+12)=S2*0.25*S1XXP1*(1.-YY**2)
      CHIX(JP+16)=-0.5*XX*S1YYP1*S2ZZP1
      CHIY(JP+16)=S1*0.25*S2ZZP1*(1.-XX**2)
      CHIZ(JP+16)=S2*0.25*S1YYP1*(1.-XX**2)
      DO 30 K=1,2
      S3=2*K-3
      KP=4*(K-1)+JP
      S3ZZP1=S3*ZZ+1.
      CHIX(KP)=S1*0.125*S2YYP1*S3ZZP1*(S1*2.*XX+S2*YY+S3*ZZ-1.)
      CHIY(KP)=S2*0.125*S1XXP1*S3ZZP1*(S2*2.*YY+S1*XX+S3*ZZ-1.)
30    CHIZ(KP)=S3*0.125*S1XXP1*S2YYP1*(S3*2.*ZZ+S1*XX+S2*YY-1.)
C     CALCULATE JAC=PARTIALS X XYZ
      DO 40 I=1,3
      DO 40 J=1,3
      SUM=0.0
      DO 41 K=1,NPTS
41    SUM=SUM+CHI(K,I)*XYZ(K,J)
40    JAC(I,J)=SUM
      DO 42 L=1,3
      PX(L)= JAC(1,L)
42    PY(L)= JAC(2,L)
      CALL SURFN(TZ)
C     INVERT JAC AND CALCULATE DET JAC
      CALL MINVDP(JAC,3,3,DETJ,ID,IEXP)
      IF(ID-1) 31,31,33
```

```
   33  PRINT 91, ID
   91  FORMAT (1X,I10,*TH ORDER PRONCIPAL MINOR IS ZERO* )
C
       STOP
   31  CONTINUE
C     CALCULATE PATIALS WITH RESPECT TO X, Y, AND Z FROM PARTIALS WITH
C     RESPECT TO XX, YY, AND ZZ BY
C     NEW.PARTIALS=JAC INVERSE X OLD.PARTIALS
       DO 50 I=1,NPTS
       CHIXI=CHIX(I)
       CHIYI=CHIY(I)
       CHIZI=CHIZ(I)
       CHIX(I)=J11*CHIXI+J12*CHIYI+J13*CHIZI
       CHIY(I)=J21*CHIXI+J22*CHIYI+J23*CHIZI
50     CHIZ(I)=J31*CHIXI+J32*CHIYI+J33*CHIZI
       WRITE(4) IXX,IYY,IZZ,(CHIX(I),CHIY(I),CHIZ(I),I=1,NPTS),TZ,ZZ
       IF(IZZ.GT.NPZ) GO TO 22
C
C     CALCULATE INTEGRATION CONSTANT
       CON=DETJ*DK*HXXHYY*H(IZZ+IPT)
C     DO SUMMATION FOR HALF OF MATRIX
       DO 60 I=1,NPTS
       X1=CHIX(I)
       Y1=CHIY(I)
       Z1=CHIZ(I)
       DO 60 J=1,NPTS
       X2=CHIX(J)
       Y2=CHIY(J)
       Z2=CHIZ(J)
       SK(I,J+NPTS)=SK(I,J+NPTS)+CON*(BB*X1*Y2+CC*Y1*X2)
       SK(I,J+LNPTS)=SK(I,J+LNPTS)+CON*(BB*X1*Z2+CC*Z1*X2)
       SK(I+NPTS,J+LNPTS)=SK(I+NPTS,J+LNPTS)+CON*(BB*Y1*Z2+CC*Z1*Y2)
       IF(J.LT.I) GO TO 61
       X2=X1*X2
       Y2=Y1*Y2
       Z2=Z1*Z2
       SK(I,J)=SK(I,J)+CON*(AA*X2+CC*(Y2+Z2))
       SK(I+NPTS,J+NPTS)=SK(I+NPTS,J+NPTS)+CON*(AA*Y2+CC*(X2+Z2))
       SK(I+LNPTS,J+LNPTS)=SK(I+LNPTS,J+LNPTS)+CON*(AA*Z2+CC*(X2+Y2))
61     CONTINUE
60     CONTINUE
  22   CONTINUE
       CALL GLOAD (XX,YY,HXXHYY,XYZ)
20     CONTINUE
       RETURN
       END
```

REFERENCES

The following initialisms are used in the list of references:

AIAA American Institute of Aeronautics and Astronautics
ASCE American Society of Civil Engineers
IUTAM International Union of Theoretical and Applied Mechanics
NSRDC Naval Ship Research and Development Center
RINA Royal Institute of Naval Architecture
SNAME Society of Naval Architects and Marine Engineers
TAPIR Technical University of Norway
WPAFB Wright-Patterson Air Force Base

Abrahamsen, E., "Structural Design Analysis of Large Ships," Trans., SNAME (1970).

Adamchak, J. C., "User's Manual for the Modified Finite Element Program FINEL," NSRDC Report 3609 (Nov 1970).

Ahmad, S. et al., "Curved Thick Shell and Membrane Elements with Particular Reference to Axisymmetric Problems," Proc. Conference on Matrix Methods in Structural Mechanics, Air Force Institute of Technology, WPAFB (Oct 1965).

Ahmad, S. et al., "Analysis of Thick and Thin Shell Structures by Curved Finite Elements," Int. J. Num. Meth. Eng., Vol. 2 (1970).

Araldsen, P. O. and O. Egeland, "General Description of SESAM-69 (Super Element Structural Analysis Modules) European Shipbuilding Vol. No. 2 (1971).

Arantes e Oliveira, E. R., "Theoretical Foundations of the Finite Element Method," Int. J. of Solids and Structures, Vol. 4, pp. 929–952 (1968). See also later comments by B. M. Irons et al., in this Journal; Vol. 6, pp. 695–697 (1970).

Argyris, J. H., "Energy Theorems and Structural Analysis, Part I, General Theory," Aircraft Engineering Vol. 26 (Oct–Nov 1954) and Vol. 27 (Feb–May 1955).

Argyris, J. H., "Continua and Discontinue," Proc., Conference on Matrix Methods in Structural Mechanics, WPAFB (Oct 1965).

Atkinson, P., "On the Choice of Method for the Calculation of Stress in Marine Propellers," Trans. RINA (1968).

Bazeley, G. P. et al., "Triangular Elements in Bending–Conforming and Nonconforming Solutions," Proc., Conference on Matrix Methods in Structural Mechanics, WPAFB (Oct 1965).

Boswell, R. J., "Static Stress Measurements on a Highly Skewed Propeller Blade," NSRDC Report 3247 (Dec 1969).

Brockett, T. E., "Propeller Perturbation Problem," NSRDC Report 3880 (Oct 1972).

Chu, T. C. and W. C. Schnobrich, "Finite Element Analysis of Translational Shells," University of Illinois, Civil Engineering Studies, SRS 368 (1970).

Clough, R. W., "Comparisons of Three-Dimensional Finite Elements," Conference on the Application of Finite Element Methods in Civil Engineering, Vanderbilt University; Proc. published by ASCE (1969).

Cohen, J. W., "On Stress Calculations in Helicoidal Shells and Propeller Blades," Netherlands Research Center TNO for Shipbuilding and Navigation, Delft, Report 21S (Jul 1955).

Comstock, J. P. (Editor), "Principles of Naval Architecture," SNAME, New York, N. Y. (1967).

Conolly, J. E., "Strength of Propellers," Trans. RINA, Vol. 10 (1961).

Courant, R., "Variational Methods for the Solution of Problems of Equilibrium and Vibration," Bull. Am. Math. Soc., Vol. 49 (1943).

Cox, G. G. and W. B. Morgan, "The Use of Theory in Propeller Design," Meeting of Chesapeake Section, SNAME (Feb 1972).

Cumming, R. A. et al., "Highly Skewed Propellers," Trans. SNAME (1972).

Dainora, J., "An Evaluation of the STARDYNE Systems," ONR Symposium on Numerical and Computer Methods in Structural Mechanics, Urbana, Illinois (Sep 1971).

Dhir, S. K. and J. P. Sikora, "Holographic Displacement Measurements on a Highly Skewed Propeller Blade," NSRDC Report 3680 (Aug 1971).

Dhir, S. K. and J. P. Sikora, "Holographic Analysis of a General Displacement Field," Proc. of Symposium on the Engineering Application of Holography, Los Angeles (16 Feb 1972).

Dunne, P. C., "Complete Polynomial Displacement Fields for the Finite Element Method," J. Roy. Aeron. Soc. Vol. 72, pp. 245–246 (1968). See also comments by B. M. Irons et al., on pp. 709–711 of that issue.

Ergatoudis, J. et al., "Curved, Isoparametric, Quadrilateral Elements for Finite Element Analysis," Int. J. Solids and Structures, Vol. 4 (1968).

Felippa, C. A., "Refined Finite Element Analysis of Linear and Nonlinear Two-Dimensional Structures," Univ. of Calif., Berkeley, UCSEL Report 66-22 (1966).

Flugge, W., "Stresses in Shell," Springer-Verlag, Berlin (1960).

Fraeijs deVeubeke, B., "Upper and Lower Bounds in Matrix Structural Analysis," AGARD-ograph 72, Pergamon Press (1964).

Gallagher, R. H., "Large-Scale Computer Programs for Structural Analysis," ASME Annual Winter Meeting, New York City (Nov 1970).

Gallagher, R. H. et al., "Stress Analysis of Heated Complex Shapes," J. Aerospace Sc. (1962).

Genalis, P., "Structures Department Status Report on Propeller Strength Research," NSRDC Technical Note SD 730-229 (1972).

General Applied Science Laboratory, Inc., "Propeller Blade Vibration and Stress Analysis Program," Westbury, N. Y. (June 1963).

Gupta, A. K. et al., "Elasto-Plastic Analysis of Three-Dimensional Structures Using the Isoparametric Element," University of Illinois, CE Studies, SRS 381 (1971).

Hammer, P. C., "Numerical Evaluation of Multiple Integrals," in "On Numerical Approximation," edited by R. E. Langer, The University of Wisconsin Press, Madison (1959).

Hancock, N., "Blade Thickness of Wide-Bladed Propellers," Trans. INA Vol. 83 (1942).

Hartung, R. F., "An Assessment of Current Capability for Computer Analysis of Shell Structures," WPAFB, AFFDL-TR-70 (Feb 1970).

Herrmann, L. R., "Finite Element Bending Analysis of Plates," Proc. ASCE Vol. 93, EM5 (1967).

Hrenikoff, A., "Solution of Problems in Elasticity by the Framework Method," J. Appl. Mech. Vol. 8 (1941).

International Ship Structures Committee, "ISD/ISSC Symposium on Finite Element Techniques," edited by M. Sorensen, University of Stuttgart (Jun 1969).

Irons, B. M., "Engineering Application of Numerical Integration in Stiffness Method," J. AIAA (1966).

Irons, B. M., "A Frontal Solution Program for Finite Element Analysis," Int. J. Num. Meth. Eng. No. 2 (1970).

Irons, B. M. and K. J. Draper, "Inadequacy of Nodal Connections in a Stiffness Solution for Plate Bending," J. AIAA 3.5 (1965).

Jennings, A. and A. D. Tuff, "A Direct Method for the Solution of Large Sparse Symmetric Simultaneous Equations," in "Large Sparse Sets of Linear Equations," edited by J. K. Reid, Academic Press (1971).

Kamel, H. A. et al., "An Automated Approach to Ship Structure Analysis," Trans. SNAME Vol. 77 (1969).

Kohnke, P. C. and W. C. Schnobrich, "A Finite Element Analysis of Eccentrically Stiffened Circular Cylindrical Shells," University of Illinois, CE Studies, SRS 351 (1969).

Langefors, B., "Theory of Aircraft Structure Analysis," Zeitschrift fur Flugwissenschaften Vol. 6 (Oct 1958).

Logcher, R. D. and C. M. Sturman, "STRUDL-A Computer System for Structural Design," J. Struct. Div. ASCE Vol. 92 (Dec 1966).

Ma, J. H., "Elastic Analysis of a Midship Compartment by the Finite Element Method," NSRDC Technical Note SML 131 (Apr 1969).

MacNeal, R. H. and G. W. McCormick, "The NASTRAN Computer Program for Structural Analysis," The MacNeal-Schwendler Corporation (1967).

Mallett, R. H. and S. Jordan, "MAGIC An Automated General Purpose System for Structural Analysis: Engineers' Manual," WPAFB AFFDL TR-68-56 (Jan 1969).

McCarthy, J. H. and J. S. Brock, "Static Stresses in Wide-Bladed Propellers," NSRDC Report 3182 (Sep 1969).

Mehrain, M., "Finite Element Analysis of Skew Composite Plate," Ph. D. Thesis, University of California, Berkeley (1967).

Melosh, R. J., "Basis of Derivation of Matrices for the Direct Stiffness Method," J. AIAA (Jul 1963).

Melosh, R. J. et al., "Efficient Solution of Load-Deflection Equations," J. Struct. Div. ASCE ST 4 pp. 661–676 (1969). See also comments in later issues of this Journal: J. S. Campbell et al., ST 12 (1969); V. B. Venkayya and B. M. Irons, ST 1 (1970); S. S. Tezcan et al., ST 2 (1970); S. Klein, ST 5 (1970); and Closure in ST 2 (1971).

Melosh, R. J. et al., "Structural Analysis and Matrix Interpretive Systems (SAMIS)- Program Report," Jet Propulsion Laboratory TM 33-307 (Dec 1966).

Moe, J. and A. Tonnesen, "Model Experiments and Finite Element Analysis of Stress in an Open Ship," European Shipbuilding Vol. XV (1966).

National Aeronautics and Space Administration, "The NASTRAN Theoretical Manual," edited by R. H. MacNeal, NASA SP-221 (Oct 1969).

Paulling, J. R., "The Analysis of Complex Ship Structures by the Finite Element Technique," J. Ship Res. (Dec 1964).

Pawsey, S. F., "The Analysis of Moderately Thick to Thin Shells by the Finite Element Method," University of California, Berkeley Civil Engineering Department SESM Report 70-12 (1970).

Przemieniecki, J. S. et al., "Proceedings of Conferences on Matrix Method in Structural Mechanics," WPAFB (1965, 1968, 1971).

Roren, E. M. Q., "Finite Element Analysis of Ship Structures," in "Finite Element Methods in Stress Analysis," edited by Holand and Bell, TAPIR, Trondheim, Norway (1969).

Rosingh, W. H. C. E., "Design and Strength Calculations for Heavily Loaded Propellers," Schip en Werf (1937).

Schoenherr, K. E., "Formulation of Propeller Blade Strength," Trans. SNAME, Vol. 71 (1963).

Schrem, E., "Computer Implementation of the Finite Element Procedure," "ONR Symposium on Numerical and Computer Methods in Structural Mechanics," University of Illinois, Urbana (Sep 1971).

Schrem, E. and J. Roy, "An Automatic System for Kinematic Analysis, ASKA," IUTAM Symposium on High Speed Computing of Elastic Structures, Universite De Liege, Belgium (1971).

Stroud, A. H. and D. Secrest, "Gaussian Quadrature Formulas," Prentice-Hall, Englewood Cliffs (1966).

Taylor, D. W., "The Speed and Power of Ships," Ransdell, Inc., Washington, D. C. (1933).

Tezcan, S. S., "Computer Analysis of Plane and Space Structure," J. Structure Div, ASCE Vol. 92 (1966).

Timoshenko, S., "Theory of Elasticity," McGraw-Hill Book Company, New York, NY (1934).

Timoshenko, S. and S. Woinowsky-Krieger, "Theory of Plates and Shells," Second Edition McGraw-Hill Book Company, New York, NY (1959).

Tong, P. and T. H. H. Pian, "The Convergence of the Finite Element Method in Solving Linear Elastic Problems," Int. J. of Solids and Structures, Vol. 3 (1967).

Turner, M. J. et al., "Stiffness and Deflection Analysis of Complex Structures," J. Aeron. Sc., Vol. 23 (1956).

Wereldsma, R., "Stress Measurements on a Propeller Model for a 42,000 DWT Tanker," Int. Ship. Prog., Vol. 12 (Sep 1965).

Wilson, E. L., "SAP, a General Structural Analysis Program," University of California, Berkeley UC SESM 70-20 (Sep 1970).

Zienkiewicz, O. C., "The Finite Element Method in Engineering Science," McGraw-Hill Book Company, New York, NY (1971).

Zienkiewicz, O. C. et al., "Three-Dimensional Stress Analysis," IUTAM Symposium, Universite de Liege (1971).

Zienkiewicz, O. C. et al., "Iso-Parametric and Associated Element Families for Two- and Three-Dimensional Analysis," in "Finite Element Methods in Stress Analysis," edited by Holand and Bell, TAPIR, Trondheim, Norway (1969).

INITIAL DISTRIBUTION

Copies

- 1 U.S. Army Eng R&D Lab, Tech Doc Cen
- 1 DDR & E
  - Peterson
- 1 ARPA
- 3 CNO
  - 1 OP 971
  - 1 OP 098
  - 1 OP 098T
- 2 CHONR
  - 1 Code 439
  - 1 Code 463
- 2 CHNAVMAT
  - 1 MAT 03T
  - 1 MAT 0333
- 1 USNA
- 2 NAVPGSCOL
  - 1 G. Cantin
- 1 USNROTC & NAVADMINU, MIT
- 1 NAVWARCOL
- 1 DNL
- 1 NRL
- 9 NAVSHIPSYSCOM
  - 2 SHIPS 2052
  - 1 SHIPS 03Z
  - 1 SHIPS 031
  - 1 SHIPS 034
  - 1 SHIPS 0341
  - 1 SHIPS 03413
  - 1 SHIPS 0342
  - 1 SHIPS 03423
- 3 NAVAIRSYSCOM
  - 1 AIR 520
  - 1 AIR 5301
  - 1 AIR 5302
- 1 NAVORDSYSCOM 913
- 2 NAVAIRDEVCEN
  - 1 ST
  - 1 STD

Copies

- 1 CIVENGRLAB
- 1 NOL 730
- 1 NLONLAB NUSC
- 1 NAVSHIPYD BREM
- 1 NAVSHIPYD BSN
- 1 NAVSHIPYD CHASN
- 1 NAVSHIPYD LBEACH
- 1 NAVSHIPYD MARE
- 1 NAVSHIPYD NORVA
- 1 NAVSHIPYD PEARL
- 1 NAVSHIPYD PHILA
- 1 NAVSHIPYD PTSMH
- 1 SUPSHIP, Seattle
  - Code 6233D
- 16 NAVSEC
  - 1 SEC 6101D
  - 1 SEC 6102C
  - 1 SEC 6110
  - 1 SEC 6112
  - 1 SEC 6113
  - 1 SEC 6114D
  - 1 SEC 6115
  - 1 SEC 6120D
  - 1 SEC 6128
  - 1 SEC 6129
  - 1 SEC 6132
  - 1 SEC 6137
  - 1 SEC 6139
  - 1 SEC 6140B
  - 1 SEC 6144
  - 1 SEC 6148B
- 1 AFOSR
  - Mechanics Div
- 1 Air Force Appl Mech Grp
  - Wright-Patterson AFB
- 12 DDC
- 2 COGARD
  - 1 Testing & Devel Div
  - 1 Ship Structures Comm

Copies	
1	Lib of Congress
2	MARAD 1 Div of Ship Design 1 Off of Res & Dev
1	NASA, Langley Res Center
1	NASA, Lewis Res Cen K. A. Faymon
1	NASA, Sci & Tech Info Fac
1	NSF Engr Div
1	BUSTAND
1	Univ of California J. R. Paulling
1	Cal Inst of Tech
1	Case Western Reserve Univ Dept Civ Engr
1	Catholic Univ Dept Mech Engr
1	George Washington Univ School of Engr & Applied Sci
3	Univ of Illinois 1 College of Engr 1 N. M. Newmark 1 W. C. Schnobrich
1	Univ of Iowa Iowa Inst of Hydr Res
1	Lehigh Univ Dept Mech
2	Univ of Maryland 1 Dept Math 1 Dept Mech Engr
1	Mass Inst of Tech Dept Ocean Engr
1	Univ of Michigan Dept NAME
1	Univ of Minnesota St. Anthony Falls Hydr Lab

Copies	
1	Southwest Res Inst
1	Stanford Univ Dept Civ Engr
1	Stevens Inst Davidson Lab
1	Virginia Poly Inst & State Univ Dept Engr Mech
1	Webb Inst
1	National Academy of Sci National Res Council Ship Hull Res Comm
1	SNAME Slamming Panel
1	American Bureau of Shipping S. G. Stiansen
1	Avco, Inc Lycoming Div
1	Boeing Company Aerospace Group
1	General Applied Science Labs
1	General Dynamics Corp Electric Boat Div
1	Gibbs & Cox
1	Grumman Aerospace Corp
1	Hydronautics
1	Itek Corp Vidya Div
1	TRG
1	United Aircraft Corp Hamilton Standard Div

CENTER DISTRIBUTION

Copies	Code	
1	11	Ellsworth, W.
1	115	Johnston, R.

CENTER DISTRIBUTION (CONTINUED)

Copies	Code	
1	1151	O'Neill, W.
1	1154	HYSTU
1	118	Brown, M.
1	1181	LTJG Wilson
1	15	Cummins, W.
1	1521	Pien, P.
1	1528	Strom-Tejsen, J.
1	1532	Dobay, G.
1	154	Morgan, W.
2	1544	
	1	Cumming, R.
	1	Boswell, R.
1	1552	McCarthy, J.
1	156	Hadler, J.
1	16	Chaplin, H.
1	163	Ford, A.
1	17	Murray, W.
1	172	Krenzke, M.
1	173	Stavovy, A.
1	1731	Sikora, J.
1	173.5	Adamchak, J.
1	174	Short, R.
1	177	Schauer, H.
1	178	Becker, L.
1	1805	Cuthill, E.
1	184	Wrench, J.
1	1844	Dhir, S.
1	1864	Pulos, J.
1	19	Sevik, M.
1	1908	Remmers, G.

Copies	Code	
1	194	Franz, G.
1	196	Zaloumis, A. (Acting)
1	1962	Zaloumis, A.
1	1966	Lee, S.E.
1	27	Nutt, H.
1	2742	Goodrich, D. G.
1	28	Wolfe, R. (Acting)
1	281	Niederberger, R.
1	9421	Schuldenfrei, M.
1	9430	Truax, R.
1	9431	Schuldenfrei, M.
1	9441	Stoiko, M.

UNCLASSIFIED
Security Classification

DOCUMENT CONTROL DATA - R & D

(Security classification of title, body of abstract and indexing annotation must be entered when the overall report is classified)

1. ORIGINATING ACTIVITY (Corporate author)	2a. REPORT SECURITY CLASSIFICATION
Naval Ship Research and Development Center Bethesda, Maryland 20034	UNCLASSIFIED 2b. GROUP

3. REPORT TITLE

STRESS ANALYSIS OF COMPLEX SHIP COMPONENTS BY A NUMERICAL PROCEDURE USING CURVED FINITE ELEMENTS

4. DESCRIPTIVE NOTES (Type of report and inclusive dates)

Final Report

5. AUTHOR(S) (First name, middle initial, last name)

James H. Ma

6. REPORT DATE	7a. TOTAL NO. OF PAGES	7b. NO. OF REFS
July 1973	106	77

8a. CONTRACT OR GRANT NO.	9a. ORIGINATOR'S REPORT NUMBER(S)
b. PROJECT NO. SF 43 422 312 c. Task 15084 d. Work Unit 1–1730–089	4057 9b. OTHER REPORT NO(S) (Any other numbers that may be assigned this report)

10. DISTRIBUTION STATEMENT

APPROVED FOR PUBLIC RELEASE: DISTRIBUTION UNLIMITED

11. SUPPLEMENTARY NOTES	12. SPONSORING MILITARY ACTIVITY
Originally submitted to University of Illinois at Urbana-Champaign in partial fulfillment of requirements for the Ph. D. in Civil Engineering.	Naval Ship Systems Command Washington, D. C. 20360

13. ABSTRACT

A numerical procedure for the structural analysis of a general three-dimensional nature has been developed to provide a reliable solution to the problem of determining the strength of propellers, particularly those with unconventional configurations. A finite element displacement model is utilized and compatible solid elements in their general form are adopted. The use of interpolation functions to define pertinent curvilinear coordinates in element space gives the finite element technique, new capabilities for dealing with structures of highly complex geometry. This formulation bypasses the contraints of simplifying assumptions (such as those imposed by classical plate theory) and allows a closer approximation to the true structural configuration than is possible by other approaches, including most analytical and numerical methods. The performance of the refined elements described in this report is distinctly superior to those obtainable with commonly available elements, for example, those in NASTRAN. A highly skewed propeller blade under prescribed pressure distributions was chosen for demonstration of the generality of the procedure. Good agreement was obtained with measured displacement and experimental stress data.

14. KEY WORDS	LINK A		LINK B		LINK C	
	ROLE	WT	ROLE	WT	ROLE	WT
Marine propeller blade						
Skewed propeller						
Stiffened plate						
Curved finite element						
Displacement method						
Elasticity						
Three-dimensional problem						
Numerical method						